



Lehrstuhl für Elektrische Energiespeichertechnik
Fakultät für Elektrotechnik und Informationstechnik
TECHNISCHE UNIVERSITÄT MÜNCHEN

Reuse of Automotive Lithium-Ion Batteries: An Assessment from the Cell Aging Perspective

Simon F. Schuster

Vollständiger Abdruck der von der Fakultät für Elektrotechnik und Informationstechnik der Technischen Universität München zur Erlangung des akademischen Grades eines
Doktor-Ingenieurs (Dr.-Ing.)

genehmigten Dissertation.

Vorsitzender:		Prof. Dr.-Ing. Ulrich Wagner
Prüfer der Dissertation:	1.	Prof. Dr.-Ing. Andreas Jossen
	2.	Prof. Dr. Jürgen Garche Universität Ulm

Die Dissertation wurde am 29.06.2016 bei der Technischen Universität München eingereicht und durch die Fakultät für Elektrotechnik und Informationstechnik am 02.09.2016 angenommen.

Vorwort und Danksagung

Die vorliegende Dissertation „Reuse of Automotive Lithium-Ion Batteries: An Assessment from the Cell Aging Perspective“ entstand während meiner Tätigkeit als wissenschaftlicher Mitarbeiter am Lehrstuhl für Elektrische Energiespeichertechnik der Technischen Universität München zwischen August 2012 und Juni 2016. Dem Lehrstuhlinhaber, Prof. Dr.-Ing. Andreas Jossen, möchte ich für die zahlreichen Denkanstöße danken, welche mir stets dabei geholfen haben meine Forschung voranzubringen. Zudem bedanke ich mich bei Prof. Dr. Jürgen Garche für die interessanten Diskussionsrunden und das Erstellen des Zweitgutachtens.

Weiterhin gilt mein Dank Martin Brand, der den Verlauf meiner Promotion durch Beantragen des Projekts „ABattReLife“ wesentlich mitbestimmt hat. In diesem Sinne möchte ich mich auch bei Tobias Bach und Jana Müller für die tolle Zusammenarbeit während des Projekts bedanken.

Bei Ehsan Rahimzei bedanke ich mich für die vorbildliche Betreuung und Koordination während der Bearbeitung der Studie „Second-Life-Konzepte für Lithium-Ionen-Batterien aus Elektrofahrzeugen“. Bei Sebastian Fischhaber, Anika Regett und Dr. Holger Hesse möchte ich mich für die intensive Zusammenarbeit während der Studienbearbeitung bedanken, welche maßgeblich zum Erfolg der Studie beigetragen hat.

Mein Dank gilt zudem sämtlichen Studenten und Kollegen am Lehrstuhl, die an meiner Forschung mitgewirkt haben. Abschließend möchte ich meiner Familie sowie Lebensgefährtin, Theresa-Maria Bauer, für die fortwährende Unterstützung danken. Diese Arbeit ist meinem Vater, Ralf Schuster, gewidmet.

München, 28. September 2016

Simon F. Schuster

Kurzfassung

Die mögliche Weiterverwendung gealterter Batterien aus elektrischen Fahrzeugen in „Second-Life-Anwendungen“ wird derzeit häufig in der Öffentlichkeit diskutiert. Neben rechtlichen und logistischen Fragestellungen bestehen bei der Umsetzung aber insbesondere auch technische Probleme, die direkt aus dem Alterungsverhalten von Lithium-Ionen-Zellen hervorgehen. Dessen tiefgründiges Verständnis stellt aber eine Grundvoraussetzung dar, um den wirtschaftlichen Nutzen sowie die Gesamtsystemkosten beurteilen zu können.

Die zwei zentralen zellalterungsbedingten technischen Probleme bei der Umsetzung sind das Phänomen der nichtlinearen Alterung (ein sprunghafter Anstieg der Alterungsgeschwindigkeit) sowie der kontinuierlichen Zunahme einer bereits im Neuzustand vorhandenen Zellstreuung während des Betriebs in vielzelligen Batterieanwendungen. Diese zwei Kernthemen werden in der vorliegenden Arbeit umfassend analysiert und beurteilt. Daraufhin werden Lösungsansätze vorgeschlagen und zwar für ersteres Problem eine alterungsabhängige Anpassung der jeweiligen elektrischen Last sowie für letzteres Problem die Anwendung von so genannten Alterungsschnelltests.

Das Einsetzen der nichtlinearen Alterung, welches bei Restkapazitäten von ca. 80 % beobachtet wird, kann durch einen Betrieb mit einer Begrenzung der Laderate und des Spannungshubs bei einem zellspezifischen Temperaturoptimum verzögert oder gar vermieden werden. Der Einfluss der betrieblichen Vorgeschichte wird dabei als unbedeutend eingeschätzt (für zyklisierte Zellen des untersuchten Typs), da eine Lastanpassung (z.B. Reduktion der Laderate und/oder des Spannungshubs) erst kurz vor Einsetzen des nichtlinearen Alterungsverhaltens dennoch die erreichbare Betriebszeit im „Second-Life“ deutlich verlängert. Daher wird davon ausgegangen, dass das zugrunde liegende technische Problem kein Hemmnis darstellt, sofern dessen Eintreten mit hinreichender Genauigkeit vorhergesagt werden kann.

Die als Folge des Zellproduktionsprozesses anfänglich vorhandene Zellstreuung nimmt während des Betriebs in vielzelligen Batterieanwendungen mit dem Alterungsfortschritt aufgrund von externen Einflüssen (z.B. Auseinanderdriften von Zellladezuständen, Temperaturgradienten im Batteriepack) kontinuierlich zu. Insbesondere Temperaturgradienten im Batteriepack können dabei die Übertragung der Zellstreuung auf Modulebene bewirken. Diese ist als besonders kritisch zu erachten, da als Folge dessen lediglich ein Teil der Module selbst aus einer Fahrzeugbatterie für die mögliche Weiterverwendung geeignet sein könnte. Um diese schnellstmöglich und mit wenig Aufwand (verglichen mit der herkömmlichen Kapazitätsmessung) zu erkennen, werden Alterungsschnelltests vorgeschlagen. Aufgrund derer begrenzter Genauigkeit wird allerdings vorerst empfohlen, Alterungsschnelltests lediglich als zusätzlichen Schritt in der Modulvorauswahl heranzuziehen (Reduktion der Anzahl an zu

vermessenden Batteriemodulen). Schließlich sollten reversible bzw. leicht lösbare Zell- und Modulverbindungstechniken (je nach Verschaltungstopologie) verwendet werden, da der Restwert gealterter Fahrzeugbatterien bei Verringerung der aufzubringenden Wiederaufbereitungskosten ansteigt.

Aus Sicht der zellalterungsbedingten technischen Probleme erscheint die Umsetzung von „Second-Life-Konzepten“ als gut durchführbar. Eine Beantwortung der rechtlichen sowie logistischen Fragestellungen erscheint, besonders in Anbetracht der hohen Anzahl an beteiligten Akteuren, allerdings als deutlich komplexer. Dabei wird insbesondere empfohlen, aktuell bestehende Standards und Normen mit Augenmerk auf Weiterverwendungsszenarien zu überprüfen, um so Rechtssicherheit für einen gänzlich neuen Markt zu schaffen.

Executive Summary

The potential reuse of lithium-ion batteries, exhausted upon electric vehicle operation, is currently a broadly discussed topic. Regarding its implementation, aside from legal and logistic issues, there are also certain technological issues, which directly arise from the nature of lithium-ion cell aging. A profound understanding of the battery aging behavior is regarded, however, as a prerequisite to assess overall system costs and economic benefit of battery reuse.

The two technological core issues of potential battery reuse are the phenomenon of nonlinear aging (a sudden increase of the aging rate) and the continuous increase of the initial cell-to-cell parameter variation in multi-cell battery applications. In this work, the two effects are analyzed in detail, and solution approaches are provided, which are, aging dependent load adaption and usage of state of health quick tests.

The effect of nonlinear aging, which is generally observed at residual capacities of approx. 80%, can be delayed or even avoided by battery operation at the cell specific temperature optimum, with a limitation of the voltage swing and the charging rate. The effect of the operational prehistory appears as marginal (for cycled cells of the investigated model), which is why aging dependent load adaption, shortly before the occurrence of nonlinear aging, clearly prolongs as well the reachable second service life. Finally, nonlinear aging is considered to be well-controllable, e.g. by reducing the charging rate and/or the voltage swing. Though, its onset must not be missed under any circumstances, which in turn underlines the importance of the refinement of state of health detection methodologies.

The initial cell-to-cell variation, which results from deviations in the cell production process, is generally increased in multi-cell battery applications with the progress of aging due to external influences like drifts of the state of charge of cells or temperature gradients in the battery pack. Especially the latter might provoke a scale-up of cell-to-cell variation up to the module level, which is critical towards battery reuse implementation. As, consequently, only a share of battery modules, even from the same automotive battery, might be reusable, state of health quick tests are capable of reducing the measurement effort compared with common capacity measurement techniques. However, with regard to their limited precision, only a supporting role should be considered in the battery module pre-selection process, in which inappropriate ones are sorted out in advance. After all, to support the profitability of battery reuse concepts, reversible and easily detachable cell and/or module interconnection techniques should be favored, as reduced refurbishing costs clearly increase the residual value of aged automotive lithium-ion batteries.

Finally, with regard to the technological barriers which emerge directly from the nature of lithium-ion cell aging, battery second life scenarios are regarded as well implementable, especially if online state of health detection is refined; in contrast, legal and logistic issues (which are

especially present due to the high number of involved actors) are considered to be the more challenging part. Here, the key is to revise present standards and norms, specifically with regard to battery reuse concepts and thus, creating legal certainty for an utterly new market.

List of Publications

Selection of Conference Contributions

S. Schuster, M. Brand, T. Bach, E. Fleder, M. Stelz, J. Müller, G. Sextl, A. Jossen, Effects of vibration loads on Li-ion cells in electric vehicles, 3rd European Electric Vehicle Congress (EEVC), Brussels, December 2014 (Oral Presentation).

S.F. Schuster, T.C. Bach, E. Fleder, J. Müller, G. Sextl, A. Jossen, Untersuchung des zyklischen Alterungsverhaltens von Li-Ion-Zellen: Ursachen für einen abrupten Kapazitätsabfall, 22. DESIGN & ELEKTRONIK-Entwicklerforum, Munich, March 2015 (Oral Presentation).

S.F. Schuster, T.C. Bach, E. Fleder, J. Müller, G. Sextl, A. Jossen, Investigations on the cyclic aging behavior of Li-ion cells: Reasons for an abrupt drop of capacity, 28th International Electric Vehicle Symposium and Exhibition (EVS), Goyang, May 2015 (Oral Presentation).

S. Schuster, P. Keil, C. von Lüders, H. Hesse, A. Jossen, New Charging Method to Avoid Nonlinear Aging of Lithium-Ion Batteries, Batteries Event, Nice, October 2015 (Poster).

S.F. Schuster, P. Keil, C. von Lüders, H. Hesse, A. Jossen, Innovatives Ladeverfahren zum Umgehen von nichtlinearer Alterung bei Lithium-Ionen-Batterien, Forum Batterietechnik, Speicher für die Mobilität 2020 und die Energieversorgung, Nördlingen, November 2015 (Oral Presentation).

S. Schuster, M. Brand, C. Campestrini, M. Gleissenberger, A. Jossen, Correlation between capacity and impedance of lithium-ion cells during calendar and cycle life, 4th European Electric Vehicle Congress (EEVC), Brussels, December 2015 (Oral Presentation).

S. Fischhaber, A. Regett, S.F. Schuster, H. Hesse, Second-Life-Konzepte für Lithium-Ionen-Batterien aus Elektrofahrzeugen, Ergebniskonferenz Schaufenster Elektromobilität, Leipzig, April 2016 (Oral Presentation).

Peer-Reviewed Scientific Reports

S. Fischhaber, A. Regett, S.F. Schuster, H. Hesse, Second-Life-Konzepte für Lithium-Ionen-Batterien aus Elektrofahrzeugen, Ergebnisrapport Nr. 18 (Begleit- und Wirkungsforschung), Frankfurt am Main, 2016.

Peer-Reviewed Journal Contributions (Co-Author)

M.J. Brand, S.F. Schuster, T. Bach, E. Fleder, M. Stelz, S. Gläser, J. Müller, G. SEXTL, A. Jossen, Effects of vibrations and shocks on lithium-ion cells, *J. Power Sources* 288 (2015) 62-69.

T.C. Bach, S.F. Schuster, E. Fleder, J. Müller, M.J. Brand, H. Lormann, A. Jossen, G. SEXTL, Nonlinear aging of cylindrical lithium-ion cells linked to heterogeneous compression, *J. Energy Storage* 5 (2016) 212-223.

C. Campestrini, P. Keil, S.F. Schuster, A. Jossen, Ageing of lithium-ion battery modules with dissipative balancing compared with single-cell ageing, *J. Energy Storage* 6 (2016) 142-152.

P. Keil, S.F. Schuster, J. Wilhelm, J. Travi, A. Hauser, R.C. Karl, A. Jossen, Calendar Aging of Lithium-Ion Batteries. Part I: Impact of the Graphite Anode on Capacity Fade, *J. Electrochem. Soc.* 163 (2016) A1872-A1880.

Journal Contributions (Lead Author)

S. Schuster, T. Bach, Jährer Absturz, DESIGN & ELEKTRONIK KNOW HOW FÜR ENTWICKLER 02 (2015) 27-30.

*Peer-Reviewed Journal Contributions (Lead Author) **

S.F. Schuster, T. Bach, E. Fleder, J. Müller, M. Brand, G. SEXTL, A. Jossen, Nonlinear aging characteristics of lithium-ion cells under different operational conditions, *J. Energy Storage* 1 (2015) 44-53. ⁽¹⁾

S.F. Schuster, M.J. Brand, P. Berg, M. Gleissenberger, A. Jossen, Lithium-ion cell-to-cell variation during battery electric vehicle operation, *J. Power Sources* 297 (2015) 242-251. ⁽²⁾

S.F. Schuster, M.J. Brand, C. Campestrini, M. Gleissenberger, A. Jossen, Correlation between capacity and impedance of lithium-ion cells during calendar and cycle life, *J. Power Sources* 305 (2016) 191-199. ⁽³⁾

* Self-produced sections of peer-reviewed lead author journal contributions are partially contained in this doctoral thesis without any further reference in the running text (figures are continuously referenced); in particular, this involves Chapter 6 ⁽¹⁾, 7 ⁽²⁾ and 8 ⁽³⁾.

List of Contents

1	Introduction.....	1
1.1	Motivation.....	1
1.2	Review of Automotive Battery Reuse Investigations.....	2
1.3	Objectives and Further Procedure.....	6
2	Second Life Concepts.....	9
2.1	Main Process	9
2.2	Refurbishing Process	12
3	Fundamentals of Lithium-Ion Cell Aging	19
3.1	Review of Aging Mechanisms	21
3.2	Interaction of Capacity Fade and Impedance Increase.....	26
3.3	Causes of Nonlinear Aging.....	30
3.4	End of Life Criteria	38
3.5	Causes of Increasing Cell-to-Cell Variation	39
4	Methods of Descriptive Statistics	41
4.1	Univariate Analysis.....	41
4.2	Bivariate Analysis.....	43
4.3	Link to the Battery Cell and Module Interconnection Configuration.....	44
5	Experimental	48
5.1	Aging Diagnosis	48
5.2	Design of Experiments	50
5.3	Examined Battery Electric Vehicles	55
6	Lithium-Ion Cell Aging.....	60
6.1	Nonlinear Aging Behavior under Different Operational Conditions.....	61
6.1.1	Dependency on the Voltage Swing.....	62
6.1.2	Dependency on the Current Rate.....	64
6.1.3	Dependency on the Temperature.....	69

6.2	Influence of the Operational Prehistory.....	73
6.2.1	Controllability of Nonlinear Aging Behavior.....	75
6.2.1.1	Two-Step Parameter Adaption.....	75
6.2.1.2	Continuous Charging Rate Adaption.....	79
6.2.2	Storage Conditions before Cycling.....	81
6.3	Conclusion.....	84
7	Lithium-Ion Cell-to-Cell Variation.....	87
7.1	Distribution Fit Analysis.....	88
7.2	Influence of Operational Histories of Examined Vehicles.....	97
7.3	Characterization of Cell Outliers.....	98
7.4	Conclusion.....	99
8	Correlation between Capacity Fade and Impedance Increase of Lithium-Ion Cells.....	102
8.1	Single Aging State Analysis.....	103
8.2	Aging Progress Regression Analysis.....	106
8.3	Validation of the State of Health Quick Test Approach.....	108
8.4	Extended Single Aging State Analysis.....	110
8.5	Conclusion.....	111
9	Final Conclusion.....	113
9.1	Summary.....	113
9.2	Recommendations for Action.....	116
	List of References.....	118
	List of Abbreviations.....	134

1 Introduction

In the beginning of this thesis, investigated issues are put into a topical context at first. Then, a comprehensive review of former and recent automotive battery reuse investigations is given to point out the central idea, the temporal development and the still present challenges of the practical implementation of so called second life concepts (SLC). Thereof, objectives of this thesis are derived and the further procedure is presented.

1.1 Motivation

A global wide launch of battery electric vehicles (BEV), accompanied by an increased share of renewable energies in the grid, is without any serious alternative to tackle major issues of society like high greenhouse gas (GHG) emissions, air pollution, oil depletion, energy security and continuous population growth [1-3]. In addition to large parts of known oil reserves being situated in politically unstable regions, current projections predict oil depletion in approximately 50 years [1]. GHG emissions lead to global warming which in turn e.g. results in glacial and sea ice melting, sea level rise and expanded aridity zones. Such effects are directly connected with species extinction or a degradation of ecological life conditions in general. Air pollutants (especially from diesel vehicles) like NO_x , PM_{10} and other volatile organic compounds are e.g. responsible for a variety of respiratory diseases [4]. The progressive global population growth additionally complicates the finding of effective approaches to aforementioned issues.

However, regarding the situation in Germany for example, neither the desired number of one million BEV until 2020, nor the aim of climate policies with a GHG emission reduction of 40% until 2020 and at minimum 80% until 2050 referred to 1990 (Kyoto base year), will likely be reached. On the 1st of January in 2015, the share of BEV and hybrid electric vehicles (HEV) in the pool of passenger cars was vanishingly low with only about 0.3% (18.948 BEV, 107.754 HEV, 44.403.124 vehicles in total) [5]. Commissioned by the German government, a recent study predicts a reduction of GHG emissions in the energy sector of 36% until 2020 and 65% until 2050 [6]. Although the government's aims refer to all sectors in complete, it is mentioned that the unconsidered sectors like transport or agriculture will not be able to compensate the deficits of the energy sector. The additional aim of a halved energy consumption until 2050 will probably be failed with reaching only 42% referred to 2008. As the only positive trend, the government's aims for the share of renewable energies in the electricity sector with 35% until 2020 are expected to be surpassed which mainly originates from the ongoing increase of using decentralized photovoltaic systems for self-generation as well as wind power plants [7].

Principal factors which impede the launch of BEV are a limited maximum range in comparison with internal combustion engine vehicles, an underdeveloped charging infrastructure and a high price which in turn is mainly caused by the costly battery storage. The latter factor is also the main cause to impede a wider use of lithium-ion batteries (LIB) in stationary energy storage applications [8]. Furthermore, the resale value of actual BEV is supposed to be low due to upcoming technological leaps which lead to a strong price decline of then outdated BEV versions. As the recycling of LIB in contrast to lead-acid batteries (PbB) is currently not economically feasible but prescribed by the German battery law “Batteriegelgesetz” (BattG), a distinct approach which could create a residual value in contrast to directly arising recycling costs is the reuse of aged automotive batteries in applications with a minor challenging load profile (such as in the field of stationary energy storage) [9, 10].

Major advantage of such a SLC is the potential of reducing the total costs of ownership (TCO) of BEV and simultaneously creating a market with cheap batteries for stationary energy storage. In addition, as LIB recycling processes are expected to become more energy-effective, current costs of up to 0.5 €/kg automotive battery system are likely to move for profits in the near future (due to the presence of precious metals like cobalt and nickel) [11-13]. So, the reuse of aged automotive lithium-ion batteries (ALIB) in SLC can even be imagined as a *temporal bridge* from uneconomical to economical recycling [14]. However, the ongoing price reduction of new LIB systems (e.g. due to an increase of produced quantities) generally promotes the launch of BEV and stationary battery storages, but simultaneously counteracts the profitability of SLC as a second life battery (SLB) system has always to compete with the costs of a new one [14-16]. So, reusing degraded ALIB in second life applications (SLA) might be a viable option to foster both the launch of BEV and stationary battery storages in the next few years, but probably lose its economic efficiency in the long-term. In the next subchapter, a comprehensive review of former and recent battery reuse investigations is given, wherefrom objectives of this thesis are derived.

1.2 Review of Automotive Battery Reuse Investigations

The potential reuse of aged ALIB is currently a hotly debated topic which mainly aims at a reduction of the TCO of electric vehicles. Simultaneously, stationary energy storage applications would be promoted by making cheaper batteries available. As the recycling of disused ALIB is currently not economically feasible but prescribed by German law (§ 5 BattG), by implementation of SLC, in other respects directly arising recycling costs could at least be offset for years [10, 17].

As the zero-emissions vehicle mandate entered into force in California in 1990, aiming at a share of 2%, 10% and 18% until 1998, 2003 and 2018, respectively, this led to intensified BEV research and development [18]. At the same time, suggestions of reusing aged automotive

batteries in SLA came up. In a first investigation, the Argonne National Laboratory compared the aging behavior of PbB with the one of pre-aged nickel metal hydride (NiMH) batteries for the United States Advanced Battery Consortium (USABC) in 1998 [19]. Results showed that NiMH automotive batteries which had already been used in BEV still fulfilled the requirements of stationary energy storage applications, and particularly could compete with new PbB. By taking up these first findings, Sandia National Laboratories evaluated the economic efficiency of SLC with aged NiMH prototype-BEV battery modules in 2003 [20]. The authors demonstrated technical feasibility but doubted their profitability. They cited a standardized, modular construction of automotive battery packs to be inevitable for an economic realization of SLC. As most promising fields of application, back-up storages for telecommunication systems, decentralized storages to avoid grid extension and interim storages for renewable energies in the residential and mid-scale industrial domain, were identified. Additionally, regarding the evaluation of a SLC's profitability, the difficulty of predicting the aging behavior of NiMH batteries was designated to stand for a material uncertainty.

This serious issue is also explicitly pointed out in [21] to exist for LIB. Furthermore, the usage of aged ALIB in the consumer field (like interim storage for renewable energies in the domestic domain) is preferred before the field of large-scale energy storage as the modification and refurbishment is estimated to be easier to handle and thus more cost-effective. Contrarily, a profitable realization of grid-related large-scale storage systems is mentioned in [22] and [23] to be feasible if distinct applications, like e.g. primary control reserve regulation (PCRR) and intraday electricity market trading, are run combined in one storage. By deploying SLB instead of new LIB for PCRR or in a home energy storage system, it was shown in [14] that net present values increased about 33% or 26% within a depreciation time of 20 years, respectively. However, latest studies consistently state, anyway, that the potential of reducing the TCO of BEV by implementation of SLC must be regarded as rather low [24-26]. The maximum TCO reduction is mentioned in [14] to be mainly limited by the ongoing price decline of new LIB systems. Possibly, there are further financial benefits for the final user at the last stage of the vehicle's life cycle. In addition, storage and integration of renewable energies could be fostered due the availability of cheaper batteries with effects like reduced GHG emissions or a deceleration of the ongoing electricity price increase. So, the main aim of reducing the TCO of BEV is most likely unreachable or vanishingly low, but there are other positive side effects for society which can be reached by a broad distribution of SLC.

Besides of several technological hurdles regarding SLC implementation, there are also legal and logistic questions (like warranty claims or battery ownership structure), which have to be answered [27, 28]. A standardized, modular construction method of ALIB, which is applied beyond the boundaries of a single vehicle manufacturer, is needed to minimize SLB refurbishing costs. As such a refurbishing process basically consists of the disassembly of aged ALIB packs, the selection of battery units (cells, modules, etc.) suitable for reuse and

finally the construction of “new” SLB in desired topology and size, especially *cost-effective methods of state of health (SoH) detection* (like online-tracking of aging dependent battery parameters or SoH quick tests) are required to maximize the profitability of SLC [16]. Thereby, it has to be considered that even within one ALIB only a fraction of battery units might be suitable for reuse because of an *increasing lithium-ion cell-to-cell parameter variation* during the progress of aging. As stationary energy storage systems are usually run for a quite long period of time, moreover, a profound understanding and predictability of the aging behavior of LIB are a prerequisite to assess overall system costs and economic benefit of battery reuse. Thus, understanding the aging behavior of LIB is directly linked with the decision to invest in a battery reuse project. However, lifetime projections are challenging, especially as a *turning away from regular aging behavior to increased aging rates* is observed at deep residual capacities of lithium-ion cells (LIC). This aging phenomenon is regarded as a major barrier of profitable SLC implementation as it may strongly limit the second service life [29].

Due to the presence of several challenging hurdles to overcome, as well as the low availability of aged ALIB packs, at present, there are mainly research projects dealing with the subject matter of SLC. The project “Second Life Batteries” of an alliance of Vattenfall, Bosch and the BMW Group is currently in its initial phase in which a 2 MW SLB storage, consisting of aged ActiveE and i3 ALIB packs, is built up in Hamburg. The storage is planned to be used for PCRR from the mid of 2016 until 2020 [30]. Another large-scale battery storage consisting of approx. 650 aged ALIB with a total capacity of 13 MWh and a power of 13 MW is currently built up in North Rhine-Westphalia by a joint venture of Daimler Automotive, The Mobility House and the GETEC Group [31]. The storage is planned to be used for PCRR as well. In an already finished project, Vattenfall and the BMW Group tested the viability of using aged ALIB as buffer storage for BEV fast charging stations. The feasibility of such buffer storages for fast charging stations with SLB was also simulated and confirmed experimentally in [32]. Another large ALIB reuse project has been started in the autumn of 2015 by EDF, Forsee Power, Mitsubishi Motors Corporation and PSA Peugeot-Citroën in the domicile of Forsee Power in the near of Paris [33]. In this project, photovoltaic modules and BEV (incl. charging stations) are connected with new LIB and SLB in a bidirectional flow to be used for grid-stabilization and to cover the energy need of the company’s main building. Finally, in terms of completeness, a selection of publicly promoted projects in Germany which dealt with SLC shall be mentioned here: Sun2Car@GAP, EOL-IS, StaTrak and ABattReLife.

As already described before, a reuse of aged ALIB could be used to build a temporal bridge from times of uneconomical to economical recycling, or at least to offset directly arising recycling costs from the present. However, as the recycling process of ALIB is prescribed by German law and can only be postponed, SLC are no alternative to recycling, but remanufacturing of aged ALIB is an alternative to SLC. If only a small fraction of battery units are damaged and thus limit the capacity and power capability of the whole pack, these could be

replaced by new (or already used but still suitable) units to restore required pack properties. Advantage of this distinct approach is the avoidance of costly SLB manufacturing processes, but, however, cost-effective methods of SoH detection like online-tracking of aging dependent battery parameters or SoH quick tests are needed as well. Additional costs could occur if removed battery units had to be stored temporarily before tracking a suitable car to be deployed in [28]. It may be assumed, however, that none of both approaches, i.e., remanufacturing and reuse, will drive its opponent completely from the (at present imaginary) market. Instead, the authors of [14] postulate that remanufacturing of aged ALIB will be a useful supplement of battery SLC.

Besides of new LIB, another direct competitor of SLB is the PbB which is still by far the most commonly used secondary battery with a total market share of approximately 50% [34]. In many applications which are regarded as suitable for SLB (e.g. vehicle starter batteries, back-up storages for telecommunication systems, emergency power supply, traction batteries for forklift trucks, etc.), the PbB represents the type of battery which is, at present, usually used by default [24, 35, 36]. In spite of several technological advantages of LIB (like a longer service life), a widespread drive from the market of PbB is not forthcoming because of the presence of currently still higher LIB system costs as well as unanswered technological disadvantages like a poorer low temperature behavior and increased safety problems at high temperatures. However, as e.g. the price decline of LIB home energy storage systems surpasses the one of PbB systems, the share of LIB will further increase in the future [7]. The Eidgenössische Technische Hochschule (ETH) Zurich compared costs and technical specifications of PbB with those of LIB in a comprehensive literature review which was published in 2013 [8]: Regarding the mean calendar life, the LIB slightly outperformed the PbB with 11.5 years in contrast to 8.5 years. For the mean maximum number of cycles at a charge and discharge cycle depth of 80%, the technological superiority of LIB with 10.250 cycles in contrast to PbB with 1.250 cycles was considerable. Also the mean round-trip efficiency of LIB with 90% surpassed the one of PbB with 82%. However, these technological advantages of LIB faced higher battery system costs with 844 €/kWh compared to 171 €/kWh for PbB systems.

Especially for the battery system costs which are listed in [8], it has to be considered, though, that mentioned values are no longer current. In the meanwhile, LIB system costs declined to values between 300 €/kWh and 400 €/kWh, whereas actual PbB systems are settled within a range from 100 €/kWh to 150 €/kWh [15, 24]. In spite of the strong decline of LIB system prices, nevertheless, there is still a heavy demand for PbB systems. As SLB would be significantly cheaper available than new LIB, however, this offered the chance of being cost-competitive with PbB which in turn principally enabled the entry in the large, already existing market of PbB. For the costs of new LIB and SLB, a relationship could be derived in [14], which quoted *the price limit of SLB (at residual capacities of 80%) to be approximately the half from new LIB (in €/kWh, regardless of the price development of new LIB)*. If it is assumed that the

price decline of LIB continues to surpass the one of PbB, this could lead to a price advantage of SLB compared with PbB in a few years. So, in combination with aforementioned technological advantages (assumed here to be valid for LIB and also SLB), SLB might bear a real chance to absorb parts of the PbB market.

An additional field of application in which SLB could replace currently deployed technologies, which are PbB or diesel generator sets, is the electrification of rural areas in developing nations by using micro- or mini-grid systems. Regarding the application-related reachable service life, for SLB values between six and eight years in contrast to three and four years for PbB, are mentioned in [37]. One reason for the inferior service life of PbB is their greater sensitivity towards high ambient temperatures which, however, are typical for developing nations like Central Africa or South East Asia. The limited service life of certain types of PbB is further reduced if the water filling level is not maintained by regularly inserting purified water. Furthermore, with a gravimetric (70 Wh/kg - 100 Wh/kg at SoH = 70%) and volumetric energy density (175 Wh/l - 280 Wh/l at SoH = 70%) of SLB, still being approximately two and three times higher than values of PbB, respectively, economical and also ecological benefits both emerge e.g. at freighter transportation of batteries [37].

Generally, battery reuse is regarded as a promising approach to reduce emissions and resource requirements associated with electromobility. If the production of new batteries (e.g. PbB or LIB) is avoided by deploying SLB, an ecological savings potential can be assumed [38, 39]. As is shown in [29, 40, 41], this potential depends on the investigated application, the respective electricity mix and the competing technology. Exemplarily, based on substitution of new LIB with SLB and the German electricity mix, an ecological savings potential of 34 kg - 106 kg CO₂ equivalent (CO₂e) and 30 kg - 95 kg CO₂e per initial kWh battery nominal capacity was calculated in [14] for PCRR and deployment in a home energy storage system, respectively. Hereby, increased losses during operation, due to a decreased efficiency of SLB compared with new batteries (for the period of the service life), were not considered, but just the savings from refurbishing aged ALIB rather than producing new storage systems (the electricity mix was referred to the energy expenditure of the refurbishing or the production process of application specific storage systems). After this comprehensive review of previous battery reuse investigations, in the following subchapter, main issues of this thesis are concisely summarized, objectives highlighted and the further procedure is presented.

1.3 Objectives and Further Procedure

Currently, the presence of several technological, legal and logistic hurdles impedes a widespread implementation of SLC. Main topic of this thesis is, as the title already suggests, the investigation of technological barriers which originate *from the nature of LIC aging*. First core issue is, thereby, the phenomenon of a suddenly increasing cell aging rate which severely

challenges lifetime projections. These, however, are necessary for assessing the profitability of SLC. Henceforth, the phenomenon of a suddenly increasing cell aging rate at deep residual capacities is denoted as *nonlinear aging*. Second core issue is the lithium-ion *cell-to-cell parameter variation* which is observed to increase with the progress of aging. Regarding the implementation of SLC, as a consequence, this is crucial as only a fraction of the units of a BEV battery pack might be worthy to refurbish from an economic point of view. Both of these core issues are investigated in detail and solution approaches are provided to promote SLC implementation. The scheme in Figure 1 is henceforth used in this thesis for progress control and clarification of connecting chapters.

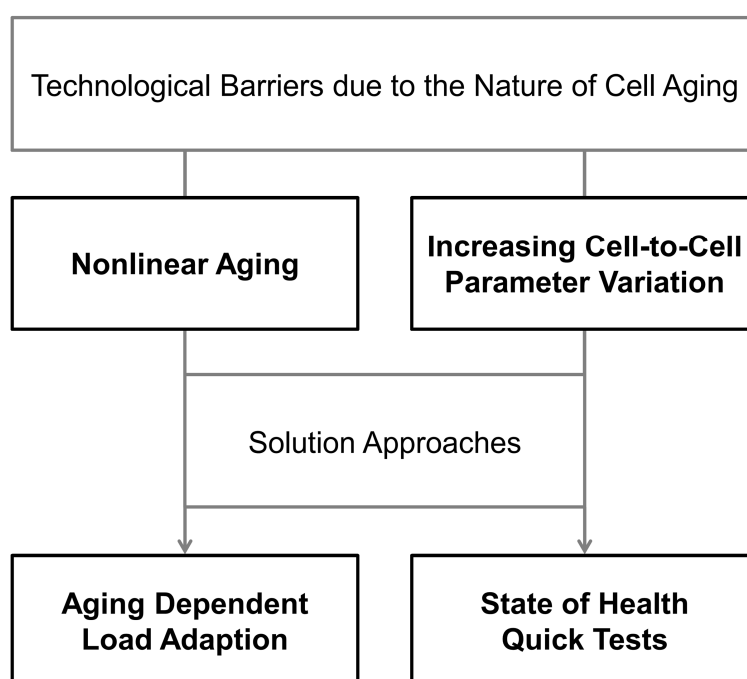


Figure 1: Scheme of investigated core issues and provided solution approaches.

Considering nonlinear aging characteristics of LIC, at first, load profile parameters are varied to identify those which promote the underlying aging mechanism(s). Additionally, by that, perfect foresight, when nonlinear aging characteristics will start, is obtained for a certain type of load. With this knowledge, ways of *mitigation or prevention by load adaption* are examined. Regarding the ALIB reuse scenario, a “two-step” load profile adaption (from BEV to SLA) thus aims at extending the battery’s total service life by preventing nonlinear aging characteristics.

The aging dependency of lithium-ion cell-to-cell parameter variation is examined by gauging large LIC batches in the new and aged state (approximately three years of BEV operation). Yielded results are statistically analyzed and compared with the operational histories of

investigated BEV. The increase of cell-to-cell parameter variation is the reason for needing *cost-effective SoH detection methods*, for which there is basically either the online-tracking of aging dependent battery parameters or the so called SoH quick tests. One approach for the latter is based on the *correlation between capacity fade and impedance increase* of LIC, which is investigated and evaluated in this thesis. With a reliable and cost-effective method of SoH detection, profitability of SLC can effectively be fostered by reduction of SLB refurbishing costs.

The thesis “*Reuse of Automotive Lithium-Ion Batteries: An Assessment from the Cell Aging Perspective*” is structured as is shown in Figure 2. In Chapter 1, the topical context and a comprehensive review of former battery reuse investigations were given. In Chapter 2, the distinct stages and processes of SLC are described. Completing the “*Framework & Fundamentals*” block, basic information on the aging behavior of LIC is reviewed in Chapter 3. Regarding the next block which is denoted as “*Modeling & Setup*”, in Chapter 4, statistical methods which are used afterwards to analyze yielded experimental data sets are explained. Additionally, the presented theoretical methods are referred to interconnection configurations of cells and modules in ALIB. Information on the setup of performed experiments is given in Chapter 5. In the “*Results & Discussion*” block, experimental findings regarding nonlinear aging characteristics, cell-to-cell parameter variation and the correlation behavior (between capacity fade and impedance increase) are shown and interpreted in Chapter 6, 7 and 8, respectively. In the concluding Chapter 9 (not shown in Figure 2), main issues and results of this thesis are summarized and an outlook is given in which forthcoming scientific steps are recommended.

Framework & Fundamentals	Introduction	1
	Second Life Concepts	2
	Lithium-Ion Cell Aging	3
Modeling & Setup	Statistical Methods	4
	Experimental	5
Results & Discussion	Nonlinear Aging	6
	Cell-to-Cell Variation	7
	Correlation Behavior	8

Figure 2: Structure of the thesis “Reuse of Automotive Lithium-Ion Batteries: An Assessment from the Cell Aging Perspective” with assigned numbers of chapters.

2 Second Life Concepts

In spite of a variety of imaginable constellations of SLC (like regarding the battery ownership structure), there are certain stages or processes yet which define a battery reuse scenario. In this chapter, relevant processes of SLC and a general definition of SLB are presented. As part of the main process, the refurbishing process, i.e., all necessary steps from automotive battery removal to the development of new SLB, plays an essential role in reaching profitability of SLC. Thereof, in turn, the detection of the SoH of disassembled battery units is regarded to be the most relevant part to do so.

2.1 Main Process

The three characteristic battery life cycle stages which define the main process of SLC are shown in Figure 3 as black boxes (instead of grey boxes representing sub-level or externally docking process steps). In the battery's first stage, i.e., the deployment as automotive battery, reachable service life is influenced by a variety of factors like battery dimensioning, management, operational strategy, user's driving style and charging habits, as well as ambient conditions. With an expected automobile lifetime of slightly more than ten years, main aim is that the battery of an electrified vehicle withstands this period's everyday use and thus, no premature battery exchange becomes necessary [16]. Insignificant for the SLC process, by all means, as soon as the BEV requirements cannot be fulfilled anymore (i.e., the automotive battery's end of life (EoL) is reached), the automotive battery must be removed. In the literature, the end of first life (Eo1L) is usually mentioned for BEV to be reached when the remaining capacity is between 70% and 80% of its nominal capacity [16, 42-45]. Definition and value range of Eo1L are critically analyzed and discussed later in Subchapter 3.4 after explanation of therefore needed fundamentals of LIC aging.

In the second stage of the main process of SLC, i.e., the refurbishment, at first, the aged battery is removed from the BEV and disassembled into its single units (not mandatory). In the field, the maximum disassembly level to be economically viable is most likely limited to modules because e.g. a breakup of single cells' soldered joints might be too costly even for large cells. As the reuse possibilities of ALIB are yet assessed in this thesis from the cell aging perspective, the interrelationship between battery cell-to-cell and module-to-module parameter variation is comprehensively analyzed and discussed in Subchapter 4.3. Alternatively, for the construction of large-scale battery energy storages, several refurbished packs may be interconnected in complete to minimize refurbishing costs. In this case, the fundamental relationships which are presented in Subchapter 4.3 can easily be transferred.

Anyway, if battery units are available in the desired disassembly level, those suitable for reuse are selected and classified. Finally, new SLB are built in desired topology and size. Thereby, to maximize profitability, further components of the original automotive battery like casing components, sensors, the cooling system or the battery management system (BMS) must be checked for the possibility of reuse. In case of the BMS, for example, to fulfill the distinct requirements of the SLA, software modifications might become necessary. Though, as car manufacturers usually protect the related software by encryption methods, in practice, this is only viable if the car manufacturer is involved in the software modification process. A more detailed description and analysis of the single steps of the refurbishing process, especially of its battery unit characterization and selection process, is presented in the next subchapter.

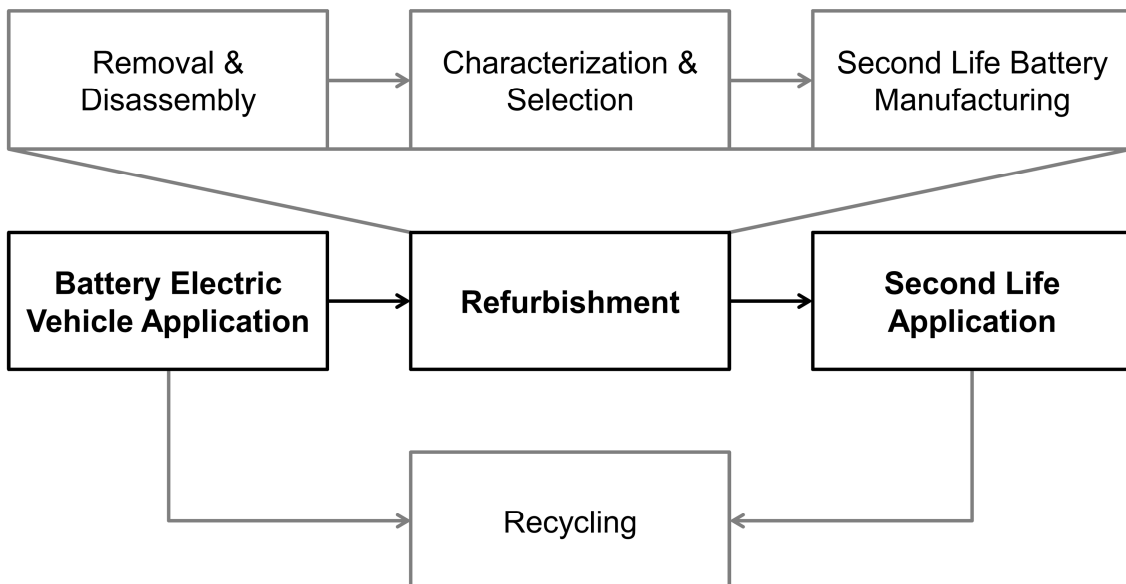


Figure 3: Battery life cycle stages in the main process (black boxes) of a second life concept; in terms of completeness, sub-level and externally docking processes are additionally marked (grey boxes).

Finally, in the third stage of the main process of SLC, after installation in the respective SLA, the SLB is deployed in a manner to optimize profitability by reaching a maximized extension of the second service life. This may be at most effectively reached by a suitable operational strategy which takes into account the battery’s pre-aged state. In general, severe ambient conditions (like sub-zero temperatures) should be avoided and load profiles of suitable SLA be characterized by only a low number of shallow cycles with mild currents. In case of stationary energy storage, as weight and volume is not an issue, load profiles with desired properties can be created by sensible and systematic battery oversizing as long as profitability still can be maintained (same earnings, higher investment costs). Same is for the field of potential mobile SLA like forklift trucks, where especially weight is even needed as a counterpart of the loaded freight. In the

literature, even if partially contradictory, several suitable fields of SLB application like as interim storage for renewable energies, back-up storage for telecommunication systems, decentralized storage for mini-grids or to avoid grid extension, as forklift truck traction battery, or storage for PCRR and peak shaving, have been identified [14, 20, 24, 37].

So, important finding is that SLB aging may be decelerated by battery oversizing (independent of SLA type) which is feasible as long as profits still exceed expenses. Especially for the case of avoiding SLB exchanges within fixed project periods, battery oversizing is lucrative as involved reinvestment costs can be considerably reduced [46]. Finally, if the requirements of SLA cannot be fulfilled anymore, i.e., the end of second life (Eo2L) is reached, the main process of SLC ends and the SLB must be brought to a recycling facility. In the literature, values of the Eo2L criterion for SLB in an arbitrary SLA are given within a range of 20% and 40% residual capacity [29]. However, as this value range appears to be strongly undifferentiated, same as for the Eo1L criterion, it is critically analyzed and assessed later in Subchapter 3.4.

As already mentioned before, the recycling process is prescribed by German law and so mandatory either directly after the first, or after the second life of the respective battery. Jurisdiction hereof depends on the battery ownership structure: in accordance with § 5 BattG, the manufacturer of an end product with battery storage is obliged to recycle it for the end consumer [10]. Regarding SLC, instead of this to be the car manufacturer by default, after alteration of the ownership structure, distinct constellations with a transferred recycling obligation are conceivable as well [14]. In any case, if the offset of directly arising recycling costs and the aforementioned temporal bridge from uneconomic to economic times of recycling are excluded, battery recycling is an external docking process of SLC and thus not further investigated in this thesis. In the next subchapter, the single steps of refurbishment are analyzed and assessed in more detail. Before, based on the lessons recently learned, a henceforth valid definition of a SLB is given.

Definition of a second life battery:

The term second life battery characterizes a battery system, consisting of automotive battery units which were used in battery electric vehicles and refurbished for reuse (in a second life application with a minor challenging load profile, especially taking into account the battery units' pre-aged state). [14]

With regard to this definition of SLB, constellations without battery removal and refurbishment, such as BEV reselling from long-distance to short-distance drivers or city leasing companies, sometimes also referred to as SLA, are especially excluded in this thesis.

2.2 Refurbishing Process

The increasing cell-to-cell (and module-to-module) parameter variation in an automotive battery during BEV operation is the reason for needing SoH detection of battery units to separate those suitable for reuse from those which should be immediately recycled. The refurbishing process basically consists of battery removal and disassembly, battery unit characterization and selection, and finally the manufacturing of new SLB (see Figure 3). The refurbishment expenses considerably reduce the residual value of aged automotive batteries. For the complete refurbishing process, in the literature, values between 150 \$/kWh and 15 \$/kWh are given, whereby a broader distribution of SLC would lead to lower values [20, 24, 26, 36]. It must be considered, though, that values given in the literature not even refer to a certain SLA, and thus, only represent a rough guide which must be rechecked in the field.

In any case, if there is a hypothetical cost limit of a SLB, which the prospective customer is willingly to pay at maximum, refurbishment expenses must be subtracted thereof to yield the residual value of an aged automotive battery [14, 24, 35, 36]. Regarding the customer side, the hypothetical cost limit of SLB depends on the actual price of new batteries of the respective technology (LIB in this thesis), the aging state of the used batteries and a psychological “second hand” factor [35, 47]. The latter is e.g. comparable with the disproportionate fall in value in the first year of use of a new passenger vehicle. Additionally, the hypothetical cost limit of SLB at the customer side is always as low as costs of competing technologies like PbB (if technological properties are assumed to be equal) [14]. Regarding the vendor side, relevant criterion is that the residual value of an aged automotive battery is positive because, otherwise, in the base case scenario, it would be immediately given to recycling (not to refurbishment). However, in alternative case scenarios, negative residual values may be allowed if a profit from the offset of recycling costs leads at least to break-even (for covered expenses only, there is at least an ecological benefit). Finally, suggested scenarios strongly depend on the battery ownership structure and the related jurisdiction of the obliged recycling process.

Generally, compliance with several legal regulations is mandatory in the context of battery production and distribution [10]. Regarding a specific application in the second life compared with the application “BEV”, if there are any additional battery regulations, it must be ensured in the refurbishing process to satisfactorily comply with them. Additionally, to assess refurbishment expenses of aged automotive batteries, it has to be checked how far existing regulations are influenced by the battery’s first life and the refurbishing process itself. As there are no specific regulations addressing the modification of already certified battery systems, a retesting procedure is not compulsorily prescribed even if e.g. a new SLB system is built partially from certified old and new but untested parts (like deploying old modules with a new BMS). Especially if integrated safety precautions of ALIB are modified in the refurbishing process, retesting is nevertheless useful in conclusion and a regulation regarding this should be added to existing

norms and standards. However, as there are no *reuse regulations* yet at present, assumptions are made hereafter.

Due to the nonexistence of relevant regulations, principally, no additional information must be provided which has not been already before in the new state. It must be assumed, though, that disposition to buy is small for customers being uninformed of relevant data like product age, residual capacity or power capability. In the following, as this thesis deals with the technology of LIB, respective legal regulations are analyzed and costs of single refurbishment steps are qualitatively assessed. Finally, major matters of expense are highlighted and recommended actions are provided.

Regarding the UN 38.3 transport standard which is a global prerequisite for road, rail, maritime and air transportation, unaffectedness by the operational ALIB prehistory and the refurbishing process is restrictedly assumed. This is based on the battery units not being altered regarding their safety precautions, but only be removed from their corresponding battery pack compounds. However, the UN 38.3.2.2 must especially be considered, as this passage prescribes retesting of battery units with a capacity fade of more than 20%. The individual tests (vibration, shock, overcharging, external short-circuiting, altitude simulation, etc.) of the transport standard are estimated to be very time-consuming and costly. Thus, battery units with 80% residual capacity are assumed to be just allowed for transportation without retesting. Additionally, as shown in [48], although LIC pass the respective vibrational tests of UN 38.3 without failure, long-term accumulated vibrational loads like in BEV, where vibration is a constant companion, may lead to spontaneous cell failure. With regard to stationary SLA, associated risks are presumably small but recheck of the UN 38.3 standard is suggested for mobile SLA like the deployment of SLB in forklift trucks.

The directive of electromagnetic compatibility 2014/30/EU is assumed to stay unaffected of battery prehistory and refurbishment. In contrast to that, quotation of the nominal capacity of LIB (mandatory in accordance to § 17 BattG, DIN EN 61960 and the European directive 1103/2010) is recommended for SLB to be renewed during/after refurbishment. Besides of discussed legal regulations, there is a variety of voluntary quality standards which mainly recommend methodologies of measuring characteristic values of LIB like actual capacity, power capability or aging behavior like DIN EN 62660-1/2, ISO 12405-1 DIS and ISO 12405-2 WD. [14]

Main aim of effective refurbishing process implementation is to separate those steps of quality assurance which are inevitable, from those, which can be cancelled or at least be operated with little effort (compared with standards in the new state of LIB). Reducing refurbishing costs directly leads to increased residual values of aged ALIB. The single steps of the exemplary refurbishing process which is shown in Figure 4 are critically discussed hereafter. Additionally, reduction potentials are highlighted. It has to be considered, though, that the illustrated refurbishment process is just an example, as there is, principally, a variety of constellations

which in turn strongly depend on the underlying battery ownership structure. The following assessment of reduction potentials of single refurbishing steps was worked out by the authors of [14] in cooperation with a study related advisory board.

In terms of the take-back obligation of the car manufacturer, removal costs of the aged ALIB are already included by default in the BEV sales price. Associated costs are regarded as low. As the pack disassembly is limited at the module level in the field, related costs are also likewise low. The disassembly process can even be avoided by in complete connection of refurbished ALIB in large-scale battery energy storage systems. Disassembly up to the cell level is regarded to be economically infeasible, as the breakup of single cells' soldered joints or welding spots is extremely costly. However, also for large LIC which are only bolted, economic feasibility is questionable but must be ad hoc evaluated in the field.

In the next process step, battery units are optically inspected for failures like leaking spots, burn marks or an accident inflicted loss of physical integrity. In accordance to the UN 38.3 standard, transport is prohibited for units which exhibit optically detectable failures. Thus, respective units are excluded from the further selection process. By serial number and relevant BMS data retrieval (like error logs, load profile logs and aging dependent state variables), additional units might be excluded in advance to the costly characterization process and directly given to the recycling facility. Ideally, no further battery unit classification based on costly measurements is needed after retrieval of aging dependent BMS state variables. A comprehensive review of theoretically available SoH estimation methodologies is given in [49]. A further promising approach, which even takes cell-to-cell variation into account, is given in [50]. However, broadly distributed in the field implementation of such cost-efficient approaches is currently not yet state-of-the-art. Optical failure inspection, serial number based aging detection and BMS data retrieval is altogether regarded as a cost-effective battery unit pre-selection process. Related costs are regarded as minimal.

Next, pre-selected battery units are packaged by the car manufacturer or a third party (like a scrap merchant) and brought by a carrier to the respective service provider (exemplary case). There, measurement based classification finally decides which battery units are suitable for reuse or alternatively recycled. Generally, used but functional batteries must comply, in accordance with the packaging instruction P903 (see ADR 2015), with the same terms of transport like new batteries [51]. Merely for batteries with optically observable failures, there are special directives but respective units have already been sorted out in advance with regard to the process which is illustrated in Figure 4. In accordance to P903, following package properties or arrangements must be ensured [51]:

- robustness of outer packaging
- existence of protective enclosures (like in fully enclosed or wooden slatted crates)
- fastening on pallets or distinct handling precautions

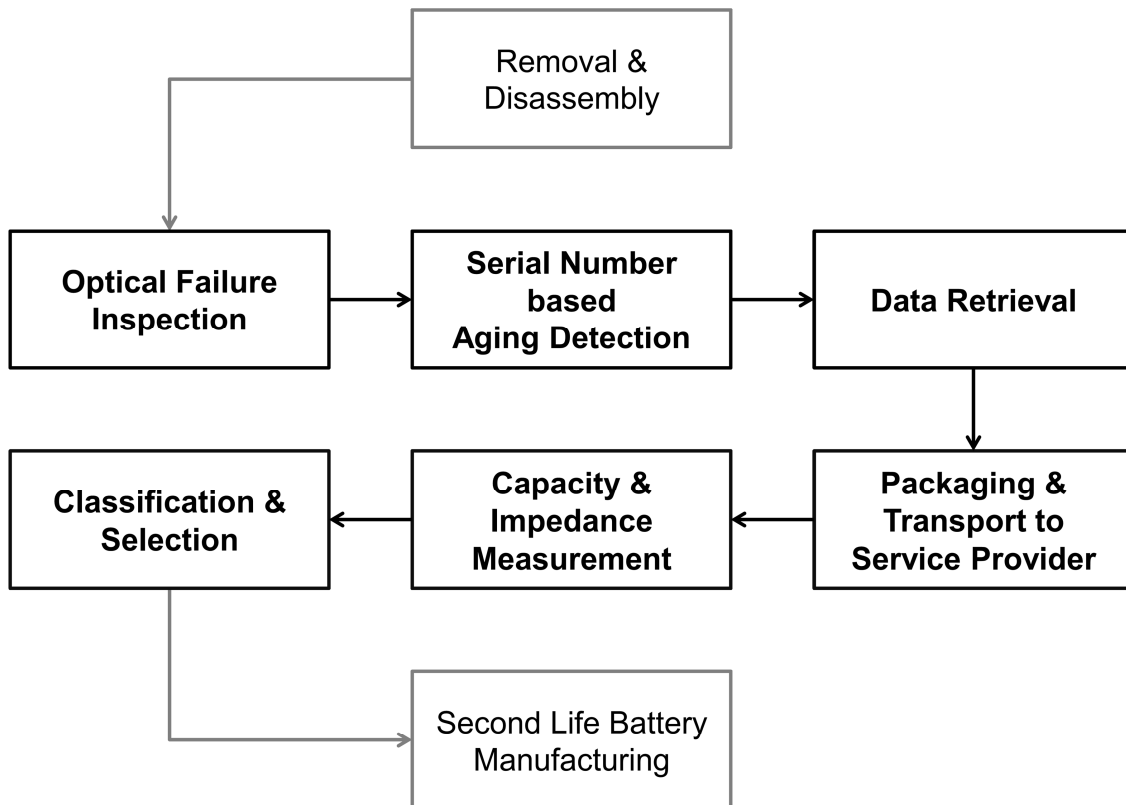


Figure 4: Flow chart of an exemplary refurbishing process of aged automotive batteries with a closer examination of the contained battery unit characterization and selection process. Based on [14].

Battery units must especially be secured against unintentional movement. Furthermore, direct loading on top of the units, imposed by other freight material, is prohibited. In complete, packaging and transport costs are assessed as moderate or even high. However, as new LIB and SLB must be packaged and transported to their place of action in the same fashion, no additional costs emerge in the SLC for the final transport to the end user. In contrast to that, for each interposed transport process, like in Figure 4 from the car manufacturer to a not in-house service provider (where battery unit selection and SLB manufacturing is performed), additional costs emerge which directly reduce the residual value of aged ALIB. So, recommended action is that the car manufacturer takes over measurement based battery unit selection and SLB manufacturing to avoid additional packaging and transport processes. Alternatively, an in-house service provider can be commissioned.

To finally decide whether a battery unit should be reused or immediately recycled, the SoH must be measured which is defined by its actual power capability or residual capacity referred to a reference value. In general, methodologies of measuring characteristic battery parameters like capacity, power capability or aging behavior are e.g. recommended in DIN EN 62660-1/2, ISO 12405-1 DIS and ISO 12405-2 WD. Regarding an energy-optimized application like BEV, the

SoH is ordinarily quantified by the ratio of the actual referred to the nominal or the initial capacity [52, 53], as per:

$$\text{SoH} = C_{\text{act}} / C_0 \quad (1)$$

Thereby, C_0 and C_{act} are the capacity in the new and the actual state, respectively. The term “aging rate” is henceforth used in this thesis to approx. give an idea of the rate of the aging progress and could be defined as:

$$\alpha_C = \Delta C_{\text{act}} / \Delta t \quad (2)$$

However, whereas the reference to time is useful to characterize calendric aging, for cyclic aging also reference to the charge throughput or number of cycles is conceivable. In addition, depending on the context, the parameter capacity can also be replaced by impedance parts.

In any case, with regard to time effort and required machinery, conventional capacity measurement techniques are costly [54]. For example, capacity determination according to standards or manufacturer guidelines usually requires at least a complete charge and discharge cycle with a current rate equal or less than 1.0 C [55]. In DIN EN 62660-1, capacity measurement is even recommended to be performed with a current rate of 1/3 C (resulting in approximately 6 h per full cycle and battery unit). Additionally, as the performance of LIB strongly depends on the temperature, preconditioning waiting periods must be precisely kept. So, a quick and easy SoH test, without the need of costly machinery, might be of great use and could especially improve the economic feasibility of reusing aged ALIB by reducing costs of refurbishment.

To assess the actual power capability of a battery unit, the impedance can be determined either in the frequency or in the time domain [56, 57]. Regarding the applicableness for SoH quick tests, the *raised impedance part must be independent of the state of charge (SoC)*, which is defined as follows [14]:

$$\text{SoC}(t) = \frac{1}{C_{\text{act}}} \cdot \int_{t=t_0}^{t_1} I(\tau) d\tau \quad (3)$$

Equation (3) basically describes the methodology of Ah-counting in which the actually stored amount of charge is referred to C_{act} . In any case, a prior adjustment of the SoC would be as time-consuming as capacity measurement itself; thus, in a SoH quick test, this is not a viable option. As an alternative to the required SoC independency of the raised impedance part, a SoC correction function could be implemented.

In the frequency domain, for LIC made of different active materials, the complex impedance value at which the imaginary part is zero, i.e., the ohmic resistance (in this thesis denoted as R_{zc} , see Subchapter 5.1), can approximately be regarded as independent of the SoC [54, 58, 59]. Figure 5 depicts the R_{zc} (normalized to the respective value at a SoC = 100%) versus the full SoC range for LIC models of different manufacturers. As is observable, the assumption of the

R_{zc} to be independent of the SoC is justified with one exception; for the IHR18650A by E-One Moli Energy Corp. (with $R_{zc} = 66.59 \text{ m}\Omega$ at a SoC = 100%), a SoC correction function is required (in this thesis, though, statistical analysis is anyway based on data with adjusted SoC). The clear SoC dependency is possibly linked to characteristics of the contained electrolyte components but this must further be investigated. The R_{zc} values at a SoC = 100% of the Panasonic NCR18650PD, the A123 APR18650m1A, the Sony US18650VT1 and the Sanyo UR18650E are $23.70 \text{ m}\Omega$, $17.54 \text{ m}\Omega$, $29.67 \text{ m}\Omega$ and $32.88 \text{ m}\Omega$, respectively. The presented data sets have been recorded by Peter Keil and Martin Brand (and/or by students under their supervision) at the Institute for Electrical Energy Storage Technology of the Technical University of Munich.

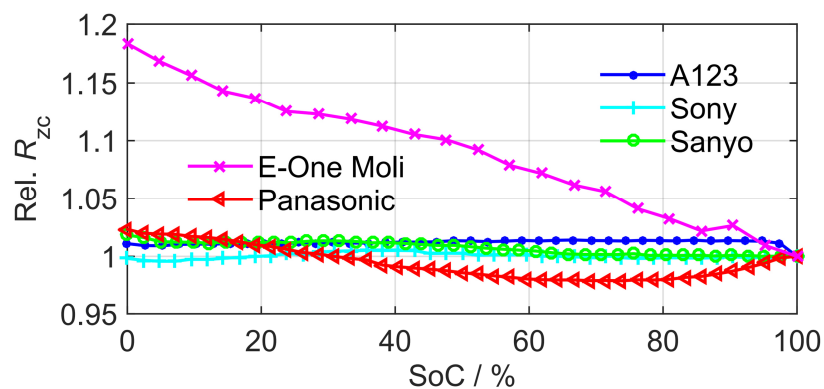


Figure 5: Dependency of the impedance part R_{zc} of the state of charge for lithium-ion cell models of different manufacturers; data sets are normalized to the respective value at a state of charge of 100%.

This part of impedance is also quickly to measure because of its occurrence at high frequencies in the magnitude of 1 kHz, as reported in [57] for LIC comprising graphite on the negative and lithium-nickel-manganese-cobalt-oxide (NMC) on the positive electrode. In addition to the independency of the SoC (for the majority of LIC models) and the quick measurability, another advantage of the R_{zc} is its negligibly dependency of the operational prehistory (impedance parts at lower frequencies are well known to be affected from relaxation processes for up to 40 h after operation) [60]. Besides, with regard to the high temperature sensitivity of the impedance of a LIC, precise temperature preconditioning is of major importance.

In terms of acceleration possibilities of SoH detection (and thus increasing cost-efficiency), approaches of reasoning the actual capacity from the corresponding impedance value were e.g. recommended in [54] and [61] to be auspicious. Main idea is to calculate a functional dependency for the variables capacity and impedance, e.g. by simple linear regression. Therefore required value pairs must be collected in advance within a laboratory aging experiment. If functional dependencies are known and so, correlation behavior is described mathematically, the residual capacity of a battery unit can quickly be calculated by inserting the

respective impedance value in the detected equation (like $C_{act} = C_y + a \cdot R_{zc}$, with the axis intercept C_y and the slope a). However, as regression curves presented in [54] and [61] were only parameterized with data from one single type of load (and due to the absence of further investigations), correlation behavior must yet be analyzed and assessed for distinct types of load (different storage and operational conditions). In any case, such a SoH quick test must be universally applicable as e.g. load profiles and ambient conditions of BEV strongly differ. So, independency of storage and operational conditions is needed for successful implementation. If this is reachable, costs of refurbishment could considerably be reduced. Possible causes of interaction of capacity fade and impedance increase, i.e., reference to the underlying aging mechanisms, is presented in Subchapter 3.2. Required statistical methods are explained in Chapter 4. Finally, the results of the correlation analysis are presented in Chapter 8.

After the respective battery units have been measured, final decision can be made with the options of either recycling or reuse. Then, battery units with similar characteristics are classified and can finally be selected for the manufacturing of proper SLB. To deploy SLB in a manner which takes into account their pre-aged state, and thus to optimize the second service life, understanding of the aging behavior and mechanisms of LIC is of major importance. Therefore, fundamentals of LIC aging (behavior, mechanisms) are comprehensively described and discussed in the next chapter.

3 Fundamentals of Lithium-Ion Cell Aging

Regarding the aim of an economic SLC implementation, profound understanding and predictability of the aging behavior of LIB are a prerequisite to assess overall system costs and economic benefit. Thus, the ability of assessing the aging behavior to expect within the project period is directly linked with the decision to invest. The fundamentals of LIC aging which are needed for such challenging lifetime projections are presented in this chapter.

Basically, the aging behavior of a LIC consists of a calendric and a cyclic component, i.e., *calendric and cyclic aging*. For a BEV, exemplarily, this means that even in inactive periods, when the vehicle is parked, the ALIB suffers from calendric aging. In addition to that, cyclic aging is caused by the driving operation and the charging process [43, 62]. Especially the latter is said to remarkably influence the aging behavior. Consequences of aging are, generally, a loss of capacity and power capability with the latter originating from an increase of impedance.

For both kinds of aging, there are certain *stress factors* which affect the respective aging rate: calendric aging is mainly influenced by the storage SoC and temperature; cyclic aging by the current rate, the cycle depth, and the mean SoC and temperature. As the latter two basically correspond with the stress factors of calendric aging, simple (equivalent circuit based) aging models split a charging or discharging event in a cyclic and a calendric component. Regarding laboratory aging experiments, such a *superposition principle* enables a reduction of experiments' complexity [63]. By that, the need of measurement equipment can effectively be reduced. Figure 6 schematically assigns the described stress factors to corresponding kinds of aging, besides of giving a hint of the aforementioned superposition principle.

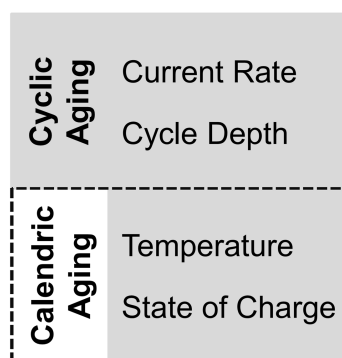


Figure 6: Main stress factors of cyclic and calendric aging with hinted superposition principle.

It must be considered, though, that for a cyclic event, mean values of temperature and SoC are raised in such models: due to the polarization of cells, their temperature is increased during

current load which is why the temperature of cells must be averaged; for the SoC, the mean value of the upper and lower bound SoC of a *half cycle event* (charging, discharging) is usually used [63].

Regarding the stress factors of *pure cyclic aging*, basically, an increase of current rate (especially for charging) and cycle depth leads to enhanced aging for all common models of LIC [64-66]. The basic idea of SLC is based on that relationship as the reuse of an aged automotive battery in a SLA normally should come along with a reduction of current rate and cycle depth (for SLA with deep cycles like photovoltaic interim home storage, oversizing is conceivable) [14]. However, for the stress factors of calendric aging, relationships vary for LIC models comprising (graphite anodes but) differently structured cathode materials: whereas the aging rate is basically increased with increasing SoC for cathodes with a layered (like NMC) or olivine (like lithium-iron-phosphate (LFP)) structure, the relationship is more complex for spinel cathodes (like lithium-manganese-spinel (LMO)) [67, 68]. In addition, it was recently shown in [69] that for cells with graphite anodes and cathodes with a layered or olivine structure, the aging rate is not continuously increased with increasing SoC, but is characterized by the occurrence of plateaus and stages which directly arise from the staging phenomenon of graphite anodes.

Considering the relationship of aging rate and temperature, trends are equal for distinct LIC models. However, it must be distinguished from calendric and cyclic aging: for stored cells, a reduction of temperature leads to reduced aging; for cells in operation, there is an optimal operation temperature around 25 °C with increased aging at lower and higher temperatures [70]. Reasons for the existence of such an optimal operation temperature are described in the next subchapter. Anyway, as all experiments, which are presented in this thesis, have been conducted with a classic LIC model with layered transition metal oxide cathode (NMC) and graphite anode, the relationship between stress factors and aging rate is comparably simple: the calendric aging rate is increased with increasing SoC and temperature; the cyclic aging rate with increased current rate, cycle depth, mean SoC and temperatures which deviate from the aforementioned operating temperature optimum.

In Subchapter 3.1, relevant aging mechanisms of LIC are concisely summarized. At this, statements and findings are mainly based on studies presented in the literature which deal with LIC models with graphite anodes and layered structure type cathodes (especially NMC). Thus, the review of aging mechanisms is basically valid for the variety of LIC with layered metal oxide cathodes (like NMC, lithium-nickel-cobalt-aluminum-oxide (NCA), lithium-cobalt-oxide (LCO), etc.). In Subchapter 3.2, an explanation for the interaction of capacity fade and impedance increase is given, which is regarded as the theoretical background for the later presented SoH quick test approach. Afterwards, assumptions and hypotheses with regard to the cause of nonlinear aging characteristics are comprehensively described in Subchapter 3.3. Based on the lessons learned in this and the prior chapter, the end of life criteria of SLC (Eo1L, Eo2L) are

critically analyzed again and discussed in Subchapter 3.4. Finally, in Subchapter 3.5, different causes of a rising cell-to-cell variation (in a multi-cell battery application) with the progress of aging are given.

3.1 Review of Aging Mechanisms

As already mentioned before, all types of LIC suffer from calendric and cyclic aging. Basically, consequences of aging are a loss of capacity and power capability (as impedance increase results in higher overpotentials). The reasons for aging can generally be divided into three groups, which are, namely, the loss of active materials, the loss of usable lithium and a deterioration of ionic kinetics [71]. The latter mainly originates from passive layer growth, which in turn is a result of electrolyte decomposition. To understand the aging of LIC is rather complex in terms of the quantity of distinct but partially interacting aging mechanisms. Because of that, in the following, a terse and concise review of most relevant aging mechanisms, as well as their dependencies and interactions, is given.

The formation and evolution of passive layers in the electrode-electrolyte interfaces take on a key role in the aging of LIC [72]. Usually, the layer at the anode is referred to as the solid electrolyte interphase (SEI) and the one at the cathode as solid permeable interphase (SPI). Whereas the SEI strongly suppresses electrolyte reduction at the anode after formation (so called *formation cycle*, further information in [72]), unimpeded electrolyte oxidation continuously takes place in the cathodic interface due to the SPI's eponymous characteristic of being only slightly passivating [73-75]. As far as is known, both passive layers are usually in the magnitude of several nm [68]. In general, electrolyte decomposition (by reduction at the anode and oxidation at the cathode) leads to an increase of the ohmic resistance. Both layers tend to grow at high temperatures and SoC (due to increased electrolyte decomposition). Furthermore, the layers can break due to volumetric changes of active materials caused by insertion and extraction of lithium cations (explanation follows shortly) [76-78]. Destruction of the protective layers results in automatic reconstruction due to the electrodes' restored exposition to the electrolyte and thus, new onset of electrolyte decomposition. In contrast to that, under permanent extreme conditions like at high SoC and temperature, the passive layers are even said to be capable of isolating active material by growing into its porous structure or clogging the separator's pores [68].

As the formation, thickening and reconstruction of both passive layers occur under the consumption of active lithium, the occurrence of these processes directly correlates with capacity loss. Besides, as the layers must be regarded as obstacles through which the lithium cations have to penetrate (when inserted into or extracted from the electrodes), there is also a link to increased impedance [76, 77, 79-81]. As an intermediate result, the importance of passive layers regarding the aging behavior of LIC is based on their unavoidable existence due to

protective (but also adverse) effects, and a strong interaction with several aging mechanisms (which are described in the following). More in-detail knowledge regarding both passive layers is presented afterwards in Subchapter 3.2.

At the cathode, a high delithiation degree (or high cell SoC), such as $x < 0.35$ or $x < 0.5$ for $\text{Li}_x\text{Ni}_{1/3}\text{Mn}_{1/3}\text{Co}_{1/3}\text{O}_2$ or Li_xCoO_2 , respectively, may result in irreversible structural changes [67, 79, 83]. By these, the altered area at the surface of the cathodic active material exhibits so called *rock-salt structure* with the result of capacity fade and impedance increase. The occurrence of that structure can be explained as follows: if a LIC is charged, lithium cations move to the anode, whereas simultaneously, electrons are released in the external electric circuit. With an increase of the SoC, vacancies in the lithium layers of the cathode active material are enhanced as well. Thereby, repulsion forces between encompassing transition metal layers rise due to the missing virtue of compensation. Due to similar ionic radii, 0.76 \AA for Li^+ and 0.67 \AA for Ni^{2+} , the latter tend to migrate to the lithium layers and compensate the repulsion forces between transition metal layers by filling these vacancies irreversibly [84]. The imagination of unaltered active material to be covered by, at first, a layer of rock salt structure, and second, on top of it, a layer of the before described SPI, is regularly denoted as *core-shell structure model* [84, 85]. Figure 7 shows the superficial composition of cathode active material with adhesive layers of rock-salt structure and SPI. For clarification, insets schematically illustrate the layered atomic structure of unaltered cathode active material as well as of an affected area with rock-salt structure.

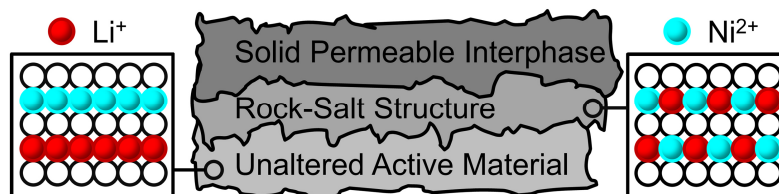


Figure 7: Superficial composition of cathode active material with an adhesive layer of rock-salt structure and solid permeable interphase. Based on [68] and [84].

As a consequence of the occurrence of rock-salt structure, cathodic oxygen release is enhanced leading to promotion of electrolyte oxidation which in turn thickens the SPI [68]. Both adhesive layers in common, i.e., rock-salt structure and SPI, are often referred to as the reason for the cathode to exhibit the main portion of charge transfer resistance of a LIC [73, 86, 87]. In addition, with an increased amount of oxygen vacancies, metal dissolution of the cathode active material is fostered. The thereby emerging oxidation products are reported to migrate to the anode where they are reduced to metals again. These in turn catalyze the SEI growth by forming electron conducting tunnel paths [79, 88]. Partially, the products also clog the pores of the separator on their way of migration, which leads to increased ohmic resistance [68]. For NMC cells, the most of the oxidation products detected at the anode is manganese, but there

are also traces of nickel and cobalt; proposed dissolution mechanisms are a Mn^{3+} disproportionation reaction or an acid corrosion (which occurs due to the presence of moisture traces in the electrolyte) [67, 89]. Whereas the anode material is principally not damaged by these deposits, a deterioration of ionic kinetics takes place [90-94]. Besides, in [66], it is mentioned for anodes of cells, which have been continuously charged to a high upper boundary SoC, to be more contaminated with oxidation products than cells stored at that SoC. Thus, cell operation (with a high upper boundary SoC) maybe eases cathodic metal dissolution and oxidation product migration.

As aforementioned, aging can be inflicted by volumetric changes of active materials during intercalation or deintercalation processes. When lithium cations are inserted into or extracted from active material, the concomitant volumetric change, approx. 10.2% for graphite anodes [95, 96] and 2.4% for NMC transition metal layer cathodes [96, 97], can lead to a loss of particles' bonds due to micro cracks or a loss of the contact of particles to the current collector. Electrically unconnected clusters of active material (anode or cathode), as is shown in Figure 8, or clusters with highly increased contact resistances, cannot be used anymore and thus, electrode capacity is reduced. Due to higher volumetric changes, graphite anodes are generally more prone to associated detrimental effects than most common cathode materials.

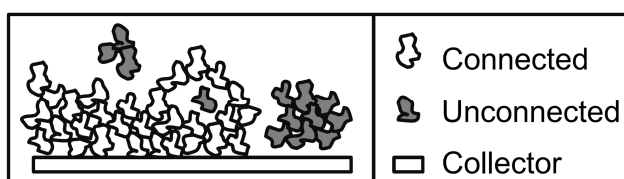


Figure 8: Current collector and electrode active material with partially unconnected clusters.

It is assumed for graphite that especially the crossing of phase transitions results in erratic volumetric changes, indicating that also small cycle depths which cross a potential of phase transitions may lead to severe aging effects [65, 98]. As the relative variation of graphite's lattice parameters is increased at two-phase reactions between different stages at the almost delithiated state, sliding and buckling of graphite planes must especially be considered when LIC are discharged to low SoC [95, 99]. Such an irreversible structural disordering in the lattice of graphite leads to active material loss and thus, capacity reduction of the anode. When the binding agent, typically polyvinylidene difluoride (PVDF), is decomposed, active materials may expand permanently which facilitates a contact loss of particle to particle or collector [75, 86]. As a consequence, active material may be isolated resulting in a loss of the electrode's capacity. Besides, passive layers may help to compensate volumetric changes but further capacity loss occurs if the layers break and need to be reconstructed [66, 77].

At a high SoC, the potential of graphite anodes can come close to the critical value of 0 V vs. Li/Li⁺. Low temperatures generally lead to a higher polarization due to slower diffusion processes and a hampered charge transfer [100, 101]. Thus, when charging LIC at low temperatures with high currents, the graphite potential may drop below 0 V vs. Li/Li⁺ [102]. In addition, as the cathodic compared with the anodic overpotentials increase more slowly with decreasing temperature, limitation of the charging end voltage at the cell level cannot reliably prevent lithium plating. As a consequence of negative potentials vs. Li/Li⁺ at the graphite anode, lithium cannot be intercalated and is plated between graphite active material and SEI. The thickness of such a metallic lithium layer could be determined in [103] for a C//LFP cell with structural 26650 shape and 2.5 Ah nominal capacity to be approx. 5 μm. For a C//NMC pouch type cell with a nominal capacity of 20 Ah, a relationship of 16 μm per plated Ah (regardless of the number of electrode layers) could be derived in [104]. In any case, plated lithium layers in the magnitude of several μm can impose serious mechanical stress onto respective cell components (like the jelly roll) as metallic lithium at the anode takes up more space than when intercalated into graphite [104, 105]. Additionally, in case of a thermal runaway of LIC, plated lithium is reported to increase heat formation and thus, safety is considerably reduced [105].

Lithium plating is a reversible process as long as the plated lithium exhibits a conductive connection to the graphite active material [106-108]. In that case, there are basically two different possibilities of the so called *stripping of plated lithium*:

- dissolution in a subsequent discharge process
- electrochemical intercalation into graphite during cell relaxation

Dissolution of conductively connected parts of plated lithium in the subsequent discharge process starts before deintercalation of intercalated lithium as the oxidation potential of plated lithium is approx. 100 mV higher than the deintercalation potential [109, 110]. Therefore, at the beginning of the discharge process, plated lithium is removed at first which is apparent from a specific voltage plateau [111]. As long as the reversibly plated lithium layer is dissolved during discharge and thus, the voltage plateau is visible, the ratio of LiC₆ and LiC₁₂ is reported to stay constant [112]. Principally, the mentioned voltage plateau is a promising candidate for the challenging in-operando detection of lithium plating. However, with sufficient precision, it is only observable for small discharge currents at very low temperatures around -20 °C (due to slowed kinetics) and thus, practical implementation is critical [102].

During cell relaxation, subsequent to a charging process which caused lithium plating, reversibly plated lithium is electrochemically intercalated into graphite. Thereby, the ratio of LiC₆ is observed to increase, while the one of LiC₁₂ decreases [112]. In correspondence to the dissolution of plated lithium in a subsequent discharge process, a voltage plateau emerges during cell relaxation which can be explained as follows: at the end of the charging process, i.e., when the cell current is set zero, the negative anode potential vs. Li/Li⁺ (for which plating occurs)

immediately starts to exponentially converge to positive values vs. Li/Li^+ due to the fade of different overpotentials. However, as soon as the critical value of 0 V vs. Li/Li^+ is passed, reversibly plated lithium can start to electrochemically intercalate into graphite and thus, further reduction of overpotentials is hindered [102]. With regard to the duration of the voltage plateau of approx. 10 min (at a temperature of 23 °C), especially the fade of the diffusion overpotential might be seriously impeded [102]. Only when the reversibly plated lithium is *de-plated* by electrochemical intercalation, remaining overpotentials can continue to fade in a common manner. With respect to the implementation of an in-operando detection method for the reversible part of lithium plating, analysis of the voltage plateau upon cell relaxation is regarded as a viable approach without the problem of peak flattening due to the current load [113].

Despite of presented stripping possibilities of reversibly plated lithium, plating is often associated with a severe irreversible loss of lithium and thus, also reduction of cell capacity [68, 79, 108]. The occurrence of irreversible lithium plating is partially related to the *dendritic or mossy* nature of lithium growth [114]. Whereas high charging rates were found to lead to the formation of many small lithium dendrites, small currents provoke the forming of less but larger ones [115]. In any case, the conductive connection of plated lithium to graphite can get lost with respect to two different processes:

- lithium dendrite contact loss during cell relaxation
- additional SEI formation due to the contact of plated lithium with electrolyte

During cell relaxation, the single dendrites of the mossy lithium layer are reported to be prone to break and thus, lose their electrical contact to the graphite active material (internal lithium isolation). Furthermore, the SEI might get damaged with respect to the aforementioned mechanic expansion due to the plated lithium layer formation (micro cracking) or, alternatively, large dendrites directly come into contact with electrolyte after SEI puncturing (external lithium isolation) [111, 112, 116]. If an area of the SEI is destroyed with the result of graphite active material or plated lithium being exposed to the electrolyte, a new onset of electrolyte decomposition leads to new SEI formation. For dendrites which come in contact with electrolyte after SEI puncturing, reactions are just similar with the effect of respective external lithium isolation. Anyway, these different processes lead to irreversible loss of lithium and thus, reduction of cell capacity. For clarification, the described processes and associated effects on the SEI are schematically illustrated in Figure 9.

Advanced charging strategies like boost charging, i.e., using a high charging rate only at the beginning of the charging process and reducing it at a SoC \approx 70%, are a possibility to reduce the risk of lithium plating to occur [117, 118]. Furthermore, an oversized anode (referred to the cathode) or additives to improve the anode conductivity (and thus reducing overpotentials) like carbon black are effective to avoid lithium plating [76]. In contrast, electrolyte additives which are

commonly used to stabilize the growth of the SEI (like ethylene or vinylene carbonate) provoke plating due to their characteristic of increasing impedance with decreasing temperature [119].

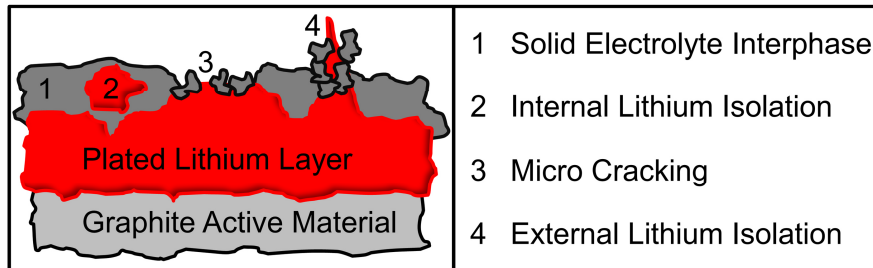


Figure 9: Graphite active material with a plated lithium layer and associated effects on the solid electrolyte interphase. Based on [68].

Besides of the variety of presented aging mechanisms of LIC, which is regarded as a required fundament of this thesis, there are further mechanisms like e.g. binder electrolyte soaking or decomposition, current collector corrosion and separator brittleness [120-122]. As an in-detail description of all known LIC aging mechanisms would go beyond the scope of this thesis, further literature is given for self-contained consultation [67, 68, 123].

3.2 Interaction of Capacity Fade and Impedance Increase

With the presented most relevant aging mechanisms as a base, in this subchapter, the reasons for interaction of capacity fade and impedance increase are explained. This interaction can be regarded as the theoretical background of the later described SoH quick test approach which is on the basis of correlation between capacity and impedance of LIC during the progress of calendric and cyclic aging.

As aforementioned, the formation, evolution and reconstruction of both passive layers, i.e., the SEI at the anode and the SPI at the cathode, take on a key role in the aging of LIC. Due to the consumption of active lithium during layer formation or growth, these processes directly correlate with cell capacity fade. Cell impedance is also increased as the layers can be imagined as obstacles for lithium cations – so, in simple terms, the thicker the passive layers the harder is it for the lithium cations to penetrate through. In addition, highly resistive passive layer compounds like LiF are known to be formed in special situations like excess temperatures or the presence of moisture traces (which both provoke decomposition of the commonly used conductive salt LiPF_6) [79, 124].

The importance of the passive layers is especially emphasized by their strong interplay with a variety of aging mechanisms: lithium plating, for example, results in additional SEI formation if plated lithium comes in contact with electrolyte (due to SEI micro cracks or puncturing);

regarding the volumetric changes of active materials during intercalation and deintercalation processes, effects are just similar with automatic reconstruction of passive layers as a consequence of their destruction. In the case of irreversible structural changes of the cathode active material, on the one hand, oxygen release is increased which leads to electrolyte oxidation and thus, thickening of the SPI; on the other hand, by the increased amount of oxygen vacancies, cathodic metal dissolution is fostered which provokes the migration of oxidation products to the SEI which in turn grows as a result of it. To suppress the causal electron conducting tunnel path effect, vinylene carbonate as electrolyte additive is known to be efficient [125]; however, by the same, the occurrence of lithium plating is favored due to the associated impedance increase especially at low temperatures [119].

As a conclusion, various aging mechanisms lead either to a growth of passive layers or a required reconstruction after their destruction. Because of that, the layers have a *central meaning regarding the aging behavior* of LIC. Their evolution is especially associated both with capacity fade and impedance increase which is why the following hypothesis is constructed:

Due to the central meaning of the evolution of the two passive layers, which is associated with continuous capacity fade and impedance increase, there is a causative negative correlation between capacity and impedance during calendar and cycle life of a lithium-ion cell.

In the literature, correlation between capacity fade and impedance increase is reported for graphite based LIC with a variety of cathode chemistries such as LCO [54], NMC [63] or LFP [98]. In contrast to that, the authors of [126] report on aged C//LMO cells with highly increased impedance but low capacity fade and the other way round, i.e., without a correlating development. Ambiguous results are also reported in [127] for C//NMC cells. However, these findings should not be solely transferred to employed cell chemistries, but could also originate from distinct types of passive layer evolution depending on the operational conditions as a result of their multilayered structure. For example, both passive layers generally exhibit a layer of mainly inorganic lithium salts close to the electrode active material (anode or cathode), and a layer of mainly organic salts near the electrolyte [77]. So, effects on capacity and impedance could vary for calendric and cyclic aging as the first may only lead to a thickening of the organic salt layer close to the electrolyte but the second necessitate complete reconstruction. As a result, capacity and impedance development could correlate for calendric and cyclic aging, but impedance increase for the same capacity fade would differ for the two kinds of aging. In the following, due to the assumed link of the multilayered structure of passive layers and the correlation between capacity fade and impedance increase, its single components are considered in more detail.

As aforementioned, in the direction from the electrode active material to the electrolyte, the passive layers exhibit a multilayered structure of inorganic lithium salts, organic salts and a mixture of semi and polycarbonates (SEI) or polymers and polycarbonates (SPI) [77]. For the

SEI, there is an additional layer of trapped gas molecules between the graphite active material and the layer of inorganic lithium salts. For clarification, the multilayered structure of the passive layers between electrode active material (anode or cathode) and electrolyte is illustrated in Figure 10. In addition, it is indicated that calendric aging might provoke only the growth of the single layers (organic salts etc.) close to the electrolyte, whereas cyclic aging is assumed to result in reconstruction likewise of all the single layers of the multilayered structure.

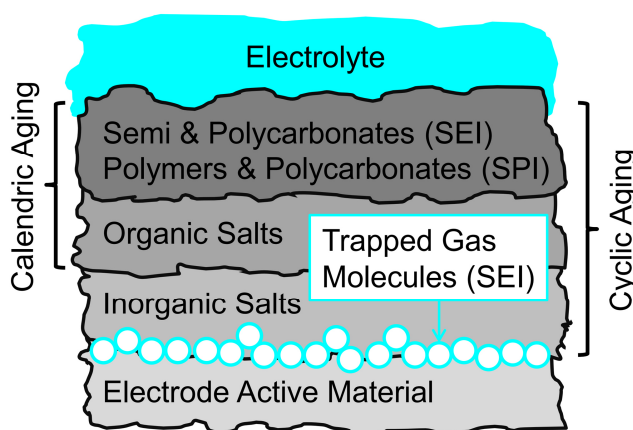


Figure 10: Multilayered structure of passive layers between electrode active material and electrolyte (based on [77]); thereby, calendric aging might only lead to a thickening of the single layers close to the electrolyte, cyclic aging provoke complete reconstruction.

In the beginning of SEI formation, solvent co-intercalation is an unavoidable process which results in gas evolution and, in extreme cases, graphite exfoliation due to the associated mechanical strain [68]. The bubble-like structure of trapped gas molecules (“blisters”) are known to partially grow even into the graphite surface area. Additives like ethylene or propylene sulfites reduce the occurrence of solvent co-intercalation in the beginning of SEI formation and thus, help to avoid graphite active material loss which can result from the mechanical strain due to gassing [128]. In the case of a maturely formed SEI, solvent co-intercalation and related processes are prevented by its feature of removing any adhesive solvent products from the lithium cations during the process of graphite intercalation (“solvent stripping”).

In general, both passive layers consist of lithium and electrolyte decomposition products. Because of that, the exact composition of the multilayered structure always depends on the used electrolyte. The inorganic lithium salts (and for the SEI, trapped gas molecules) are in the near of the electrode active material as these products emerge in a primary reaction (which is mainly the decomposition of the conductive salt LiPF_6). Regarding the inorganic salts, Li_2CO_3 is known to be the main component to protect from electrolyte decomposition [129]. In addition, compounds like LiF , Li_2O , LiCl or LiOH are commonly found. The layers of organic lithium salts

as well as of polycarbonates and polymers (SPI), or semi and polycarbonates (SEI), are more close to the electrolyte as these products emerge from a secondary reaction (which is mainly the decomposition of the solvent). Besides, at least for the SEI, it is known that these products are instable in direct contact with the anode active material. In the layer of organic salts, commonly, compounds like lithium alkyl carbonates or a variety of lithium alkoxides (e.g., ROCO_2Li , ROLi or HCOLi) are found [130-132].

As a summary assessment, the composition of the SEI and the SPI, as far as is known, is similar except for the trapped gas molecules at the anode, and polymers instead of semi carbonates at the cathode. However, their processes of formation and growth differ: the SEI is immediately formed in the formation cycle due to electrolyte reduction (and anode oxidation); after formation, the SEI strongly suppresses any further electrolyte reduction and thus, it grows comparably slow. The SPI is not formed immediately as the most of common cathode materials are within the electrochemical stability window of the electrolyte; instead, it is formed eventually with regard to released oxygen which in turn provokes electrolyte oxidation. The polymers in the SPI (which are not present in the SEI) are assumed to be created by that electrolyte decomposition reaction [133]. The significant difference of the SEI and the SPI is their different effectiveness towards the prevention of electrolyte decomposition: whereas the SEI prevents almost completely any further electrolyte reduction at the anode surface (if properly formed), at the cathode electrolyte interface, the SPI's eponymous characteristic of being only slightly passivating results in an unimpeded electrolyte oxidation throughout the service life of a LIC. To slow down this unavoidable reaction, cathode coatings like MgO , SiO_2 , AlF_3 , $\text{Ni}_3(\text{PO}_4)_2$, $\text{Co}_3(\text{PO}_4)_2$ or AlPO_4 can be incorporated [134].

As already described before, a link of the multilayered structure of passive layers and the correlation between capacity fade and impedance increase is assumed. As calendric aging is suspected to lead only to a thickening of the external layers (like the one of organic lithium salts), but cyclic aging to provoke complete reconstruction, if the respective passive layer is destroyed, the arising effects on capacity and impedance could differ.

Regarding the SEI for example, in resting periods, only the layer of organic lithium salts close to the electrolyte is assumed to grow as a consequence of electrolyte reduction; thereby, electrons tunnel from the graphite electrode through the multilayered structure of the SEI to reduce the electrolyte (accompanied by lithium cations to keep electrical neutrality). The resulting consumption of lithium cations ("lithium trapping") in the layer of organic lithium salts is mainly associated with capacity fade. Due to the porosity of the layer, impedance increase is thereby considered as rather low. However, as aforementioned, the SEI can be destroyed (e.g., due to volumetric changes of graphite or lithium plating) resulting in a direct exposure of the electrode to the electrolyte. If the electrolyte directly reacts e.g. with LiC_6 , lithium cations are trapped as well (which results in capacity fade) but predominantly, the resulting growth of the dense layer of

inorganic lithium salts is associated with impedance increase [77]. It has to be considered, though, that if a LIC is cycled, processes of calendric and cyclic aging typically emerge in superposition (see Figure 6) [63]. Furthermore, impedance increase may nevertheless be even more intense for calendric aging than for cyclic aging, as cathodic oxidation products which migrate to the negative electrode are known to catalyze the growth of the SEI by producing especially highly resistive compounds [67, 89].

In any case, correlation between capacity and impedance development is assumed for both kinds of aging, but, impedance increase for the same capacity fade could disagree (for an assumed linear relationship, gradients would differ). Due to the little information in the literature on the correlation behavior between capacity and impedance of LIC during calendar and cycle life, an in-detail analysis of it, accompanied by an assessment if it is suitable as a base for SoH quick tests, is presented in Chapter 8. In the following subchapter, the causes of the so called nonlinear aging behavior, i.e., the effect of a sudden increase of the aging rate at deep residual capacities, are comprehensively explained.

3.3 Causes of Nonlinear Aging

Most calendric aging studies of LIC reveal a capacity fade with a square root dependency on time [52, 62, 65, 94, 132]. Thereby, the related temperature influence is usually modeled by the Arrhenius law [135]. The capacity under load is commonly reported to fade nearly linear with the charge throughput [63, 65, 94, 136]. In rejection of these well-known dependencies, an enhanced aging rate upon prolonged cycling (at deep residual capacities) is observed in a few studies for distinct types of LIC. This phenomenon, entitled in the following as *nonlinear aging*, is assessed as severely challenging regarding a successful implementation of SLC due to the imposed problems of predicting the aging behavior in a SLA.

Nonlinear aging is e.g. observed for LIC with NCA [137], NMC [65, 88], LFP [98, 103, 138, 139] or NMC-LMO blend cathodes [66], and, for all in common, graphite anodes. Thus, the assumption may be indicated that the relevant aging mechanism to provoke nonlinear aging takes place at the anode – and in particular, at the graphite anode, as no study yet observed the effect for a cell with a different type of anode. However, although there are several studies which observed the phenomenon of nonlinear aging, only a few explicitly address and investigate its origins [79, 98, 103, 138, 139]. In this subchapter, the causes of nonlinear aging, i.e., the relevant mechanism(s) which provoke the effect, are comprehensively described, and, based on that, dependencies and mitigation possibilities by load adaption are derived. These are evaluated later in Chapter 6.

Figure 11 a) clarifies the appearance of nonlinear aging upon prolonged cycling by showing a capacity development versus equivalent full cycles (EFC) of the C//NMC cell which has been used in all experiments of this work (IHR18650A by E-One Moli Energy Corp., specifications are

given in Chapter 5). The load profile of the presented test case consisted of constant current (CC) charging with 0.5 C to a charging end voltage of 4.2 V, a break of 20 min between half cycles and CC discharging with 1.0 C to a discharging end voltage of 3.0 V. The ambient temperature was 35 °C. Until a residual capacity of approx. 80%, the assumption of the capacity fade to be linearly depending on the charge throughput (or EFC) seems to be justified if first data points are neglected. The slightly enhanced aging rate at the beginning of cycling could be related to a closing formation of passive layers [141]. In the literature, the turning point from linear to nonlinear aging is also observed at residual capacities of approx. 80% or increased ohmic resistances of approx. 150% [65, 137]. By comparing the aging rate before ($\alpha_C \approx 2.4\%$ per 100 EFC) and after ($\alpha_C \approx 17.2\%$ per 100 EFC) the occurrence of nonlinear aging for the capacity development in Figure 11 a), an increase by factor seven can be estimated.

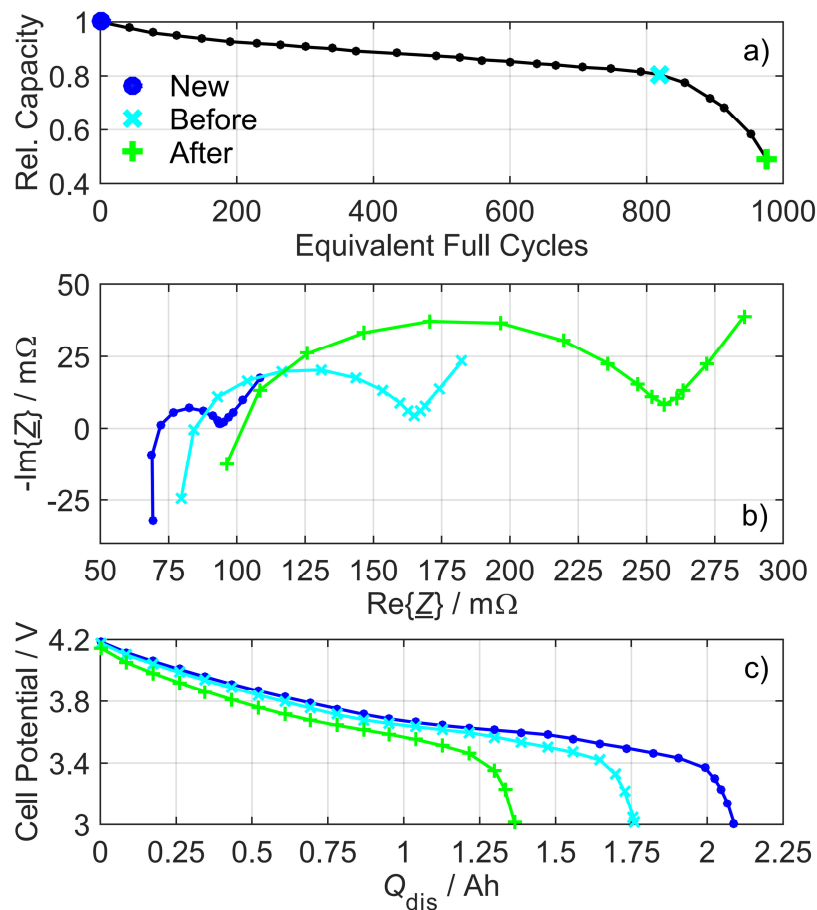


Figure 11: a) Development of the relative capacity versus equivalent full cycles; b) Nyquist plots of the impedance and c) slow discharge curves referring to the three spots in a): new cell (blue), directly before (cyan) and after (green) the onset of nonlinear aging. [140]

In Figure 11 b) and c), Nyquist plots of the impedance spectra and slow discharge curves (with a discharge rate of 0.02 C) are presented in reference to the three characteristic spots in Figure 11 a): prior to aging (new state); and before as well as after the start of nonlinear aging. The degradation in terms of impedance increase and slow discharge capacity fade in the area of nonlinear aging (from “before” at approx. 820 EFC to “after” at approx. 980 EFC) far outweighs the one in the linear area (from “new” to “before”), and thus, principally corresponds to the behavior which is shown in Figure 11 a). After all, based on the presented findings, the effect of nonlinear aging and its onset shall be defined here in more detail:

If closing formation processes of passive layers are neglected, the capacity fade can generally be regarded as linearly depending on the charge throughput, which is why its gradient is constant in this “area of linear aging”. At deep residual capacities, the (absolute) gradient of the capacity fade is observed suddenly to increase, switching into the “area of nonlinear aging”. If this increase exceeds the measurement accuracy and is likewise no more flattened onwards, it is considered as the onset of nonlinear aging.

In the area of linear aging, most relevant aging mechanisms are the SEI growth and graphite active material loss [93, 94, 98, 123, 138, 142, 143]. The SEI grows under the consumption of active lithium which in turn leads both to an increase of impedance and capacity fade [76, 77, 79-81]. Erratic volumetric changes in the crystal structure of graphite are known to provoke a severe loss of active material especially when cells are discharged to low SoC [95, 99].

At the turning point, i.e., the onset of nonlinear aging, lithium plating is assumed to occur even for moderate charging rates and temperatures as a result of the increased overpotentials and the reduced capacity of the graphite anode (which both were caused by the aforementioned aging mechanisms) [79, 98, 138]. If plated lithium reacts with the electrolyte, additional SEI is formed, and thus, the electrode balancing is further distorted with respect to the disproportionate increase of the sum of anodic overpotentials. Although dissolved cathodic oxidation products are increasingly detected at the anode from the onset of nonlinear aging, the cathode itself is found to be only negligibly deteriorated [138, 139, 144].

Altogether, the *self-reinforcing nature of lithium plating* [79], accompanied by an *increased distortion of the electrode balancing*, is supposed to create an *adverse circle* of lithium and graphite active material loss [144]. Figure 12 a) flow charts the interaction of relevant aging mechanisms which are supposed to provoke the effect of nonlinear aging. In Figure 12 b), the assumed development of maximal electrode overpotentials (for a constant charging rate) versus EFC with reference to the three characteristic aging states “New”, “Before” and “After” is shown. At a certain state of the aging progress, the anodic potential drops below the critical value of 0 V vs. Li/Li⁺, lithium plating occurs, and, in interaction with further aging mechanisms, it provokes the effect of nonlinear aging. As the effect of nonlinear aging has not been reported yet for LIC with a lithium-titanate-oxide (LTO) anode, this is presumably linked to the high potential of LTO

which makes it unsusceptible (even in the aged state) to drop below the critical value of 0 V vs. Li/Li^+ (for which lithium plating would theoretically occur as well).

The statement of a sudden onset of lithium plating to be causative for nonlinear aging is based in the literature on several supplementary measuring and analysis methods. Generally, periodic capacity and impedance measurements of investigated consumer cells during the aging experiments are performed by default. Furthermore, differential voltage and incremental capacity analysis (DVA and ICA) are carried out at the end of an aging experiment with the consumer cells and, afterwards, with out of those made laboratory cells to yield information on the degradation of single electrodes. Thereby gained results are only compared with the new state. DVA and ICA are generally used to infer to a loss of active material or usable lithium. To further support thereby gained insights, for example, X-ray diffraction (XRD) and inductively coupled plasma optical emission spectroscopy (ICP-OES) can be used. In addition, photographs and scanning electron microscopy (SEM) images of nonlinearly aged anodes are usually compared with the new state.

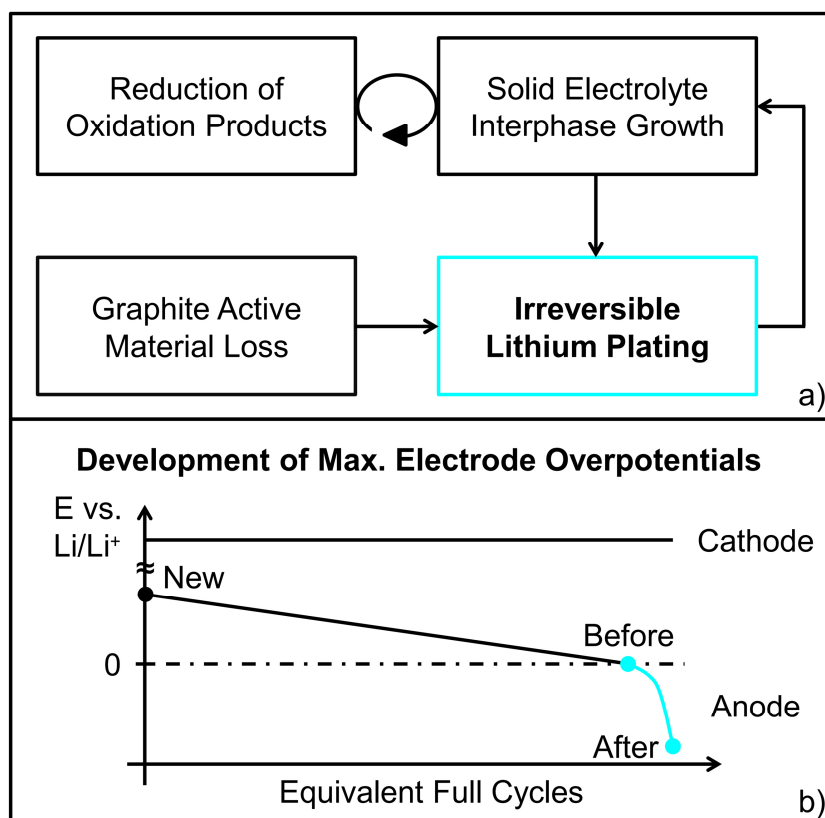


Figure 12: a) Flow chart of aging mechanisms which may lead to nonlinear aging; b) assumed development of maximal electrode overpotentials versus equivalent full cycles.

Out of the set of described measuring and analysis methods, with DVA, ICA, XRD and ICP-OES, loss of usable lithium could be identified as the main source of nonlinear aging, followed (to a lesser extent) by graphite active material loss [103, 138, 139, 144]. In combination with aforementioned anode photographs and SEM images, the authors of these studies finally concluded that lithium plating is causative for nonlinear aging, as there was a metallic sheen observable on the rolled out anode jelly rolls. SEM images additionally elucidated the presence of a thick surface film in these bright areas which could be a result of irreversibly plated lithium that had been in contact with electrolyte.

For the three characteristic spots which are marked in Figure 11 a), anode photographs and SEM images of the same type of C//NMC cell were taken within the scope of [144]. In the left box of Figure 13, the photograph of the new anode basically reveals its black appearance which is to expect for delithiated graphite. However, even in the new state (i.e., after 2 cycles for cell characterization), there is a first sign of regularly spaced vertical stripes which turn to clear metallic bright areas for the anode of the cell just before the occurrence of nonlinear aging. As this is a clear sign for a deficiency in the production process, focus is laid on it later again. The anode of the cell after nonlinear aging finally shows that the metallic patterns have spread to cover the whole anode surface area. Regarding the corresponding SEM images, in the black areas, there is only a slight surface film formation which is possibly due to an ordinary growth of the SEI. In contrast to that, in the bright areas, SEM images (before and after nonlinear aging) reveal the presence of thick surface films which could result from additional SEI growth due to the contact of irreversibly plated lithium with electrolyte.

However, although the authors of [103, 138, 139, 144] already inferred that lithium plating is causative for nonlinear aging (based on the just presented findings), final scientific evidence cannot be given only on the base of the *irreversible part of lithium plating*. Exemplarily, as the manganese content at the anode, regarding again the three characteristic spots of Figure 11 a), obviously exhibits a trend suiting to the one of nonlinear aging (from $11 \text{ nmol}\cdot\text{cm}^{-2}$ (new) to $33 \text{ nmol}\cdot\text{cm}^{-2}$ (before, mixed area) to $46 \text{ nmol}\cdot\text{cm}^{-2}$ (after, black area) or $139 \text{ nmol}\cdot\text{cm}^{-2}$ (after, bright area) [144]), distinct aging mechanisms are theoretically conceivable to provoke nonlinear aging. Principally, the related characteristic of capacity fade could also stem from a strong *ordinary* SEI growth (not due to lithium plating) which is known to be catalyzed by cathodic oxidation products which are reduced at the anode (and thus, form electron conducting tunnel paths) [79, 88].

As there is actually no satisfying analysis method to differentiate ordinary SEI growth from the additional one which results from irreversibly plated lithium, a further chance to reach scientific evidence is to add information which is based on the *reversible part of lithium plating* (see stripping and electrochemical intercalation of reversibly plated lithium in Subchapter 3.1). For plated anodes, this part was described before to result in a characteristic potential plateau

during cell relaxation – which in turn is present exactly as long as the metallic lithium needs to be electrochemically intercalated into graphite (≈ 10 min [102]).

Thus, the authors of [102] opened cells and optically investigated their graphite anodes by SEM more quickly than the observed duration of the potential plateau. As lithium plating is assumed to be predominantly reversible (but self-reinforcing), there must be, principally, a thick layer of metallic lithium which still exhibits a conductive connection to graphite. They took a SEM image of a plated anode immediately after plating had been provoked (< 10 min), as well as, for another plated anode, after having it been given enough time for relaxation. As a reference, an un-plated anode was investigated immediately after the charging process.

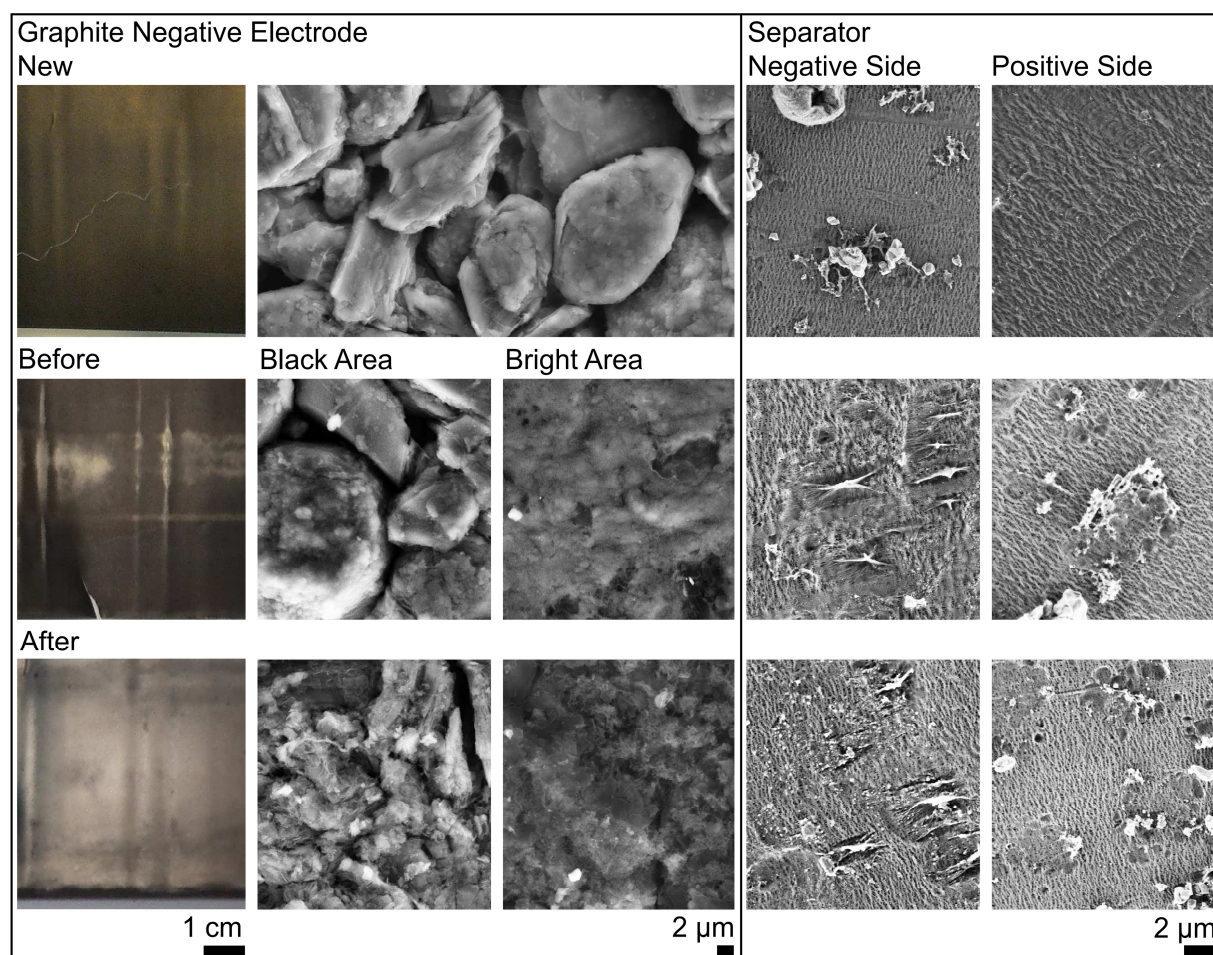


Figure 13: Left box: Photographs and scanning electron microscopy images of graphite negative electrodes; right box: scanning electron microscopy images of corresponding separators (for the negative and positive side each); the different rows correspond to the three characteristics spots in Figure 11 a). [144]

By doing so, the scientists found a thick *mossy and net-like layer of metallic lithium* covering the graphite surface of the cell which was opened immediately after plating had occurred (which is also in accordance to [114, 139, 145]). The plated anode of the cell, which had been given enough time for relaxation, only showed some inactive remnants of the net-like lithium structure, but aside from, it resembled the un-plated anode (where e.g. graphite particles were clearly recognizable). The remnants correspond to the irreversible part of lithium plating, as there is obviously no conductive connection to graphite anymore. As aforementioned, lithium is generally known to be irreversibly plated due to *internal or external lithium isolation*, as well as *SEI micro cracking*, with regard to Figure 9. The described *synergies between the time-variant optical findings on the anode surface and the characteristic relaxation behavior* (in addition to the DVA, ICA, XRD and ICP-OES results), are regarded as adequate to finally conclude that *lithium plating is the cause of nonlinear aging*. Therefore, in the following, the reasons for the observed locally distributed onset (e.g., regularly spaced vertical stripes in Figure 13) and subsequent strong propagation of lithium plating are considered in more detail.

Generally, phenomena like inhomogeneous potential distributions, current densities, mechanical strains or temperature gradients are well-known to be present in LIC [146-151]. In the linear area of aging, where the SEI growth and loss of graphite active material are considered to be prevailing, effects of such non-uniform distributions may be increasingly problematic as e.g. local overcharge or deep discharge could be the result. For cells upon prolonged cycling, at a certain SoH, the onset of local lithium plating, as is observable in Figure 13 on the left, is hence conceivable which in turn initiates the onset of nonlinear aging.

Based on ICA, the effects of local lithium plating on the electrochemical behavior of LIC are described in [144] with regard to the three characteristic spots of Figure 11 a): if the new graphite jelly roll is imagined as a parallel connection of several individual areas (like a raster), the total capacity corresponds to the sum of the single capacities of individual areas. For a cell just before the start of nonlinear aging, as the less active areas with a metallic sheen are rare and only small-sized, the effect on the total graphite anode capacity is therefore limited. However, as the less active areas instead lead to increased electrical (and mechanical) loads for the insane areas, the self-reinforcing nature of lithium plating provokes quick propagation of bright areas. Moreover, the propagation is assumed to be additionally fostered by excess currents which occur at the edge of an electrochemically more active area next to one which is less active [152]. Thus, in the end, more and more individual areas of the jelly roll are disabled with a dramatic effect on the total graphite anode capacity.

Besides of the increasing electrical loads in insane black areas, progressively inhomogeneous mechanical loads are the consequence of plated lithium which is known to take up more space than when intercalated into graphite [104, 105]. Regarding the right box of Figure 13, even the separators appear to be seriously damaged due to the contact with plated lithium: besides of a

few clogged pores due to impurities or effects of compression, areas facing the cathode, or unplated sectors of the anode, stay unaffected; however, for separator areas facing plated bright sectors (before and after nonlinear aging), there are craters in the magnitude of μm which could be the result of local heating and melting or chemical degradation [144, 153]. Due to increased overpotentials in these degraded separator areas the occurrence of local lithium plating is hence additionally promoted which suits to its self-reinforcing nature (in accordance to [122]).

Furthermore, aside from the described mechanical loads which are caused by the plated lithium itself, a connection between mechanical loads as a result of external strains or cell components and the occurrence of lithium plating is observed: e.g., regarding the new graphite jelly roll in Figure 13, there are already first signs of regularly spaced vertical stripes; for the anode just before the start of nonlinear aging, exactly these stripes turn to bright areas (which is the indicator for lithium plating). This must be regarded as a clear sign of a deficiency in the production process of the investigated type of cell. By means of micro computed tomography within the scope of [144], the stripe patterns could be clearly linked to the positive current collector tab which especially inflicts deformation of the inner jelly roll layers close to the cell center as a result of the imposed mechanical load. For further clarification, the same authors conducted a control experiment *for plating susceptibility*, where a hose clamp was fixed around the diameter of a cell to externally impose mechanical strain. As a result, bright metallic areas appeared on the overlap of the hose clamp and the positive current collector tab after only a few cycles. The connection of an inhomogeneous pressure distribution and the occurrence of lithium plating might e.g. be explainable by affected lithium ion diffusion through the separator (due to alterations of its porosity and tortuosity) [121, 122, 154]. In terms of the difficulty of reaching homogeneous pressure distributions e.g. at the edges of pouch cells, this observance must be considered as a critical issue [155, 156].

As the occurrence of lithium plating is promoted by high charging rates and end voltages at low temperatures, focus is laid on these stress factors with respect to the design of the aging experiment of this work. Regarding the implementation of SLC, the possibility to delay or even prevent nonlinear aging by load adaption (in consistency with the reuse of an ALIB in a SLA) is of major importance. Thus, in a first step, for a certain set of parameters, it is investigated when nonlinear aging starts to occur for a given load; and in a second step, with the thereby gained *perfect foresight*, load adaption (with regard to the stress factors of lithium plating) is carried out just before the onset of nonlinear aging to investigate how far it can be delayed or prevented. The thereby gained results of the aging experiment are presented in Chapter 6. In the next subchapter, based on the described context of nonlinear aging and further relevant issues like norms and standards, the end of life criteria of SLC are discussed again in more detail.

3.4 End of Life Criteria

An inevitable onset of nonlinear aging at residual capacities around 80%, as is shown in Figure 11 a), would make SLC unprofitable in the field. Though, it is assumed that the mild load profiles of SLA compared with those of BEV lead to a considerable delay or even prevention of this critical aging phenomenon [14]. In the literature, usually residual capacities in a range from 70% and 80% are mentioned as the Eo1L, i.e., the criterion which defines the time of battery removal from the BEV [16, 22, 35, 36, 40-45]. For the corresponding criterion in the SLA, i.e., Eo2L, there is a lack of literature references: only in [29], a range from 20% and 40% is given, but these values can just be regarded as a rough guideline as they are not referred to the requirements of certain SLA. In any case, regarding a successful realization of SLC, $\Delta EoL = Eo1L - Eo2L$ must be maximized for a most long period of battery reuse. Figure 14 shows a schematic development of capacity versus EFC and qualitatively assigns the EoL criteria to conceivable SoH. It is observable that after the Eo1L is reached, due to a change of application, aging continues to be linearly depending on the charge throughput (possibly with a different gradient in the field), whereas without application change, nonlinear aging would immediately start to onset. Finally, after the Eo2L is reached in the SLA, the (postponed) start of nonlinear aging is regarded as the ultimate *battery failure* (more specifically discussed at the end of this subchapter). The corresponding determining factors and dependencies of Eo1L and Eo2L are presented in the following.

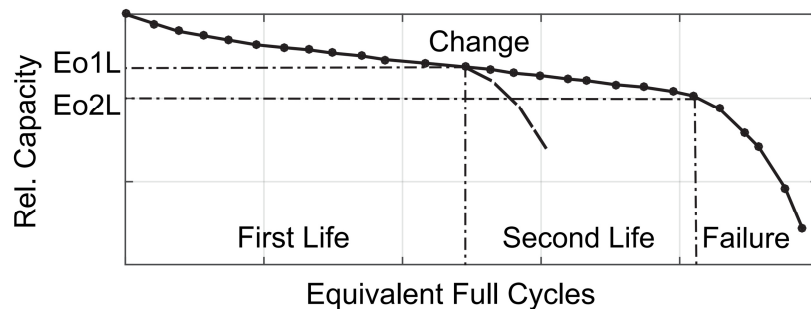


Figure 14: Schematic development of capacity versus equivalent full cycles with qualitatively indicated end of life criteria. [14]

The reason that a residual capacity of 80% is commonly assumed as Eo1L dates from a first recommendation in the “Electric Vehicle Battery Test Procedures Manual” which was published by USABC in 1996 [55]. However, the value has never been validated. In a recent American publication, based on the National Household Travel Survey, only a share of 4% of polled drivers was determined being unable to perform their daily drives at a residual capacity of 80% [157]. The share is increased to values of 7%, 11% and 17% for residual capacities of 70%, 60% and 50%, respectively. Thus, a user-dependent definition of the Eo1L criterion is principally

regarded as useful, but simultaneously making SLC implementation more complicated (e.g. due to a strongly varying SoH of battery units which are considered for reuse). Additionally, ΔEoL , and thus the reachable time of battery reuse, would be lowered which definitely reduces the profitability of SLC.

A particularly practicable approach is the orientation towards warranty details of BEV manufacturers. Usually, they promise functionality of the automotive battery for a time of 8 to 10 years or 100.000 km, which in turn is mostly defined of residual capacities greater than at least 70% [158, 159]. However, for residual capacities smaller than 80%, retesting regarding the transportability of respective battery units is prescribed in accordance to UN 38.3.2.2. As this must be regarded as elimination criterion for SLC if transportation is necessary (due to the expensive retesting procedure), *reuse is considered in this thesis only for battery units with residual capacities equal or greater than 80%*. The observed onset of nonlinear aging at residual capacities of approx. 80% supports the scope limitation, even if automotive batteries are not assumed to immediately exhibit enhanced aging rates at residual capacities of 80% (as long as suitable operational conditions are kept which particularly take the actual SoH into account). However, transport regulations must be reconsidered in any case as the transportation of disused SLB to the recycling facility is likewise critical.

Costs of a SLB system's periphery are assumed to increase with a decrease of the Eo2L criterion: to cope with the same load profile of a SLA, a smaller Eo2L results in a larger (and heavier) SLB which in turn might require a larger casing or stronger cooling system. Aside from this economical aspect, as is shown in Figure 14, the onset of nonlinear aging is regarded as the ultimate end of battery life as its origin, lithium plating, severely reduces the safety of the SLB storage (e.g. thermal runaway). Thus, the onset of nonlinear aging must not be missed under any circumstances. Hard figures are waived here for the Eo2L criterion, as in the field tests are required to assess the possibility to delay or prevent nonlinear aging. Afterwards, the reachable service life can be related to the costs of refurbishing. Additionally, reduced efficiency due to increased impedance must be likewise considered for batteries with a very low SoH. The correlation between capacity and impedance of LIC during calendar and cycle life is analyzed in Chapter 8.

3.5 Causes of Increasing Cell-to-Cell Variation

Although having been removed from one aged BEV battery pack, only a fraction of its single units might be worthy to refurbish from an economic point of view, since an unavoidable cell-to-cell parameter variation (capacity, impedance, etc.) in the new state is known to even increase with the progress of aging [142, 160-162]. As a result of it, the necessity of time-consuming and costly measurements to classify battery units and select most suitable ones clearly reduces the

profitability of SLC (see Subchapter 2.2). Here in this subchapter, the origins of cell-to-cell variation in the new state and its increase with the progress of aging are concisely summarized.

In the new state, cell-to cell (and lot-to-lot) parameter variation must be attributed to *deviations in the production process*, such as changes in the weight fraction of active materials or the thickness of electrodes [50, 163, 164]. Reducing the mixing or thickness tolerance leads to excessive manufacturing costs at a comparably low improvement of the cells' performance [163]. However, e.g. thicker electrodes result in higher cell capacities, but, contrarily, also promote cyclic aging due to stronger volumetric changes upon intercalation and deintercalation processes. Thus, there is a direct interplay between cell-to-cell variation which results from the production process and its increase with the progress of aging [127].

Aside from this *intrinsic origin* of cell-to-cell parameter variation, in multi-cell battery applications, there are *extrinsic origins* which e.g. comprise [165]:

- temperature gradients in the battery pack
- SoC drifts due to uneven current loads (parallel strings)
- deviations in the cycle depth (serial strings; for LFP based cells: also parallel strings)
- deviations in the conductor or cells' contact resistances

For a parallel string, differences in the cells' resistances lead to an uneven current distribution, which in turn causes a drift of corresponding SoC [166]. Cells connected in series are loaded with the same current but distinct cycle depths, as the weakest cell always determines the performance of the whole string [50, 58]. In conclusion, intrinsic cell-to-cell variation leads to different cell loads in multi-cell battery applications, which in turn results in different aging mechanisms and rates. As an example, for two C//LFP cells connected in parallel, a 20% mismatch in the ohmic resistance led to a lifetime reduction by 40% when compared to a compound with optimally matched resistances [166].

As a consequence of a continuously increasing cell-to-cell variation (with the progress of aging), in multi-cell battery applications, effective balancing algorithms must be implemented in BMS to ensure a safe and efficient mode of operation. To do so, relevant parameters of new and aged batches of cells are investigated by distribution fit analysis in Subchapter 7.1. For a summary of the presented chapter "Fundamentals of Lithium-Ion Cell Aging", the reader is hereby referred to Subchapter 9.1. In the following chapter, the statistical methods, which were used to analyze the experimental data of this work, are presented. At its end, in Subchapter 4.3, the interrelation between cell-to-cell parameter variation and the battery (cell and module) interconnection configuration is analyzed and discussed from a theoretical point of view.

4 Methods of Descriptive Statistics

As the name already suggests, methods of *descriptive statistics* basically aim to describe and present (one- to multi-dimensional) data sets in a most clear way. By the so called *univariate analysis* of descriptive statistics, distributions of one-dimensional data sets (i.e., single variables like capacity or impedance parts) are investigated in terms of central tendency and dispersion. Respective univariate methods were used for the investigation of the development of cell-to-cell parameter variation which is presented in Chapter 7. Contrarily, *bivariate analysis* is used to describe the relationship between pairs of variables. In Chapter 8, the correlation between capacity and corresponding impedance parts of LIC during calendar and cycle life is analyzed by respective bivariate methods. Thereupon, it is assessed whether the correlation behavior is a suitable base regarding the implementation of SoH quick tests. In the following, most relevant univariate and bivariate analysis techniques are tersely described.

4.1 Univariate Analysis

The symmetric normal (or Gaussian) distribution is commonly used to describe the intrinsic cell-to-cell parameter variation in the new state. Hence, basically, production processes can be evaluated by it [167-170]. In the field, a total dispersion is mostly composed of multiple smaller dispersions. If these are normally distributed, same is obtained for their sum. Otherwise, if the distribution is unknown or abnormal, the central limit theorem helps stating that the sum of a sufficiently large number of stochastically independent dispersions can approximately be regarded as normally distributed [171]. In other words, if a distribution appears to be normal, only random errors underlie, which characterizes a high-quality production process without any systematic errors. The normal probability density function of the normal distribution is expressed as follows:

$$f(x, \mu, \sigma) = \frac{1}{\sqrt{2\pi} \cdot \sigma} \cdot e^{-\frac{(x-\mu)^2}{2\sigma^2}} \quad (4)$$

Thereby, the parameter μ is the arithmetic mean value of the distribution, σ its standard deviation and σ^2 the variance. To be able to compare different sets of data, the relative coefficient of variation $\kappa = \sigma \cdot \mu^{-1}$ is used. As an example, the distribution of capacity or internal resistance of 20,000 pristine LFP based LIC was reported in [160] to correspond to a normal distribution with $\kappa_C = 1.3\%$ or $\kappa_R = 5.8\%$, respectively (i.e., the relative coefficient of capacity variation κ_C was observed to be lower than the one of the internal resistance κ_R).

Another well-known parameter to characterize if a variation is normally distributed is the skewness s , which is calculated as follows with the expected value E :

$$s(x, \mu, \sigma) = \frac{E(x-\mu)^3}{\sigma^3} \quad (5)$$

The skewness describes the asymmetry of the data around the mean value. If $s < 0$, the distribution is left-skewed, which means that the data is more spread to the left, and for $s > 0$, distribution is right-skewed. For a symmetrical distribution (like normal distribution), s is equal to zero.

In contrast to the normal distribution, the Weibull distribution is typically used in materials engineering for reliability analysis, i.e., to describe probabilities of failure and make predictions of it within confidence bounds [132, 171-176]. As such, there is a major distinction in the typical field of application of these two distributions: while the normal distribution is generally used to describe the dispersion of a parameter for a fixed period of application, the Weibull distribution is usually raised to characterize the *life cycle* or the spread of maximal periods of application before the failure of an electronic device.

As Chapter 7 aims to compare the cell-to-cell parameter variation in the new state to that after BEV operation, the normal distribution is used in its typical field. However, this suggests a new and alienated area of use for the Weibull distribution as cell-to-cell parameter variation at a fixed period of application is investigated. The Weibull probability density function in terms of a two-parameter distribution (β, η) is expressed as follows:

$$f(x, \beta, \eta) = \frac{\beta}{\eta} \cdot \left(\frac{x}{\eta}\right)^{\beta-1} \cdot e^{-\left(\frac{x}{\eta}\right)^\beta} \quad (6)$$

Thereby, β is the shape parameter which can be raised to refer to different types of failure in case of classical use of Weibull for lifetime analysis. According to [177], a $\beta < 1.0$ represents a defect in the initial step caused by manufacturing errors with a decreasing failure rate vs. time ($x = t$), a $\beta = 1.0$ a random failure with a constant failure rate and a $\beta > 1.0$ a failure caused by abrasion or aging and therefore an increasing failure rate vs. time. The scale parameter η quantifies the expected life of a device by giving the value for which 63.2% will have failed. In case of failures which definitely do not start at $t = 0$ days, years, cycles, etc., the three-parameter Weibull distribution should be used instead with the additional failure-free time, minimum life or location parameter γ [177]. Substitution of x in Equation (6) by $x - \gamma$ transforms the two- to a three-parameter distribution which is expressed as follows:

$$f(x, \beta, \eta, \gamma) = \frac{\beta}{\eta} \cdot \left(\frac{x-\gamma}{\eta}\right)^{\beta-1} \cdot e^{-\left(\frac{x-\gamma}{\eta}\right)^\beta} \quad (7)$$

There is no definite rule which one of the two Weibull distributions is the better choice for a certain set of data of a product without known lifetime expectation. Decision has to be made based on engineering expertise and experience, and by assumptions about the expected lifetime of the investigated product. However, Equation (7) is only valid if a finite failure-free time γ can absolutely be ensured.

It has to be considered, that in classical reliability analysis, the length of operation time until failure is investigated. In Chapter 7, the parameter variation of aged ALIB cells, all employed for the same operation time and without having remarkably failed, is compared with the Weibull distribution. Not a classical life cycle distribution at a *predefined EoL* is investigated, but the distribution of characteristic cell parameters at a concrete charge throughput. Therefore, the values of parameters (β , η) which are given in Subchapter 7.1 deviate from typical values of reliability analysis and thus cannot be interpreted as known from the past. Anyway, regarding the capacity of aged LIC, the Weibull distribution should be left-skewed with $\beta > 3.6$, according to [171], which can be interpreted as a surplus of capacities below the mode of distribution. For the special case of $\beta \approx 3.6$, the skewness of the Weibull distribution can be neglected and thus principally resembles the shape of a normal distribution [171]. Theoretically, with respect to resistances of LIC in the aged state, the Weibull distribution in the relevant range of β , which is much greater than 3.6, as will be shown and explained in Subchapter 7.1, is only useful to compare with its reciprocal value, i.e., the conductance, because resistances are assumed to be distributed right-skewed. In simple terms, if a cell capacity or conductance distribution proficiently corresponds to Weibull, disproportionately more cells exhibit a lower capacity or conductance as e.g. compared with a normal distribution. In the following subchapter, after the description of most relevant methods of univariate analysis of descriptive statistics, corresponding methods for two-dimensional data sets are explained.

4.2 Bivariate Analysis

Bivariate analysis basically describes two-dimensional data sets e.g. by scatter plots, the Pearson product-moment correlation coefficient (PPMCC) or regression functions. To mathematically quantify the grade of correlation by direction and strength, the PPMCC $r_{X,Y}$ can be raised. Thereby, the variables X and Y with $X = (x_1, x_2, \dots, x_n)$ and $Y = (y_1, y_2, \dots, y_n)$ represent the investigated two-dimensional data set [178]. Throughout in this work, the one variable is cell capacity, the other a corresponding impedance value. So, for each measurement, a pair of capacity and investigated impedance part is created. The PPMCC $r_{X,Y}$ describes the extent of linear relationship between these two variables [179]. Its values range from -1 to 1 , whereby a negative sign represents a negative correlation which is to expect for capacities and corresponding impedance parts of a LIC. The PPMCC $r_{X,Y}$ is described by Equation (8) [167]:

$$r_{X,Y} = \frac{\text{cov}_{X,Y}}{\sigma_X \cdot \sigma_Y} = \frac{\sum_{i=1}^n (x_i - \bar{x}) \cdot (y_i - \bar{y})}{\sqrt{\sum_{i=1}^n (x_i - \bar{x})^2 \cdot \sum_{i=1}^n (y_i - \bar{y})^2}} \quad (8)$$

Thereby, the covariance $\text{cov}_{X,Y}$ is standardized by division by the standard deviations σ_X and σ_Y . The following gradations of absolute $r_{X,Y}$ can be interpreted as:

$ r_{X,Y} < 0.3:$	Missing Correlation
$0.3 \leq r_{X,Y} < 0.5:$	Weak Correlation
$0.5 \leq r_{X,Y} < 0.8:$	Moderate Correlation
$0.8 \leq r_{X,Y} < 1.0:$	Strong Correlation
$ r_{X,Y} = 1.0:$	Perfect Correlation

Finally, the negative correlation is modeled by linear regression analysis in accordance with $Y = b + a \cdot X$ which in turn is optimized by the least squares method. Raising $r_{X,Y}$ in combination with linear regression analysis, it can be assessed whether there is a linear dependency between the development of capacity and impedance as assumed in [54] and [61]. Especially for linear regression, the coefficient of determination is the square of $r_{X,Y}$. If e.g. $r_{X,Y}^2 = 95\%$, this means that 95% of the variation of X can be explained by the values of Y and vice versa [168].

4.3 Link to the Battery Cell and Module Interconnection Configuration

The effect of cell-to-cell parameter variation on the performance of a battery module and pack strongly depends on the battery (cell and module) interconnection configuration. On that score, the interrelation between cell-to-cell parameter variation and the interconnection configuration is discussed in this subchapter with reference to the recently learned fundamentals of descriptive statistics. Figure 15 shows the equivalent circuit diagram of a multi-cell battery which consists of s serially connected modules; each of the s modules again consists of p cells which are connected in parallel. The presented $XsYp$ interconnection configuration is often found in multi-cell batteries and, in particular, is basically the same as in the BEV batteries which are investigated in this work (see Subchapter 5.3).

For each of the s modules, the relation $U_{Ms,Total} = U_{Ms,1} = \dots = U_{Ms,p}$ applies due to the parallel interconnection of p cells. Regarding the complete battery system, the total system voltage corresponds to $U_{Total} = U_{M1,Total} + \dots + U_{Ms,Total}$, as the s modules are serially interconnected. For the total system current, the relation $I_{Total} = I_{M1,1} + I_{M1,2} + \dots + I_{M1,p} = \dots = I_{Ms,1} + I_{Ms,2} + \dots + I_{Ms,p}$ applies with regard to the series interconnection of the s modules, and, the current division in the p parallel branches of modules according to the current divider rule. [28]

With regard to the parallel interconnection of cells in a module, if one cell fails with high impedance, the module is still usable with reduced capacity and increased current load of the remaining cells (for the same total system current I_{Total}). The capacity of the battery system is reduced in the same extent (if other modules are assumed to be unaltered), as the capacity of a series string is defined by its weakest unit. However, these adverse effects are usually minimized in the field by the interconnection of a great number of cells in parallel. For an exemplary battery module with 50 cells in parallel (1s50p), if one cell fails completely with high

impedance (which is regarded as a seldom event), its share of $1/50 = 2\%$ of the current load is then divided up the remaining 49 cells (ideal case). For the same setting, the capacity of the module, and thus likewise of the complete battery system, is reduced by 2% as well. Therefore, it can be said that the effects of single cell outliers on modules with a great number of cells in parallel are regarded as only small. The presented findings can also be transferred in the same manner to a setting in which more cells fail with high impedance. In contrast to the given example, if the single modules are each replaced by a large cell with high capacity (e.g., p times the capacity of the shown small cells), then a single cell failure would mean a total failure of the battery system; whereas for the presented example with small cells, a total failure of the battery system would only emerge in case of the entirety of a module's cells would fail.

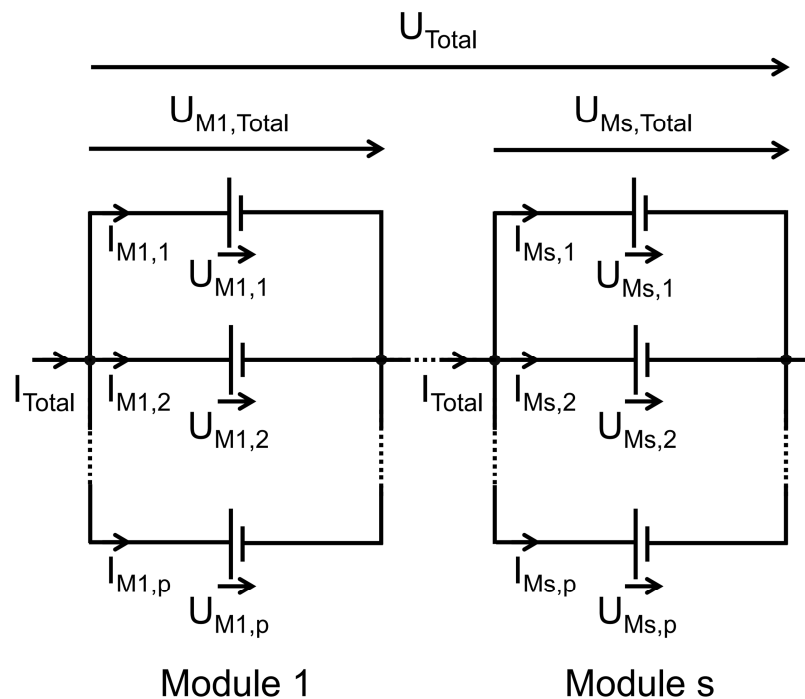


Figure 15: Equivalent circuit diagram of a multi-cell battery in an exemplary battery cell and module interconnection configuration ($XsYp$).

As described in Subchapter 4.1, a high-quality cell production process which is characterized by the absence of systematic production errors results in production lots of cells with normally distributed cell parameters (capacity, impedance, etc.). It is assumed here that battery packs and their modules, respectively, represent randomly selected partial quantities of such production lots. As a consequence, the cell parameters of battery packs and their modules are normally distributed as well (in the new state) [171].

In general, the sum $Z = X + Y$ of two independent, normally distributed random variables $X \sim N(\mu_X, \sigma_X^2)$ and $Y \sim N(\mu_Y, \sigma_Y^2)$ is again normally distributed [168]:

$$Z \sim N(\mu_X + \mu_Y, \sigma_X^2 + \sigma_Y^2) \quad (9)$$

In the following, the entirety of battery cells (which is available for battery module and pack construction) is assumed to consist of independent cell groups which are characterized by normally distributed cell parameters (capacity, resistance, conductance, etc.). Furthermore, it is assumed that the *arithmetic mean values and standard deviations of cell parameters are even* for distributions of the different cell groups.

Then, with regard to Equation (9), if p cells are randomly selected from those groups and *interconnected in parallel*, the interrelation between the mean capacity $\mu_{\text{Mod},C}$ of the battery module (which consists of p cells in parallel) and the one of a single cell $\mu_{\text{Cell},C}$ from the entirety of available cells is calculated as follows:

$$\mu_{\text{Mod},C} = \mu_{\text{Cell},C} \cdot p \quad (10)$$

Simultaneously, the interrelation between the standard deviation of a battery module and its p cells in parallel is yielded as per:

$$\sigma_{\text{Mod},C} = \sigma_{\text{Cell},C} \cdot \sqrt{p} \quad (11)$$

By that, the relative coefficient of variation $\kappa_{\text{Mod},C}$ of a battery module which consists of p cells in parallel is lastly derived from Equation (10) and (11):

$$\kappa_{\text{Mod},C} = \sigma_{\text{Mod},C} / \mu_{\text{Mod},C} = \sigma_{\text{Cell},C} / (\mu_{\text{Cell},C} \cdot \sqrt{p}) \quad (12)$$

Thereby, it is obvious from Equation (12) that $\kappa_{\text{Mod},C}$ decreases with an increase of p (which is the number of cells in parallel). Furthermore, for a *parallel cell interconnection*, aside from the parameter “capacity”, Equations (10-12) are valid in the same manner for the parameter “conductance”. For a *serial cell interconnection*, Equations (10-12) are likewise valid for the parameter “resistance” (which is the reciprocal value of the parameter “conductance”).

Regarding the parameter “capacity” for a serial cell interconnection, though, relations between statistical values of a battery module and its cells are more complex as the performance of a serial string is always limited to its worst cell. If p battery cells from a cell batch with a normal capacity distribution are randomly selected and interconnected in series, with an increase of p , the probability is continuously increased to select a cell with a capacity which is lower than the capacity distribution modus. Finally, if a battery cell is selected, which is an outlier cell towards small capacities, the capacity of the serial string is likewise strongly limited. With regard to the common serial interconnection of battery modules in a battery pack, this is critical as SLC are most likely realized at the battery module level (as aforementioned, though, effects of cell outliers in battery modules are usually minimized by interconnecting a large number of cells in parallel).

However, if battery cells from different production lots or from BEV with different operational histories are interconnected, the assumption of normally distributed parameters with even arithmetic mean values and standard deviations is problematic. Likewise, battery cells might be divided into different cell groups during operation in a battery pack, e.g. due to the presence of temperature gradients. By the simplifying assumption that there are only two groups of cells which are still normally distributed around two arithmetic mean values μ_1 and μ_2 , the resulting distribution of all cells in common would be bimodal. With regard to the central limit theorem, only for a sufficiently large number of independent distributions, the sum is approx. normally distributed again. Nevertheless, with the progress of cell aging, though, it is furthermore assumed that the symmetric normal distributions of cell parameters continuously gain in skewness (see Chapter 7).

In any case, contrary to the effect of a cell outlier which is compensated in a battery module with a great number of cells in parallel, by the formation of cell groups with different properties, whole areas of inferior and superior modules (in which all cells each are particularly bad or good) are created in a multi-cell battery. By that, cell-to-cell variation is basically scaled up to the next level which is *module-to-module variation*. This is critical as SLC implementation is presumably realized at the module level; as a consequence, SoH detection of battery modules is inevitable. Regarding the interconnection of complete battery packs, the presented relations can be transferred with regard to the battery interconnection configuration of the former ALIB and the planned SLB.

From the description of the required fundamentals of descriptive statistics, as well as of the interrelation between cell-to-cell parameter variation and the interconnection configuration, it is led over to the experimental part of this work, beginning with an overview of the experimental setup and general framework.

5 Experimental

Throughout in this work, the BEV high-energy type LIC “Molicel IHR18650A” by E-One Moli Energy Corp. with a nominal capacity of 1.95 Ah was raised for investigation. For this cell, the manufacturer recommends an operational voltage swing ΔV from 3.0 V to 4.2 V, and maximum current rates of 1.0 C for charging and 2.0 C for discharging. With regard to the manufacturer’s data sheet, the nominal capacity is reached within the given voltage swing for discharging rates smaller than 0.5 C at room temperature. The active materials of the investigated type of cell are graphite and NMC regarding the anode and cathode, respectively. Cells out of two identical BEV were compared with new cells of the same type and manufacturer.

Within the scope of [144], the type of cell was characterized in more detail. By ICP-OES, the cathode material was detected to be $\text{Li}_{1.06\pm 0.02}\text{Ni}_{0.33\pm 0.01}\text{Mn}_{0.33\pm 0.01}\text{Co}_{0.33\pm 0.01}\text{O}_2$ in the fully lithiated state after cell formation (hinted measurement accuracy, oxygen derived from the crystal structure). Regarding the total initial content of lithium, a share of 4.5% is assumed to be unavoidably lost due to either the SEI formation or the *buffering effect* of the graphite anode (thus, before cell formation, lithium content in the crystal structure amounted to be 1.11 ± 0.02). Furthermore, the cathode, and thus likewise the cell, was determined (by measurements with commercial EI-Cell three-electrode laboratory cells) to have a capacity of $3.0 \text{ mAh}\cdot\text{cm}^{-2}$ [144].

In the following, regarding the conducted aging experiment, the methodology of diagnosing the current aging status and its design itself are presented; in addition, comprehensive information with respect to the investigated BEV is provided.

5.1 Aging Diagnosis

The large aging experiment within the scope of this work was periodically stopped to track the current aging status. The weekly basis of measuring in the beginning of the experiment had been switched to a two weekly one in a later phase, as the aging behavior of cells was yet better known. The *periodical checkup procedure*, which consisted of capacity and impedance measurements, was conducted at a controlled ambient temperature of 25 °C. Utilized test devices were a Cell Test System (CTS) by BaSyTec for capacity measurements and cycling of cells as well as a VMP3 potentiostat by Biologic Science Instruments for impedance measurements; both in combination with custom-made climate chambers. Figure 16 flow charts the single steps of the one/two-weekly checkup procedure, which are described in the following in more detail.

After interruption of the aging experiment and temperature preconditioning for 1 h at 25 °C, the checkup procedure started with the measurement of capacity. Cells were charged with a CC of

0.5 C until the charging end voltage of 4.2 V was reached, then switching to a constant voltage (CV) phase for as long as the current was greater than 0.1 C. After a break of 6 min, cells were discharged with a CC of 1.0 C until the discharging end voltage of 3.0 V was reached, again switching to a CV phase with an absolute current greater than 0.05 C as termination condition. Hence, the capacity values in this work consist of the sum of CC and CV discharge capacities. After capacity measurement, cells rested again for 6 min and then were charged with a CC of 0.5 C to a target voltage of 3.73 V which corresponded to a SoC of approx. 50%. The voltage of 3.73 V was kept in a following CV phase for as long as the current was greater than 0.1 C. Figure 17 shows the voltage and current development versus time of a new Molicel IHR18650A in the capacity determination part of the steadily used checkup procedure.

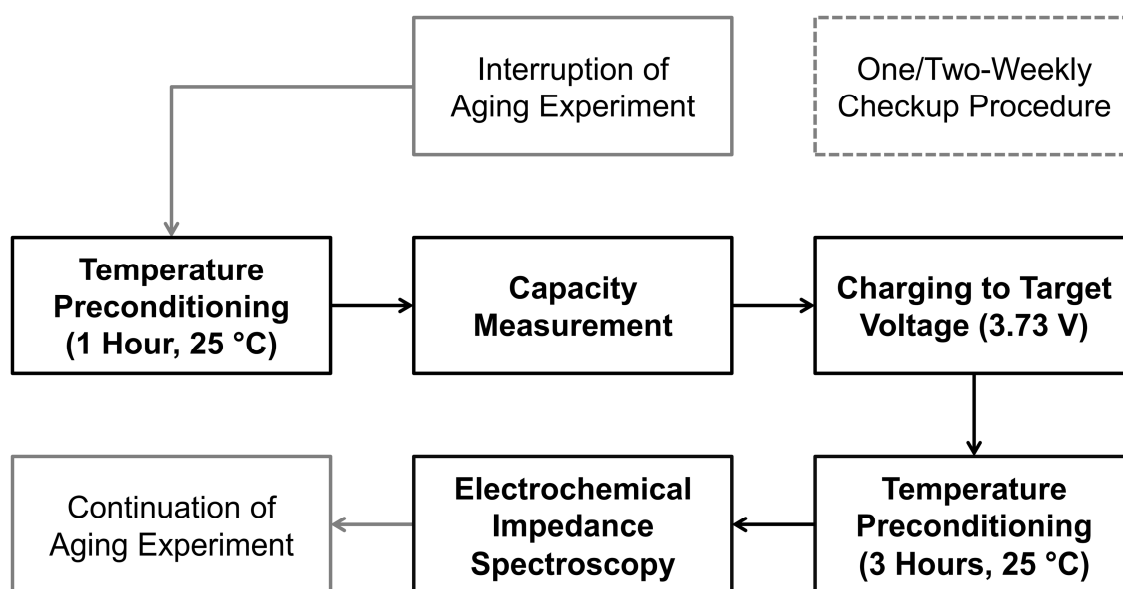


Figure 16: Flow chart of the single steps of the one/two-weekly checkup procedure.

The CV phase in the discharging process basically aimed at eliminating the influence of impedance in the CC discharging process by a continuous depletion of polarization. This in turn enabled a better inference to the available amount of active lithium; and furthermore, made the measurement less sensitive to temperature fluctuations in the custom-made climate chambers (± 0.5 K). Though, regarding the investigation of correlation between capacity and impedance which is presented in Chapter 8, higher values of $r_{x,y}$ would have been reached regarding the correlation between CC capacities and corresponding impedance parts as the resulting overpotentials are directly influenced by the impedance while the discharge itself is voltage limited. But, in contrast to that, the reference on concrete aging mechanisms leading to capacity loss due to the consumption of active lithium accompanied by impedance increase would then not be feasible.

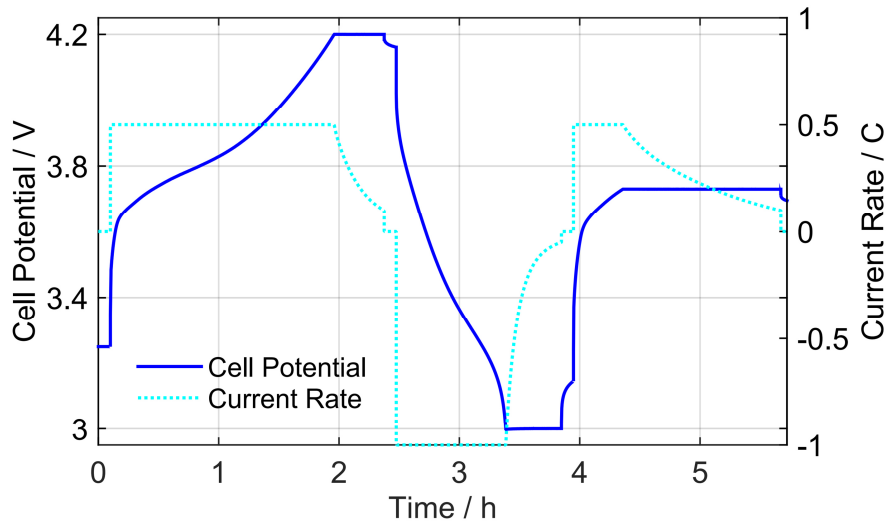


Figure 17: Voltage and current development versus time in the capacity determination part of the steadily used checkup procedure.

After adjustment of the SoC ($\approx 50\%$), cells had to rest for 3 h at 25 °C before measuring their actual impedance. The impedance spectra were determined by electrochemical impedance spectroscopy in galvanostatic mode regarding a frequency range from 10 kHz to 10 mHz. Figure 18 shows a Nyquist plot with averaged impedance spectra of all classified new cells as well as of all those investigated of both BEV (see Subchapter 5.3), which are called *BEV1* and *BEV2* from now on. In the averaged spectrum with the highest impedance, i.e., that of *BEV2*, characteristic impedance parts are marked, which are raised henceforth throughout in this work to quantify the current aging status (next to corresponding capacity values). These are the real part of impedance at zero crossing, R_{zc} , and the part which corresponds to the diameter of the semi-circle appearing in the Nyquist plot, R_{pl+ct} . The first is often mentioned as the ohmic resistance and is attributed to the sum of resistances of current collectors, active materials and electrolyte (also within the porous separator). The latter is attributed to the passive layers, the double layer capacity and the charge transfer resistance and is defined by $R_{pl+ct} = \text{Re}\{Z_{total}\} - R_{zc}$ [57-60, 180]. A distinction between two semi-circles, which principally represent either only the characteristics of the passive layers or the double layer capacity and the charge transfer resistance, appears not to be feasible for the used type of cell at a temperature of 25 °C (due to too similar time constants of underlying processes) [57, 59].

5.2 Design of Experiments

In complete, 484 new and 954 aged cells out of two identical BEV each (i.e., 1908 BEV cells in total) were characterized to yield a broad set of data regarding a concrete *state of aging*. These data sets were raised for the statistical analyses (cell-to-cell variation, correlation between

capacity and impedance) which are presented in Chapter 7 and 8. Out of the 484 new cells, most similar ones were selected with respect to $\text{Re}\{Z_{\text{total}}\}$ for the conducted laboratory aging experiments. In a *first phase* of experiments, aging data of cells during the *progress of aging* was collected within calendric and cyclic aging experiments. The yielded data of this first phase was used in terms of the investigation of correlation between capacity and impedance (next to aforementioned cell batches). Therefore, all in all, 83 cells from laboratory tests were raised. As only data from 62 laboratory test cells (see Table 1 and Table 3, plus three cells of the special test case “2CCCV”) is presented in this thesis (except from Chapter 8), the difference is explainable by the addition of cells from supplementary measurements in order to yield larger cell batches. Aging data from the *second phase*, i.e., experiments which were conducted in the course of load adaption (to delay or prevent nonlinear aging) were not considered in Chapter 8.

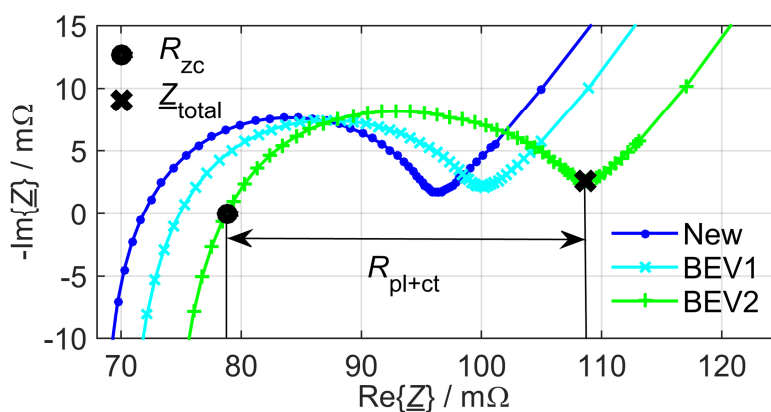


Figure 18: Nyquist plot of averaged impedance spectra of all new cells and of all those investigated of BEV1 and BEV2 (at a SoC \approx 50%). [127]

As aforementioned, *cyclic aging* depends on numerous parameters like cycle depth, mean SoC, current rate and temperature. As the mean SoC of all test cases presented in this work is approx. 50%, the effect of this parameter is excluded and not further investigated. However, with respect to the *superposition principle*, it is assumed that aging is enhanced with increasing mean SoC. Regarding the cycle depth, fixed charging and discharging end voltages were used throughout in this work which is why the term *voltage swing* ΔV is used instead in the following. Thereby, it has to be considered that the accumulated charge throughput per cycle decreases upon prolonged cycling as polarization is increased due to growing impedances.

Table 1 lists the investigated parameters of the *first phase of the cyclic aging experiment* which are the voltage swing ΔV , the charging and discharging rate as well as the temperature. Cells were either charged with a CC or with a constant current constant voltage (CCCV) process, whereas the termination condition for the latter was a current smaller 0.1 C in the supplementary

CV phase. In all test cases, cells were discharged with CC and a break of 20 min was kept between half cycles.

Additionally in Table 1, for each test case, the amount of inspected cells and an explicit identifier (ID) of the respective experiment is given. The column “Cell Batch” refers to the laboratory cell batch of the correlation analysis of Chapter 8, which is subdivided into the cell batches “Cyclic” (ID 1-11 + cells from supplementary measurements, see Table 1), “Calendric” (ID 21-30 + cells from supplementary measurements, see Table 2) and “Mild Cyclic” (ID 12, see Table 1). The supplementary measurements had same or similar setups than those within associated batches. For most test cases which were executed from the start of the aging experiment, three cells were used to be able to average the aging behavior and exclude outliers, if necessary. For test cases which were started at a later stage of the aging experiment, the number of cells could be reduced, as prior tests had already revealed a sufficiently homogeneous aging behavior of cells cycled with the same load profile at same ambient conditions. Before the start of all experiments, selected cells were preloaded with four cycles to avoid ongoing formation processes.

The *second phase of the cyclic aging experiment* aimed to assess the possibility of delaying or preventing nonlinear aging by load adaption (which corresponds to the central idea of SLC). Based on experiences from the first phase of the aging experiment, a *reference base case* (ID 3) was chosen for which it was known when nonlinear aging would start to occur. The load profile of the reference base case consisted of CC charging with 0.5 C to a charging end voltage of 4.2 V (without CV phase), a break of 20 min between half cycles and CC discharging with 1.0 C to a discharging end voltage of 3.0 V. The ambient temperature was 35 °C. Nonlinear aging characteristics for cells cycled with this load profile were shown in Figure 11; furthermore, it corresponds to the cycling base case in the course of [144] (see Figure 13).

Anyway, if the cells of one adaption test case had been fallen below a mean *residual capacity of 85%*, the load was adapted with respect to experiences from the first phase of the cyclic aging experiment (here mentioned beforehand just for clarity): ΔV was reduced from 1.2 V to 0.94 V (ID 13); the charging rate from 0.5 C to 0.2 C (ID 15); the temperature was both decreased and increased from 35 °C to 25 °C (ID 17) and 50 °C (ID 19). In addition, regarding the test case “All” (ID 20), all investigated parameters were simultaneously adapted (temperature: 35 °C \rightarrow 50 °C). The discharging rate was excluded in the second phase of the experiment. As the temperature and charging rate adapted load profiles are not included in the matrix of Table 1 (only with CCCV charging), as mild reference test cases, cells were additionally cycled with these profiles beginning from the new state (ID 14, 16, 18). Table 2 presents the aging matrix of the second phase of the cyclic aging experiment.

Table 1: Matrix of the first phase of the cyclic aging experiment in dependency on the investigated parameters: ΔV , current rate (charging and discharging) and temperature. Based on [140].

Investigated Parameter	$\Delta V / V$	V_{\max} / V	V_{\min} / V	Charging Rate / C	Discharging Rate / C	Temp. / °C	Cells	ID	Cell Batch
Voltage Swing ΔV	0.56	3.89	3.33	0.5 (CC)	1.0	35	3	1	Cyclic
	0.94	4.11	3.17	0.5 (CC)	1.0	35	3	2	Cyclic
	1.2	4.2	3.0	0.5 (CC)	1.0	35	3	3	Cyclic
	1.2	4.2	3.0	0.5 (CCCV)	1.0	35	3	4	Cyclic
	1.3	4.3	3.0	0.5 (CCCV)	1.0	35	2	5	Cyclic
Charging Rate	1.2	4.2	3.0	0.2 (CCCV)	0.5	35	2	6	Cyclic
	1.2	4.2	3.0	0.5 (CCCV)	0.5	35	2	7	Cyclic
	1.2	4.2	3.0	1.0 (CCCV)	0.5	35	2	8	Cyclic
Discharging Rate	1.2	4.2	3.0	0.5 (CCCV)	0.5	35	2	7	Cyclic
	1.2	4.2	3.0	0.5 (CCCV)	1.0	35	3	4	Cyclic
	1.2	4.2	3.0	0.5 (CCCV)	2.0	35	2	9	Cyclic
Temperature	1.2	4.2	3.0	0.5 (CCCV)	1.0	25	2	10	Cyclic
	1.2	4.2	3.0	0.5 (CCCV)	1.0	35	3	4	Cyclic
	1.2	4.2	3.0	0.5 (CCCV)	1.0	50	2	11	Cyclic
	0.94	4.11	3.17	0.5 (CC)	1.0	35	3	2	Cyclic
	0.94	4.11	3.17	0.5 (CC)	1.0	50	3	12	Mild Cyclic

Aside from the described two-step parameter adaption (in analogy to SLC), the effect of continuous charging rate adaption was investigated in a quick test procedure: regarding the test case with the maximum charging rate I_{\max} in Table 1 as the reference base case (i.e., 1.0 C, CCCV, ID 8), the rate was periodically reduced as per:

$$I(t) = I_{\max} \cdot \left(1 - \delta \cdot \frac{C_0 - C_{\text{act}}(t)}{C_0}\right) = I_{\max} \cdot \left(1 - \delta \cdot \frac{C_{\text{loss}}(t)}{C_0}\right) \quad (13)$$

C_0 and $C_{act}(t)$ are the capacity in the new and the actual state, respectively; $C_{loss}(t)$ is the current capacity loss (i.e., C_0 referred to $C_{act}(t)$), and $\delta \in \{1; 2; 4\}$ a gain factor which controls the proportion of charging rate adaption. For a $\delta = 1$, principally, the adaption leads to a constant capacity-related charging rate, as it is reduced in the same manner as the capacity fades. In contrast, without charging rate adaption, the capacity-related charging rate is increased as it is usually referred to the fixed value of nominal capacity (like in this work) [181].

Table 2: Matrix of the second phase of the cyclic aging experiment in dependency on the load adapted parameters: ΔV , charging rate and temperature. For each adapted test case, cells were cycled with the respective mild load profile from the beginning in addition to the base case reference.

Investigated Parameter	$\Delta V / V$	V_{max} / V	V_{min} / V	Charging Rate / C	Discharging Rate / C	Temp. / °C	Cells	ID
Base Case	1.2	4.2	3.0	0.5 (CC)	1.0	35	3	3
Voltage Swing ΔV	0.94	4.11	3.17	0.5 (CC)	1.0	35	3	2
	1.2 \rightarrow 0.94	4.2 \rightarrow 4.11	3.0 \rightarrow 3.17	0.5 (CC)	1.0	35	3	13
Charging Rate	1.2	4.2	3.0	0.2 (CC)	1.0	35	3	14
	1.2	4.2	3.0	0.5 \rightarrow 0.2 (CC)	1.0	35	3	15
Temperature	1.2	4.2	3.0	0.5 (CC)	1.0	25	2	16
	1.2	4.2	3.0	0.5 (CC)	1.0	35 \rightarrow 25	2	17
	1.2	4.2	3.0	0.5 (CCCV)	1.0	50	3	18
	1.2	4.2	3.0	0.5 (CC)	1.0	35 \rightarrow 50	3	19
“All”	1.2 \rightarrow 0.94	4.2 \rightarrow 4.11	3.0 \rightarrow 3.17	0.5 \rightarrow 0.2 (CC)	1.0	35 \rightarrow 50	3	20

In order to investigate the effects of *calendric aging* in the laboratory, cells were stored (without float charging) either at a SoC of 0%, 10%, 50%, 90% or 100%, and a temperature of 35 °C (ID 21-25) or 50 °C (ID 26-30). The relevant data is listed again in Table 3. Stored cells were given to checkup only once a month in contrast to cycled cells. As the output SoC of the checkup procedure was 50%, the SoC of cells which were stored at a SoC = 50% had not to be adjusted afterwards. For cells stored at a different SoC, the adjustment was conducted by CC discharging (SoC < 50%) or charging (SoC > 50%) with 0.5 C until the desired target voltage was reached (3.0 V, 3.5 V, 3.69 V, 4.01 V and 4.2 V, respectively), switching to a CV phase for as long as the

(absolute) current was greater than 0.01 C. At the end of the calendric aging experiment (after 84 weeks), cells were started to be cycled with the aforementioned reference base case load profile (with respect to the two-step load profile adaption experiment, see Table 2, ID 3), to investigate the effects of storage conditions before first time operation.

Table 3: Matrix of the calendric aging experiment.

Temp. / °C	SoC / %	Cells	ID	Cell Batch
35 °C	0%, 10%, 50%, 90%, 100%	5 · 3	21-25	Calendric
50 °C	0%, 10%, 50%, 90%, 100%	5 · 3	26-30	Calendric

The variety of cell aging experiments (calendric aging, cyclic aging, load adaption, etc.) is presented in Chapter 6. Thereby, based on the first phase of the laboratory aging experiments, the effects of investigated parameters (ΔV , charging and discharging rate, temperature) on the phenomenon of nonlinear aging are presented at first in Subchapter 6.1. Afterwards, in Subchapter 6.2, the effects of the operational prehistory are assessed with respect to the aforementioned experiments regarding load adaption and storage conditions before cycling. In the next subchapter, auxiliary background information in terms of the construction and operational histories of examined BEV is presented.

5.3 Examined Battery Electric Vehicles

Both examined BEV (BEV1, BEV2) were identical in construction and part of a fleet-test with more than 500 passenger cars which were operated in everyday customer use. In the following, most relevant information regarding the construction and operational histories of BEV is given, whereas the effects of the latter are clarified by additionally delivering respective mean values of cell capacities and impedance parts. The discussion of operational histories and possibly available inhomogeneities (temperature, SoC, etc.) in the respective battery packs are the base of the statistical analysis of cell-to-cell variation which is presented later in Chapter 7.

The BEV battery packs which consisted of 5088 single LIC had a nominal energy content of 35 kWh, a nominal voltage of 355.2 V and were subdivided into 48 serially connected modules with a 2s53p cell interconnection configuration. For every parallel block of cells (1s53p, 103.35 Ah) within a module, one temperature and voltage sensor each was available with a measurement accuracy of ± 1 K and ± 10 mV, respectively. Voltage and current values were logged with 5 Hz, those of the temperature with 1 Hz. However, values were only logged during

driving operation (incl. recuperation); thus, no data is available regarding the charging processes.

The battery packs were cooled with air from the passenger compartment which was blown through the battery modules and deflected by fans out of the car. To further diminish aging effects, the allowed voltage swing ΔV of cells in the BEV battery packs was limited in terms of a charging and discharging end voltage of 4.0 V and 3.4 V, respectively. A drift of the battery modules' SoC in the serial connections was counteracted by an active dissipative charge equalization system [182].

To investigate effects of temperature gradients within the battery packs or SoC drifts of battery units (cells, modules) on cell-to-cell parameter variation, each out of BEV1 and BEV2, nine modules were completely characterized by single cell measurements. So, as one module consisted of 106 cells, this resulted in 954 cells in total per BEV. The nine of 48 modules of each BEV were chosen in a way to cover a maximum of different exemplary positions in the battery pack. Thereby, it was especially important to choose modules which were situated at the beginning, in the middle and at the end of the cooling air flow. Six of nine modules of BEV1 comparing to BEV2 were located completely identical to be able to ensure car-to-car comparison of yielded findings.

Figure 19 shows the construction of the BEV battery pack which is segmented in an upper main box and two lower side boxes. The marked cooling air flows ought to give an impression of possible temperature gradients in the examined type of automotive battery pack. In addition, measured modules of both BEV are drawn in to clarify overlaps which enable car-to-car comparison. The upper main box is just schematically segmented here in two parts in terms of clarity; the air flow enters the housing of the main box against the driving direction through lateral and central channels at the bottom (with an angle of inclination). Thus, cells which are located in their modules close to the bottom of the upper main box might be cooler on an average than those which are located at the top. Regarding the two lower side boxes, the air flow enters through the lateral and central channels on top with an angle of inclination, at both sides each, and is also only capable to leave on top; thus, there might be a horizontal instead of a vertical temperature gradient within modules. Possible hot spots, which originate from the construction of the investigated type of battery pack and the direction of the cooling air flows, are given in Chapter 7 for interpretation of cell-to-cell parameter variations.

BEV1 and BEV2 were used by different drivers at different operation sites with different ambient conditions. At first, both cars were deployed in California for a period of 1.75 years, where the average module temperature was measured to be 25.2 °C. The mileage of BEV1 was 14,849 km; the one of BEV2 was 19,641 km. Subsequently, however, BEV1 was further used in Paris for a period of 1.42 years and reached there a mileage of 6,548 km; BEV2 was then used in Shenzhen for 1.25 years and reached 7,104 km. The average module temperature in Paris and

Shenzen was 20.2 °C and 27.8 °C, respectively. The most relevant information on both examined BEV (and their LIC) is summarized in Table 4.

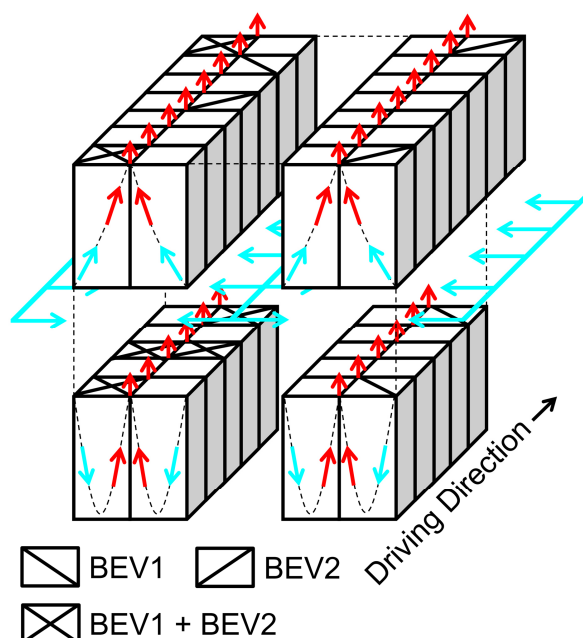


Figure 19: Construction of the examined automotive battery packs with hinted air flows of the integrated cooling system; measured modules of respective BEV are additionally marked.

Comparing the total mileage of both cars, BEV1 was deployed approx. a quarter less with 21,397 km compared to BEV2 with 26,745 km. 79% of the total mileage of BEV1 and 84% of BEV2 were driven in town. The total application period of BEV1 with 3.17 years was only slightly higher than that of BEV2 with 3.00 years; though, the average module temperature was higher for the latter. The average cell (parallel block) voltage was identical for both cars with 3.78 V. The higher average energy consumption of BEV2, with 19.0 kWh per 100 km compared with the one of BEV1 with 16.9 kWh per 100 km, could originate from an enhanced energy consumption of the air-conditioning system with regard to the higher ambient temperatures in Shenzen.

A further reason of the higher average energy consumption of BEV2 could be the more aggressive driving style of its drivers, as the share of the charge throughput of currents beyond the manufacturer's limitations (i.e., 1.0 C for charging and 2.0 C for discharging) of BEV2 was nearly twice as large ($\approx 1,000$ Ah) as the one of BEV1. Referred to the total charge throughput of BEV2 with 35,948 Ah, consequently, a share of 2.78% of the total charge throughput was critical. The given total charge throughput is composed by the one of the charging and the driving process. Thus, if the total charge throughput is divided by the number of cells in parallel and by two times of the nominal capacity, i.e., $35,948 \text{ Ah} / 53 / 3.9 \text{ Ah} \approx 174$ for BEV2, the

number of EFC per cell for the total period of application can be estimated. The number of EFC per cell of BEV1 is lower with 123. If the number of EFC per cell is estimated by the total mileage and the average energy consumption, the resulting charge throughput must be referred to only one time of the nominal capacity as only the driving process is considered.

Table 4: Summary of the most relevant information on examined BEV. Based on [127].

Parameter	BEV1	BEV2
Operation Site 1	California	California
Period of Application	1.75 y	1.75 y
Mileage	14,849 km	19,641 km
Av. Module Temperature	25.2 °C	25.2 °C
Operation Site 2	Paris	Shenzen
Period of Application	1.42 y	1.25 y
Mileage	6,548 km	7,104 km
Av. Module Temperature	20.2 °C	27.8 °C
Total Period of Application	3.17 y	3.00 y
Total Mileage	21,397 km	26,745 km
Av. Energy Consumption	16.9 kWh / 100 km	19.0 kWh / 100 km
Total Charge Throughput *	25,376 Ah	35,948 Ah
Av. Charge Throughput / Cell	479 Ah	678 Ah
Equivalent Full Cycles	123	174
Av. Cell Voltage	3.78 V	3.78 V
Av. Cell Capacity	1.91 Ah	1.85 Ah
Av. Cell Resistance R_{zc}	74.08 mΩ	78.64 mΩ
Av. Cell Resistance R_{pl+ct}	25.35 mΩ	29.95 mΩ

* The total charge throughput is composed by the one of the charging and the driving process.

The higher total charge throughput and the enhanced average module temperature of BEV2 compared with BEV1, in combination with the presumably more aggressive driving style of its drivers, might be causative for the slightly advanced aging progress of its battery. This is reflected by a lower average cell capacity and higher impedance parts of BEV2 compared with BEV1 which are also listed in Table 4. In comparison with an average cell capacity of 1.97 Ah, average $R_{New,zc} = 71.15 \text{ m}\Omega$ and $R_{New,pl+ct} = 24.67 \text{ m}\Omega$ for the investigated batch of 484 new cells, the average performance of the cells of both cars decreased due to the progress of aging. Same tendency regarding the progress of aging, i.e., new < BEV1 < BEV2, is also observable in Figure 18 for the increase of impedance parts.

Furthermore, by comparing the parameter values of BEV cells with those of new cells, the progress of aging appears as only low for both BEV1 and BEV2, but their total period of application is likewise just about a quarter of the commonly expected lifetime of an automobile. The upcoming aging behavior can easily be estimated by e.g. assuming a linear dependency from the charge throughput and raising the nominal cell capacity as initial value, besides from the presented values after the known period of BEV operation.

From the given information on the experimental setup of the conducted aging experiments and the general framework (cell type, BEV fleet-test, etc.), it is led over to the main part of this work. In the following chapter, the results of the aging experiments (calendric, cyclic, load adaption, etc.) are presented and discussed.

6 Lithium-Ion Cell Aging

In the beginning of the main part of this thesis, the phenomenon of nonlinear aging is investigated in detail. As aforementioned, the effect is regarded as a major technological barrier towards a successful SLC implementation, since it might severely limit the reachable second service life of a refurbished ALIB. Apart from that, it basically complicates the prediction of the expectable aging behavior. These general conditions are, though, directly linked with the decision of an interested party to invest in a storage project with SLB.

In Subchapter 6.1, the dependency of nonlinear aging on the voltage swing, the current rate (charging and discharging) and the temperature is assessed. Based on the thereby yielded results, operational strategies to delay or prevent the occurrence of nonlinear aging can be derived. In Subchapter 6.2, presented experiments address a suppression of nonlinear aging by either a two-step parameter (ΔV , charging rate, temperature) or continuous charging rate adaption; in addition, the effect of different long-term storage conditions before cycling is evaluated. For clarification, Figure 20 highlights the progress of work which is reached in Chapter 6.

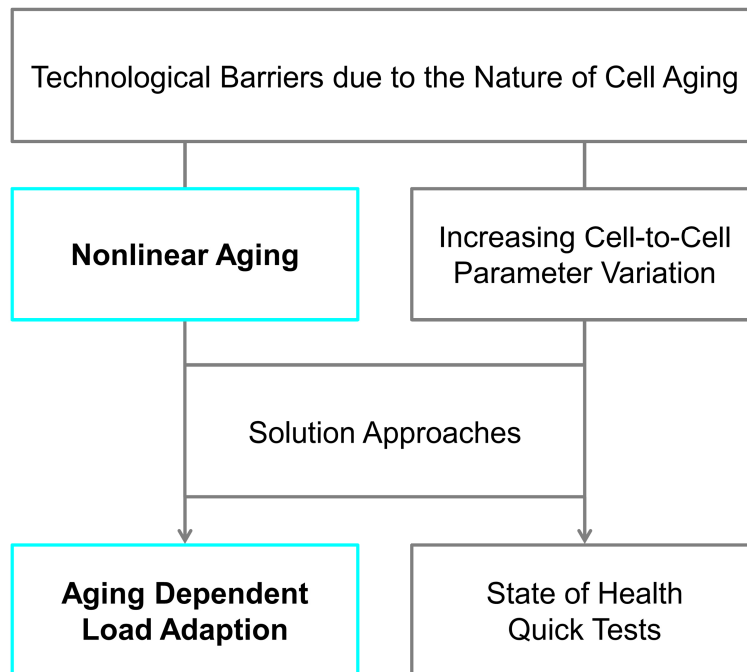


Figure 20: Progress of work in Chapter 6: the boxes of the presented core issue (nonlinear aging) and the corresponding solution approach (aging dependent load adaption) are colored in cyan.

The possibility to delay or prevent the occurrence of nonlinear aging of LIC must be regarded as a prerequisite with regard to an economic realization of SLC. Since the aging phenomenon has often been mentioned in the literature to start around 80% residual capacity [65, 137], but this value coincides with the commonly cited Eo1L criterion (i.e., the residual capacity where the ALIB is removed from the BEV) [16, 22, 35, 36, 40-45], the reachable second service life would approach zero as a consequence of being unalterable.

6.1 Nonlinear Aging Behavior under Different Operational Conditions

As aforementioned, in the majority of relevant LIC aging studies, focus is laid on the aging behavior above residual capacities of 80%. Figure 21 shows the development of the relative discharge capacity versus EFC in dependency on the voltage swing for cells charged with 0.5 C (CC) and discharged with 1.0 C (CC) at 35 °C. The different voltage swings $\Delta V = 0.56$ V (ID 1), 0.94 V (ID 2) and 1.2 V (ID 3) correspond approx. to a cycle depth of 27%, 73% and 87% in the new state of cells, respectively, referred to the nominal capacity. Thereby, it has to be considered, though, that the accumulated charge throughput per cycle decreases upon prolonged cycling as polarization is increased due to growing impedances. In general, for the test cases presented in Figure 21, the loss of capacity is increased for enhanced voltage swings. Besides, the assumption of its linear dependency on the charge throughput (or EFC) seems to be justified for all depicted test cases if first data points are neglected. The slightly increased aging rate at the beginning of cycling might originate from closing formation processes [141].

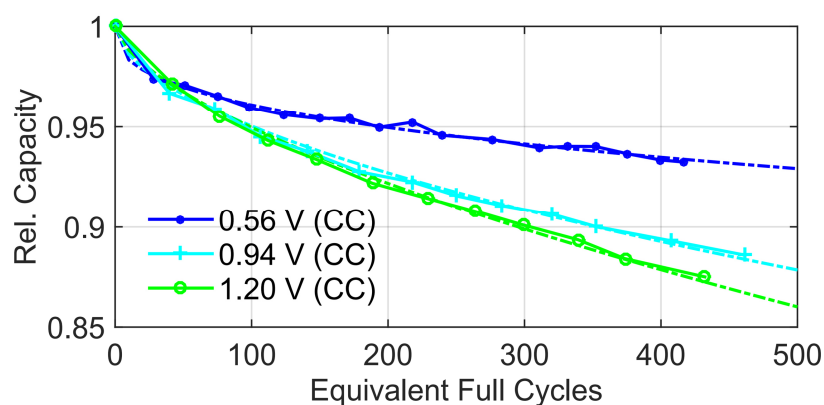


Figure 21: Development of the relative capacity versus equivalent full cycles for different voltage swings; the fitted curves indicate a prediction of the upcoming aging behavior; the abbreviations in the legend characterize the charging process. Constant parameters: $I_{Ch} = 0.5$ C, $I_{Dis} = 1.0$ C, $T = 35$ °C; ID (legend top down) = 1, 2, 3. [140]

Accordingly, if the upcoming capacity development is predicted based on the presented data (see fitted curves), by further assuming a linear dependency from the charge throughput, the maximally reachable number of cycles up to a defined EoL criterion would be overestimated, if the effect of nonlinear aging occurs but is not considered. Regarding a storage project with SLB, this would lead to severe miscalculations in the business outlook. Therefore, in the following, the aging behavior upon prolonged cycling is presented for different operational conditions to figure out the effects on the turning point from linear to nonlinear aging characteristics. The following subchapters are divided into the effects of different voltage swings, current rates (charging and discharging) and temperatures.

6.1.1 Dependency on the Voltage Swing

In this subchapter, the aging behavior upon prolonged cycling is presented for different voltage swings. In addition to the test cases which are shown in Figure 21, two load profiles with a supplementary CV phase in the charging process, and thus longer periods at high SoC and deeper cycles, were added in order to provoke an early turning point from linear to nonlinear aging. These additional voltage swings $\Delta V = 1.2$ V (ID 4) and 1.3 V (ID 5) correspond to a cycle depth of approx. 94% and 98% in the new state of cells, respectively. Thereby, it is especially apparent from the test case with the voltage swing $\Delta V = 1.3$ V (which is even larger than recommended), that the accumulated charge throughput per cycle is nonetheless smaller than the nominal capacity (due to the discharging rate of 1.0 C; the nominal capacity is reached only for rates < 0.5 C according to the cell specifications of the manufacturer, see Chapter 5).

Figure 22 a) shows the development of the relative discharge capacity versus EFC for different voltage swings upon prolonged cycling. It is clearly visible that higher voltage swings and supplementary CV phases in the charging process result in an earlier onset of nonlinear aging. For the test cases with CC charging, a reduction from $\Delta V = 1.2$ V to 0.94 V extends the area of linear aging at about 42%, and, in addition, the effect of nonlinear aging appears less intensive. Furthermore, for the test cases with CCCV charging, a reduction from $\Delta V = 1.3$ V to 1.2 V results in a prolongation of about 46%. When comparing the test cases $\Delta V = 1.2$ V with CC and CCCV charging, the longer periods at high SoC and deeper cycles accelerate the onset of the turning point at about 29%. The test case with a $\Delta V = 1.2$ V and CC charging (cyan curve with “plus” markers) represents the reference base case of the two-step parameter adaption experiments which are presented in Subchapter 6.2.

Figure 22 b) and c) show the development of R_{zc} and R_{p+ct} versus EFC, respectively. It is apparent, in general, that the increase of R_{p+ct} far outweighs the one of R_{zc} . Furthermore, a strong negative correlation to the development of the capacity is visible, i.e., a loss of capacity comes out with an appropriate rise of impedance parts and vice versa. As a consequence, there should be the possibility of perceiving or even predicting the occurrence of the turning point from

impedance measurements. The correlation between impedance parts and capacity could e.g. be used on a BMS to detect nonlinear aging by the calculation of corresponding resistances (regarding voltage changes caused by current pulses): as long as its gradient is approx. constant, the increase of the respective impedance part shows a linear dependency on the charge throughput but might turn to a nonlinear one when exceeding the measuring inaccuracy.

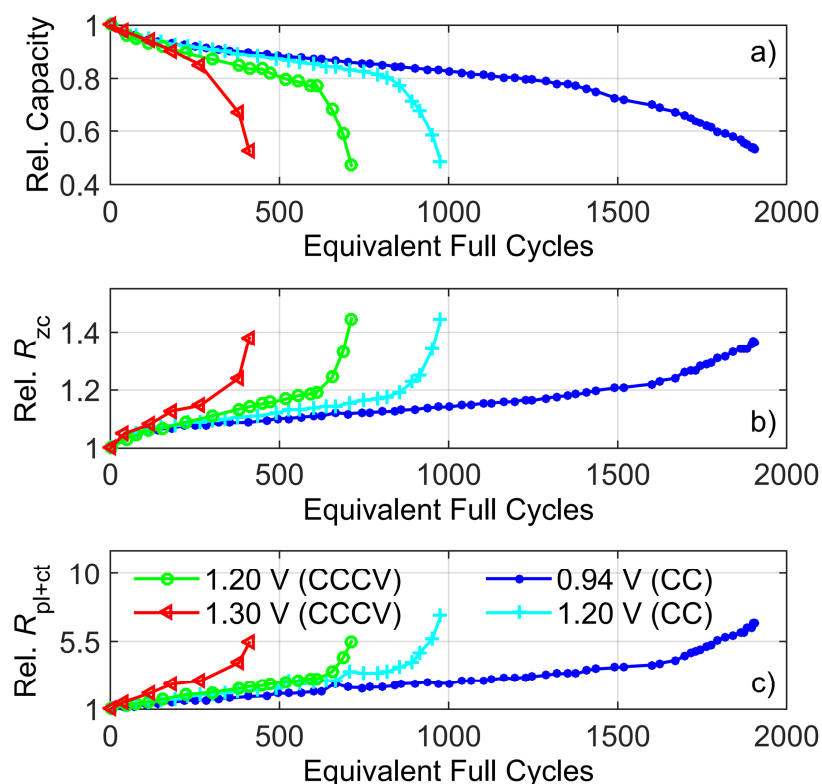


Figure 22: a) Development of the relative capacity versus equivalent full cycles in dependency on the voltage swing upon prolonged cycling; b) and c) show the corresponding development of R_{zc} and R_{pl+ct} , respectively; the abbreviations in the legend characterize the charging process. Constant parameters: $I_{Ch} = 0.5 C$, $I_{Dis} = 1.0 C$, $T = 35\text{ }^{\circ}\text{C}$; ID (legend top down, right left) = 2, 3, 4, 5. [140]

To further clarify the described negative correlation between capacity and impedance parts, Figure 23 shows a) R_{zc} and b) R_{pl+ct} versus corresponding capacity values. For both impedance parts, it is observable that even after the onset of nonlinear aging, i.e., for residual capacities smaller than approx. 80%, the correlation behavior stays linear (clarified by a dashed vertical line which separates the linear from the nonlinear area of aging); with regard to the later described correlation based SoH quick test approach, this observance means that *nonlinear aging is not critical to its feasibility as it does not affect the linear correlation between capacity and impedance parts* (for the investigated type of cell).

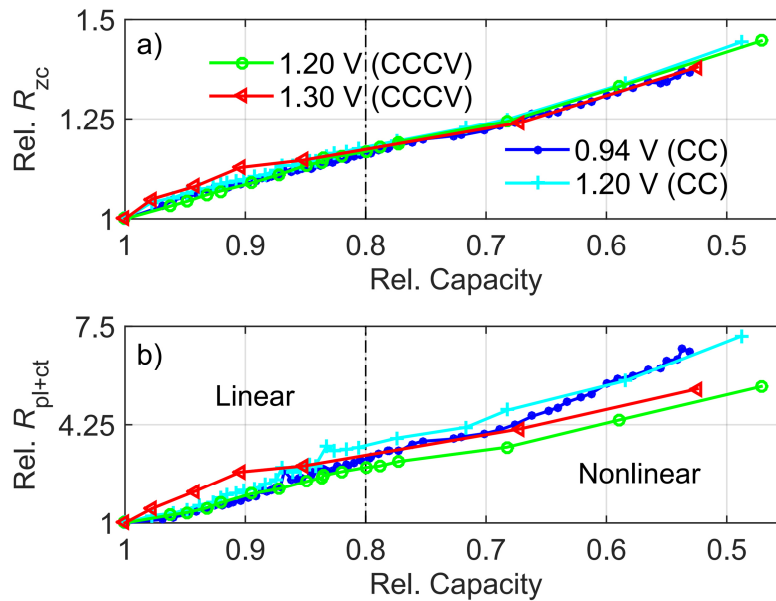


Figure 23: Clarification of approx. linear correlation between relative a) R_{zc} and b) R_{pl+ct} and corresponding values of capacity for the test cases presented in Figure 22. Constant parameters: $I_{Ch} = 0.5\text{ C}$, $I_{Dis} = 1.0\text{ C}$, $T = 35\text{ }^{\circ}\text{C}$; ID (legend top down, right left) = 2, 3, 4, 5. [140]

As the mean SoC of all test cases of conducted cyclic aging experiments is approx. 50%, a high voltage swing always results both in high charging and discharging end voltages. At high SoC, the SEI is generally known to grow, with the result of increased overpotentials at the anode; furthermore, its growth is additionally catalyzed by the reduction of oxidation products (which emerge as a result of cathode dissolution) [79, 88]. Especially when LIC are discharged to low SoC, erratic volumetric changes in the crystal structure of graphite are known to provoke a severe loss of active material [95, 99]. Thus, as a high voltage swing compulsorily leads to anodic capacity fade and increased overpotentials, at a certain state of aging, lithium plating will occur [79, 98, 138]. As aforementioned, due to its self-reinforcing nature, lithium plating (which leads to a continuously increasing distortion of the electrode balancing) is supposed to create an adverse circle of cyclable lithium and graphite active material loss, which in turn is the reason for the increase of the aging rate (see Figure 12) [79, 144]. As a conclusion, both a reduction of the charging and an increase of the discharging end voltage are effective towards a delay of the onset of nonlinear aging.

6.1.2 Dependency on the Current Rate

After the dependency on the voltage swing, the aging behavior upon prolonged cycling is shown for different charging and discharging rates. In compliance with Table 1, being equal for all test cases which are presented in this subchapter, cells were charged with a CCCV process at $35\text{ }^{\circ}\text{C}$ within a voltage swing $\Delta V = 1.2\text{ V}$. In the experiment regarding the effects of the charging rate,

the discharging rate was 0.5 C. To guarantee comparability, the charging rate of the test cases addressing the investigation of discharging rates was also 0.5 C.

Figure 24 a) shows the development of the relative discharge capacity versus EFC for different charging rates. For the test case with the maximum charging rate of 1.0 C (ID 8), the aging behavior exhibits nonlinear aging characteristics almost from the beginning of cycling. By reducing the charging rate to 0.5 C (ID 7), the maximum number of EFC before reaching the turning point is clearly extended. Regarding the test case with the minimum charging rate of 0.2 C (ID 6), the aging rate did not clearly increase within the timeframe of the experiment. Figure 24 b) and c) show the corresponding development of R_{zc} and R_{pl+ct} versus EFC, respectively. Again, as detected for the test cases in dependency on the voltage swing, a strong negative correlation between capacity and impedance parts is observable.

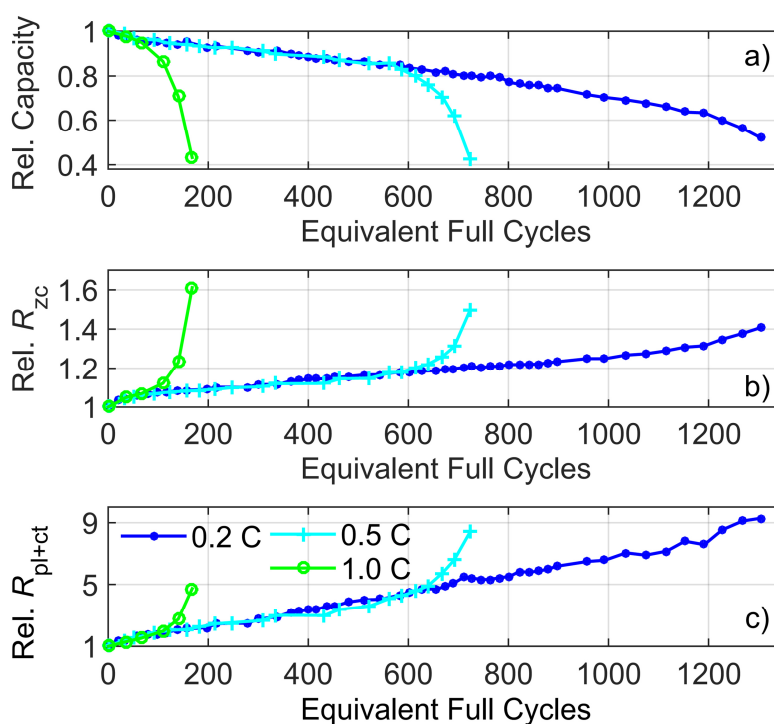


Figure 24: a) Development of the relative capacity versus equivalent full cycles in dependency on the charging rate upon prolonged cycling; b) and c) show the corresponding development of R_{zc} and R_{pl+ct} , respectively. Constant parameters: $\Delta V = 1.2$ V, $I_{Dis} = 0.5$ C, $T = 35$ °C; ID (legend top down, left right) = 6, 7, 8.

Furthermore, it is noteworthy that for all parameters and test cases in Figure 24, the aging rate appears identical until to the onset of nonlinear aging; thus, there is no effect of the charging rate in the area of linear aging. Generally, with higher charging rates, overpotentials at the anode are enhanced, which in turn increases the risk of the anode potential dropping below 0 V vs. Li/Li⁺ [102]. As a consequence of it, the occurrence of lithium plating is known to lead to an adverse

circle which in turn triggers nonlinear aging [144]. Finally, to give an assessment of the impact of the charging rate on the aging of LIC, its effect is regarded as serious but only in the case that a certain threshold value is exceeded which leads to lithium plating. As this threshold value depends on the aging state, the maximum charging rate which just does not trigger lithium plating must be continuously adapted (see Subchapter 6.2.1.2).

Figure 25 a) shows the development of the relative discharge capacity versus EFC for different discharging rates. *In contrast to the promoting effect of high charging rates towards nonlinear aging, the relationship is just contrary for discharging rates against expectations: with an increase of the discharging rate, the onset of nonlinear aging appears to be delayed.* Although the extension of the linear area is marginal with approx. 3% when comparing the test cases with 0.5 C (ID 7) and 1.0 C (ID 4), no increase of the aging rate is observed for the maximum discharging rate of 2.0 C (ID 9) within the timeframe of the experiment (even below residual capacities of 70%).

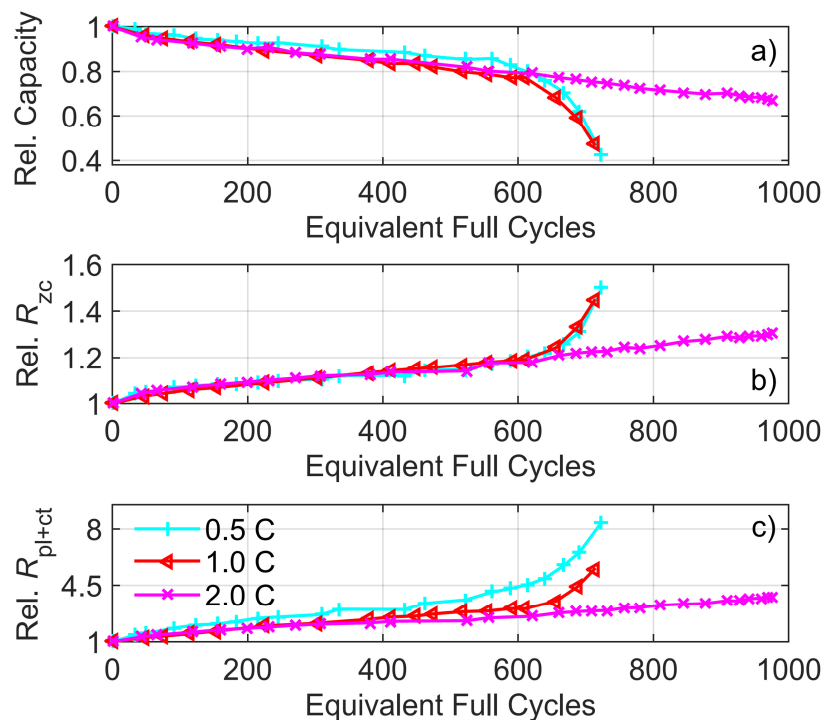


Figure 25: a) Development of the relative capacity versus equivalent full cycles in dependency on the discharging rate upon prolonged cycling; b) and c) show the corresponding development of R_{zc} and R_{pl+ct} , respectively. Constant parameters: $\Delta V = 1.2$ V, $I_{Ch} = 0.5$ C, $T = 35$ °C; ID (legend top down) = 7, 4, 9.

The slightly enhanced capacity fade rates of the test cases with 1.0 C and 2.0 C compared to 0.5 C in the area of linear aging might originate from temperature deviations due to internal heat buildup (up to 10 K deviation for cells discharged with 0.5 C and 2.0 C). However, results are

ambiguous as the test case with a discharging rate of 1.0 C exhibits the highest capacity fade rate in the linear area. In any case, if cells which are discharged with high rates are still warmer at the end of the subsequent charging process (due to the mentioned internal heat buildup), this could counteract the onset of nonlinear aging, as it is triggered by lithium plating which in turn is known to emerge facilitated at low temperatures.

Figure 25 b) and c) show the corresponding development of R_{zc} and R_{pl+ct} versus EFC, respectively. Again, both correlate negatively with the development of capacity. To further clarify the described negative correlation between capacity and impedance parts, Figure 26 shows a) R_{zc} and b) R_{pl+ct} versus corresponding capacity values for the experiments addressing the effects of different charging and discharging rates (i.e., test cases of Figure 24 and Figure 25). In the legend, the first term represents the charging rate, the second the discharging rate. Regarding the development of R_{zc} versus corresponding capacity values in Figure 26 a), the correlation behavior appears to be approx. linear. However, with regard to the development of R_{pl+ct} in Figure 26 b), correlation behavior is yet approx. linear for all test cases but there are different “branches”; the cause of their evolution is possibly related to time controlled aging mechanisms (like passive layer growth) as the two test cases with the most slowly cycled cells (i.e., 0.2 C / 0.5 C, 0.5 C / 0.5 C) are clearly distinguishable from the rest (also see Subchapter 3.2). For the same capacity fade, they exhibit a pronounced increase of R_{pl+ct} . The causes of this observance are investigated in Chapter 8 in more detail.

Returning to the discussion of the effects of different discharging rates, regarding Figure 25 c), it is astonishing that higher discharging rates seem to result in a delayed increase of R_{pl+ct} . As higher discharging rates also lead to a delay of the onset of nonlinear aging, the responsible cause might be the same: due to the voltage limitation of the (CC) discharging process, decreasing discharging rates lead to an increase of the depth of discharge. For the discharging rates of 0.5 C, 1.0 C and 2.0 C, corresponding cycle depths in the new state of cells are 98%, 94% and 76%, respectively. With the progress of aging, the values of the cycle depth are additionally reduced due to an increase of impedance. The *prevalence of the effect of the depth of discharge, compared with the one of the discharging rate itself*, is further clarified in the following example.

A break of 20 min was kept between half cycles in all test cases. As a consequence, after the discharging end voltage of 3.0 V had been reached, the cell potentials relaxed for 20 min until the start of the upcoming charging process. The relaxed value of the respective cell potentials can be used to estimate the depth of discharge, which qualitatively corresponds with the delithiation degree of the anode. A high amount of residual lithium, which cannot be deintercalated from the anode, leads to higher values of the relaxed cell potential after discharge. Figure 27 shows the development of the relaxed cell potential in the principally discharged state versus EFC for the investigated discharging rates. For the test cases with a

discharging rate of 0.5 C and 1.0 C, the values of the relaxed cell potential are increased from 3.39 V and 3.45 V to 3.63 V and 3.74 V, respectively. Regarding the test case with the maximum discharging rate of 2.0 C, the relaxed cell potential is increased from 3.57 V to 4.03 V – although nonlinear aging did not emerge.

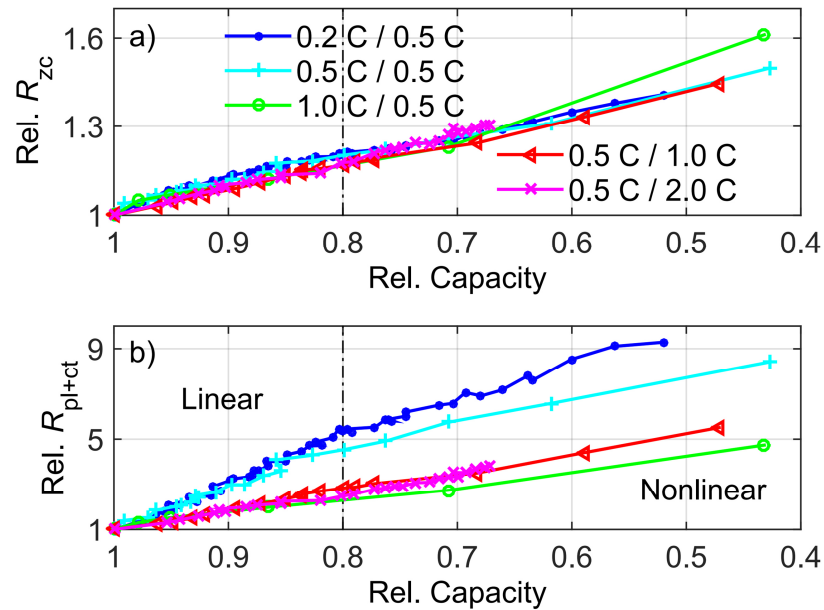


Figure 26: Clarification of approx. linear correlation between relative a) R_{zc} and b) R_{pl+ct} and corresponding values of capacity for the test cases presented in Figure 24 and Figure 25; in the legend, the first term represents the charging rate, the second the discharging rate. Constant parameters: $\Delta V = 1.2$ V, $T = 35$ °C; ID (legend top down, left right) = 6, 7, 8, 4, 9. Based on [140], extended data set.

Thus, it must be assumed that there is quite a lot of theoretically cyclable lithium buffered in the anode, which cannot be deintercalated due to excessive polarization under the discharging current load and the voltage limitation of the discharging process itself. As a consequence of this, the lower delithiation degrees of the anode might result in reduced graphite active material loss [94, 98]. In contrast, with regard to the accompanied increase of the mean SoC, also an enhanced growth of the SEI would be imaginable, but graphite active material loss is assumed to be dominating.

As a reduced depth of discharge or delithiation degree of the anode led to an avoidance of nonlinear aging, the observed effect was further examined by another experiment: therefore, a special test case with 0.5 C CCCV charging and 1.0 C CCCV discharging (2CCCV, no ID), respectively, was performed and compared to those only with CCCV charging (ID 4) or no CV phases at all (ID 3). The additional test case with $\Delta V = 1.2$ V and synchronous CCCV charging and discharging resulted in a cycle depth of 103% for new cells referred to the nominal capacity.

Termination condition in the CV phase at the discharging end voltage of 3.0 V was a current smaller than 0.1 C. In Figure 28, it is visible that the effect of nonlinear aging starts about 34% or 51% earlier referred to the test case with only CCCV charging or no CV phases at all, respectively. Thus, also this additional experiment shows the detrimental effect of discharging to low SoC, or alternatively a strong delithiation of the anode. Therefore, due to the prevailing effect of the depth of discharge, compared with the discharging rate itself, the latter is excluded from the load adaption experiments which are presented in Subchapter 6.2. The effect of the depth of discharge is anyway analyzed in terms of the voltage swing.

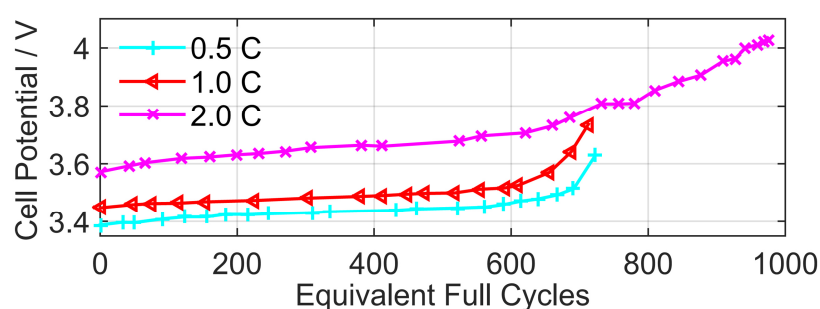


Figure 27: Development of the relaxed cell potential in the discharged state of cells versus equivalent full cycles for the investigated discharging rates (see Figure 25). Constant parameters: $\Delta V = 1.2$ V, $I_{Ch} = 0.5$ C, $T = 35$ °C; ID (legend top down) = 7, 4, 9. [140]

The different parameters, which have been analyzed so far with respect to their effect on the phenomenon of nonlinear aging, i.e., the voltage swing and the current rate (charging and discharging), are easily adaptable in a SLC. In the following subchapter, the effect of the ambient temperature on the onset of nonlinear aging is analyzed. As the sudden increase of the aging rate is associated with lithium plating, it is assumed a priori that low temperatures provoke nonlinear aging. Generally, regarding the implementation of SLC, it must be considered that cooling or heating of battery systems is energy-intensive. Thus, in comparison with excessive temperature conditioning, an adaption of electrical parameters (voltage swing, current rate) should be favored in terms of efficiency. In terms of heating, though, at least unavoidable heat buildup can be gainfully reused.

6.1.3 Dependency on the Temperature

With regard to Table 1, a first set of test cases, which address the effect of the ambient temperature, was conducted with a voltage swing $\Delta V = 1.2$ V, a charging rate (CCCV) of 0.5 C, and a discharging rate (CC) of 1.0 C. Respective cells were cycled in self-built climate chambers at 25 °C (ID 10), 35 °C (ID 4) and 50 °C (ID 11). In addition, a second set of test cases with a

reduced voltage swing $\Delta V = 0.94$ V, but same current rates, was conducted at 35 °C (ID 2) and 50 °C (ID 12).

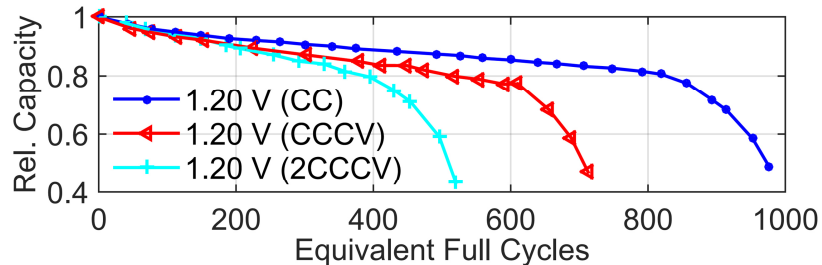


Figure 28: Development of the relative capacity versus equivalent full cycles for different cycling processes; the abbreviations in the legend characterize the charging process; 2CCCV represents a synchronous cycling with CCCV charging and CCCV discharging. Constant parameters: $I_{Ch} = 0.5$ C, $I_{Dis} = 1.0$ C, $T = 35$ °C; ID (legend top down) = 3, 4, special case (no ID). [140]

Figure 29 a) shows the development of the relative discharge capacity versus EFC for both sets of test cases. For the set with $\Delta V = 1.2$ V, cycling at the lowest temperature, i.e., 25 °C, results in the quickest occurrence of the turning point. In comparison, for the test case at 50 °C, the number of EFC before reaching the turning point is prolonged at about 8%. The test case between those boundaries, i.e., at a temperature of 35 °C, seems to be the optimum resulting in a prolongation of the linear area of roughly 40% referred to the test case at 25 °C. Regarding the reference test cases in the two-step temperature adaption experiment (identical setup except CC instead of CCCV charging, see Figure 32), same rank order is obtained regarding the emerging aging rates (35 °C < 50 °C < 25 °C). For the second set of test cases with a reduced voltage swing $\Delta V = 0.94$ V, the capacity fade rate at 35 °C compared with 50 °C is smaller at first, but only for the test case at the lower temperature, a turning point to nonlinear aging is observable (even though it appears only less pronounced). Figure 29 b) and c) show the corresponding development of R_{zC} and R_{pl+ct} versus EFC, respectively. A negative correlation with regard to respective capacity values is again noticeable with one exception: regarding the development of R_{zC} in Figure 29 b), its increase for the test case with a reduced voltage swing $\Delta V = 0.94$ V at a temperature of 50 °C is disproportionately strong and starts to stagnate at about 1100 EFC.

It is assumed that time controlled aging mechanisms have led to a strong rise of R_{zC} but to a comparably low fade of capacity for cycling with a rather mild load profile at a high ambient temperature. Such a behavior could principally originate from an excessive growth of passive layers and/or a loss of conducting salts in the electrolyte [76, 77]. However, it is astonishing that the corresponding development of R_{pl+ct} is inconspicuous. In any case, such an ambiguous behavior is known for C//NMC cells, and was e.g. associated in [141] with time controlled mechanisms.

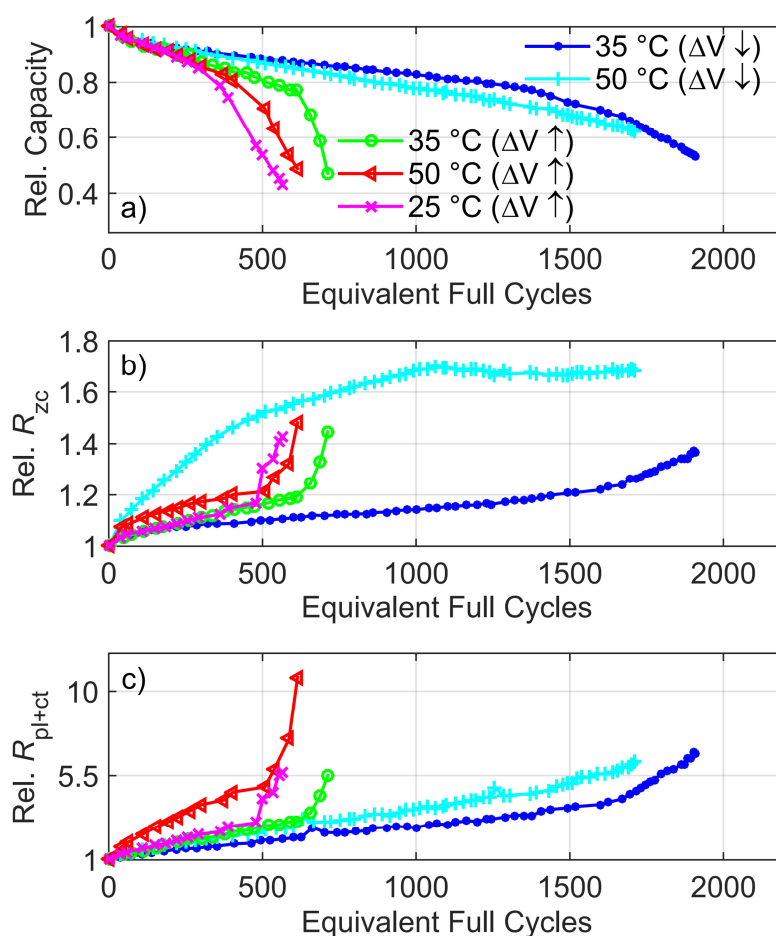


Figure 29: a) Development of the relative capacity versus equivalent full cycles in dependency on the temperature upon prolonged cycling; b) and c) show the corresponding development of R_{zc} and R_{pl+ct} , respectively; the abbreviations in the legend characterize the test cases with $\Delta V = 1.2 \text{ V}$ (\uparrow) and $\Delta V = 0.94 \text{ V}$ (\downarrow). Constant parameters ($\Delta V \uparrow$): $\Delta V = 1.2 \text{ V}$, $I_{Ch} = 0.5 \text{ C}$ (CCCV), $I_{Dis} = 1.0 \text{ C}$; constant parameters ($\Delta V \downarrow$): $\Delta V = 0.94 \text{ V}$, $I_{Ch} = 0.5 \text{ C}$ (CC), $I_{Dis} = 1.0 \text{ C}$; ID (legend top down, left right) = 10, 4, 11, 2, 12. [140]

Figure 30 a) and b) clarify the correlation behavior between R_{zc} and R_{pl+ct} and the corresponding values of capacity, respectively. The assumption of a linear relationship is again justified; except for the test case with a voltage swing $\Delta V = 0.94 \text{ V}$ and a temperature of $50 \text{ }^\circ\text{C}$, the stagnating increase of R_{zc} in combination with an ongoing fade of capacity results in a nonlinear relationship.

The observance of a temperature optimum, with an increase of the cyclic aging rate at lower and higher temperatures, is well-known in the literature. For temperatures lower than the optimum, lithium plating is said to dominate, whereas excessive passive layer growth is the prevailing mechanism at enhanced temperatures. However, as the temperature optimum is regularly found to be in the near of $25 \text{ }^\circ\text{C}$ (as e.g. in [70]), the shift to $35 \text{ }^\circ\text{C}$ in the presented experiment is regarded as a sign of the investigated type of cell of a strong susceptibility to lithium plating.

Unfortunately, if the temperature optimum is shifted to higher values, this is due to the dominating effect of lithium plating compared with the growth of passive layers (in accordance with the observed rank order of aging rates which is $25\text{ }^{\circ}\text{C} > 50\text{ }^{\circ}\text{C} > 35\text{ }^{\circ}\text{C}$). However, nonetheless, at enhanced temperatures, passive layer growth is increased with regard to the Arrhenius law. For the same LIC model as is inspected in this work (IHR18650A by E-One Moli Energy Corp.), it was shown in [93] that the area of linear aging could be extended (which corresponds to the avoidance of lithium plating) by filling the cells with a mixture of different electrolyte components which synergistically prevent excessive SEI growth. Thus, a sense of balance is needed in the mechanical design and chemical engineering of LIC to reach a desired value of optimal operational temperature. Looked at it from the other side, however, for a given type of cell, operational strategies can always be optimized by electrical engineering to maximize the reachable service life.

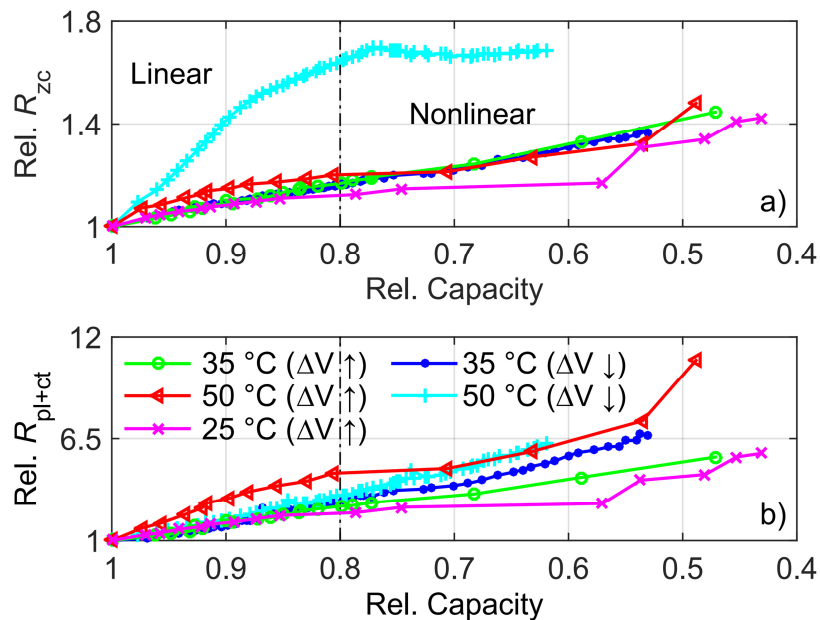


Figure 30: Clarification of approx. linear correlation between relative a) R_{zc} and b) R_{pl+ct} and corresponding values of capacity for the test cases presented in Figure 29. Constant parameters ($\Delta V \uparrow$): $\Delta V = 1.2\text{ V}$, $I_{Ch} = 0.5\text{ C}$ (CCCV), $I_{Dis} = 1.0\text{ C}$; constant parameters ($\Delta V \downarrow$): $\Delta V = 0.94\text{ V}$, $I_{Ch} = 0.5\text{ C}$ (CC), $I_{Dis} = 1.0\text{ C}$; ID (legend top down, left right) = 10, 4, 11, 2, 12. [140]

In any case, the observances implicate that, with regard to the implementation of SLC, *rather heating than cooling* is useful to avoid the effect of nonlinear aging (as lithium plating is the cause). As aforementioned, however, a suitable adaption of electrical parameters is always to prefer in terms of the battery system's efficiency. Nonetheless, as the voltage swing, the charging rate and the temperature were shown to affect the onset of nonlinear aging, these parameters are raised as *final control elements* in the following load adaption experiments.

6.2 Influence of the Operational Prehistory

Lithium plating, which results in an adverse circle of cyclable lithium and graphite active material loss, is regarded as the cause of the phenomenon of nonlinear aging [144]. The onset of nonlinear aging, which is observed at residual capacities of approx. 80%, can be delayed or even prevented by [140]:

- a reduced voltage swing (decreased charging and/or increased discharging end voltage)
- a reduced charging rate
- operation at the cell specific temperature optimum

In the first phase of the conducted aging experiments, the described relations were determined based on cycling cells from the beginning with different values of each investigated parameter. Regarding the implementation of SLC, however, the basic idea is to reuse a pre-aged ALIB in a SLA. Thus, it is of major importance to analyze the influence of the operational prehistory. In the ideal case, exemplarily, as it was shown that the charging rate does not impact the aging behavior as long as an aging dependent threshold value is not exceeded, for a certain state of aging, the threshold value would be the same, independent from the operational prehistory. Therefore, in the experiments which aim at assessing the controllability of nonlinear aging (presented in Subchapter 6.2.1.1), the control element parameters (ΔV , charging rate, temperature) are *two-step adapted at a mean residual capacity of 85%*. If the phenomenon of nonlinear aging is independent from the operational prehistory, the turning point would be exactly shifted from the *challenging base case* (see respective nonlinear aging characteristics in Figure 11 and Subchapter 5.2) to the *mild reference load profile*. In practice, however, it can be assumed that the turning point lies somewhere in between the two.

Furthermore, as the required perfect foresight, which is available for the laboratory two-step parameter adaption experiments, is missing in the field, the turning point to nonlinear aging must not be missed under any circumstances. At the *point of no return*, i.e., when the aging rate starts to increase, it is assumed within the scope of this work that the mentioned adverse circle of cyclable lithium and graphite active material loss inevitably leads to a quick breakdown of capacity (and intense impedance increase). As lithium plating is said to considerably reduce the safety of a cell, its appearance should be regarded in any case as the ultimate EoL condition (compare with the discussion in Subchapter 3.4). Nevertheless, in Figure 31, the development of the relative capacity versus EFC is shown for the reference base case (ID 3), with a reduction of the load clearly after the onset of nonlinear aging ($\Delta V = 1.2 \text{ V} \rightarrow 0.94 \text{ V}$, $0.5 \text{ C} \rightarrow 0.2 \text{ C}$ charging (CC), $1.0 \text{ C} \rightarrow 0.5 \text{ C}$ discharging (CC)). By that, the aging rate in the nonlinear area is slightly reduced, but still outclasses the one in the linear area, where lithium plating is assumed to have not emerged. As a conclusion, lithium plating might be debilitated by load adaption but nevertheless is present at every charging process.

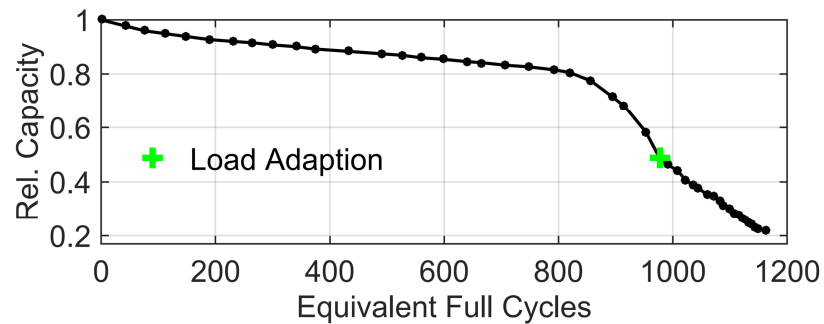


Figure 31: Development of the relative capacity versus equivalent full cycles for the reference base case (ID 3), which is adapted after the occurrence of nonlinear aging (at a residual capacity of approx. 50%).

Considering the share of the irreversible and reversible part of lithium plating, it was stated in [102] that the latter would dominate by far. However, as the authors of the study provoked lithium plating by only one overstraining charging process, the statement might not be exactly representative within the scope of this work (in which plating is provoked upon prolonged cycling). Hence, a simple explanation which basically well suits to the idea of the mentioned adverse circle is given here: beginning from the onset of nonlinear aging, with every subsequent charging process, the anodic overpotential and graphite active material loss proceeds to increase; as a consequence, with regard to the constant load parameters in the laboratory aging experiments, the total amount of plated lithium should be continuously increased as well. Thus, if only assuming that the share of both parts stays constant, the absolute amount of irreversibly plated lithium is enhanced likewise with every charging process. A methodology which reliably quantifies the share of the reversible and irreversible part of lithium plating, however, is not yet state-of-the-art, and thus, further research is recommended in this field.

As it was described before, the charging rate is observed (approx.) to not affect the aging behavior for as long as a critical threshold value is not exceeded (see Figure 24). However, if the aging dependent threshold value is exceeded, the emerging lithium plating results in an adverse circle which in turn provokes nonlinear aging. Therefore, presented in Subchapter 6.2.1.2, for an aging quick test experiment, cells were operated with the maximally allowed charging rate of 1.0 C, yet adapting it continuously (with every checkup) referred to the observed fade of capacity.

Under the assumption, that the maximally allowed charging rate, which is given by the manufacturer, exactly coincides with the mentioned threshold value (where barely no lithium plating occurs), continuous adaption would theoretically lead to the fastest charging process during the progress of aging which is possible without provoking lithium plating and thus, nonlinear aging. Although LIC manufacturers yet recommend decreasing the charging rate to increase the service lifetime of their products, this is usually not referred to the effect of nonlinear aging but to the area of linear aging (which is not useful for the inspected LIC model as the

aging behavior is only influenced by the charging rate if a critical threshold value is exceeded). Henceforth, in any case, the suggested approach is entitled as *close-to-the-edge charging*, inspired by the aforementioned critical threshold value. The respective approach has been applied for patent by the authors of [181].

Finally, in Subchapter 6.2.2, the effects of different long-term storage conditions before cell operation (at first time) are analyzed and assessed. Presented results shall give an impression on the usability of “old” LIC, like such which have been remained in the shelf for a long time; theoretically, if e.g. passive layers have excessively grown during long-term storage, also moderate charging loads might immediately provoke nonlinear aging due to increased impedances. In contrast to that, approaches to intentionally pre-store cells with the aim of optimizing the formation process and thus decelerating the aging rate in the subsequent operation, as investigated in [183], are beyond the scope of this work and thus not considered.

6.2.1 Controllability of Nonlinear Aging Behavior

6.2.1.1 Two-Step Parameter Adaption

Figure 32 shows the development of the relative discharge capacity versus EFC upon prolonged cycling for the challenging reference base case, for the respective mild reference load profiles and the ones with the corresponding two-step parameter adaption. The black circles mark the adaption moment (which is at a mean residual capacity of 85%). In Figure 32 a), by comparing the curves of the reference test cases (with $\Delta V = 1.2 \text{ V}$ and 0.94 V) with the load adapted one (ID 13), it is observable that the latter lies in between the two reference curves, as expected. In comparison with the reference base case, the onset of nonlinear aging can clearly be delayed. The gradients of the adaption test case correspond approx. with the respective reference; that is, the negative gradient is slightly attenuated after load adaption. Especially the comparably mild appearance of nonlinear aging characteristics of the reference test case with $\Delta V = 0.94 \text{ V}$ is similar to the one of the adaption test case, at what, however, starts to occur slightly in advance. Thus, as a conclusion from the findings of the first control element parameter, there might be an *effect of the operational prehistory*, which is however, *only less pronounced*.

Figure 32 b) contains the respective plots regarding the charging rate. As aforementioned, there are no different gradients in the capacity development detectable for different rates (in the linear area of aging); i.e., the aging behavior appears to be independent of the charging rate. For the mild reference with a charging rate of 0.2 C (ID 14), no onset of nonlinear aging has been detectable within the timeframe of this work. After having passed the turning point to nonlinear aging of the reference base case with a charging rate of 0.5 C , the capacity fade of the charging rate adapted test case (ID 15) continues linearly. Although the length of the mild reference curve is inadequate to give a precise statement, an ongoing linear development can be assumed, as the development of the adaption test case is likewise linear for more than 300 EFC. Thus, from

the findings of the charging rate, *independency from the operational prehistory can be concluded.*

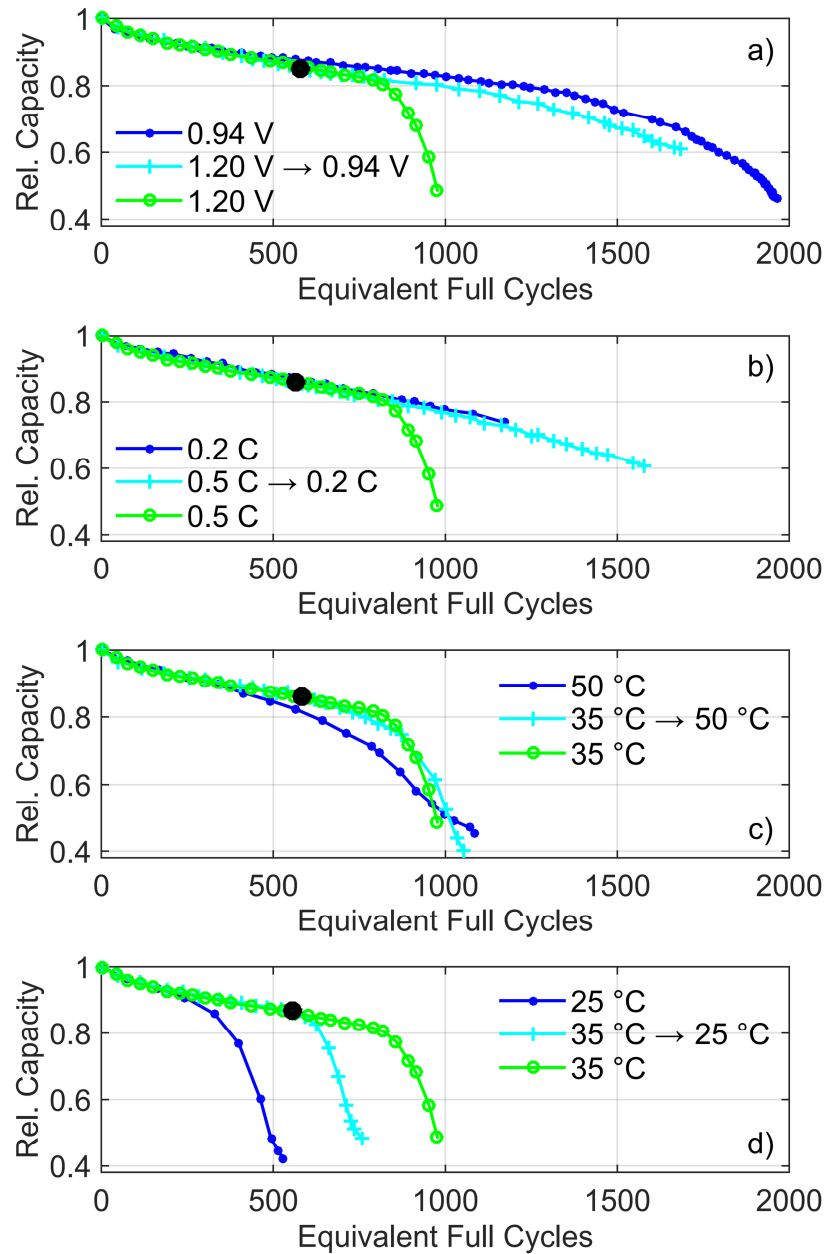


Figure 32: Development of the relative capacity versus equivalent full cycles upon prolonged cycling for the challenging reference base case, for the mild reference load profiles and the ones with the corresponding load adaption (marked by black circles): a) voltage swing, b) charging rate, c) temperature increase, d) temperature decrease. Constant parameters: a) $I_{Ch} = 0.5 C$, $I_{Dis} = 1.0 C$, $T = 35 °C$; b) $\Delta V = 1.2 V$, $I_{Dis} = 1.0 C$, $T = 35 °C$; c) & d) $\Delta V = 1.2 V$, $I_{Ch} = 0.5 C$, $I_{Dis} = 1.0 C$; ID (legend top down) = a) 2, 13, 3; b) 14, 15, 3; c) 16, 17, 3; d) 18, 19, 3.

In Figure 32 c) and d), the adaption experiments of increasing and decreasing the temperature are shown, respectively. As the temperature optimum for the investigated type of cell is at 35 °C, for both experiments, pronounced aging or, more precisely, an accelerated onset of nonlinear aging is expected. Indeed, the assumption attunes for both the temperature increasing (ID 18, 19) and decreasing experiment (ID 16, 17); as the reference base case turning point to nonlinear aging has already been passed at the moment of load adaption, after it, as a consequence, the capacity fade rate immediately starts to increase. Compared with the experiment of increasing the temperature, the onset of nonlinear aging after lowering the temperature is clearly more pronounced and erratic; a simple explanation for a smaller gradient in the nonlinear area for increasing the temperature could be a mixture of responsible causes: assuming that nonlinear aging at low temperatures originates purely from lithium plating without the occurrence of further side reactions, high temperature nonlinear aging could be lithium plating, which is, however, superposed or accompanied by strong passive layer growth. Simply said, for a given lithium inventory, the part which is lost to passive layer growth cannot be lost anymore to lithium plating, which is why the latter appears debilitated. Conclusions on the impact of the operational prehistory are not feasible with regard to the temperature adaption experiments, but there is a clear *causative relationship* detectable: if it is switched from a mild to a challenging load, at a number of EFC for which nonlinear aging has already onset for the reference of the latter, also for the adaption test case, capacity fade will immediately start to increase.

Figure 33 a) jointly shows the relative discharge capacity development versus EFC for the reference base case and the load adaption test cases (regarding the temperature, only the increase of it), which have been presented so far. By it, the even slightly pronounced effect of reducing the voltage swing, compared with the charging rate, on the aging behavior of the investigated cell, is visualized. Figure 33 b) and c) show the corresponding development of R_{zc} and R_{pl+ct} versus EFC, respectively. Again, the development of both impedance parts clearly appears to negatively correlate with the respective capacity values. Furthermore, an additional adaption test case “All” (ID 20) is included in Figure 33, which combines the different parameter adaptations of the three other test cases ($\Delta V = 1.2 \text{ V} \rightarrow 0.94 \text{ V}$, $0.5 \text{ C} \rightarrow 0.2 \text{ C}$ charging (CC), $35 \text{ °C} \rightarrow 50 \text{ °C}$). For it, the beneficial effect of decreasing the voltage swing and the charging rate is obvious with regard to the prolonged linear area of aging. Nonlinear aging does not occur for the all combining test case. However, in addition, the disadvantageous effect of increasing the temperature is observable as well, as the capacity fade rate in the linear area is higher compared with the test cases of only decreasing the voltage swing or the charging rate.

As a conclusion from the two-step parameter adaption experiments, for both the voltage swing and the charging rate, a reduction leads to a clear prolongation of the reachable service life, which is promising in terms of SLC implementation. Based on these two experiments, the impact of the operational prehistory (on the onset of nonlinear aging) can be regarded as marginal, which reduces the complexity of predicting the forthcoming aging behavior of a LIC.

Furthermore, a causative relationship can be derived from the temperature experiments, as switching away from the optimum immediately triggers nonlinear aging in both cases. Considering a temperature adaption experiment in which the temperature is switched to the optimum, a delay or prevention of nonlinear aging is regarded as the most likely result. In the following, in contrast to the described two-step parameter load adaption, the results of the continuous charging rate adaption experiment are presented.

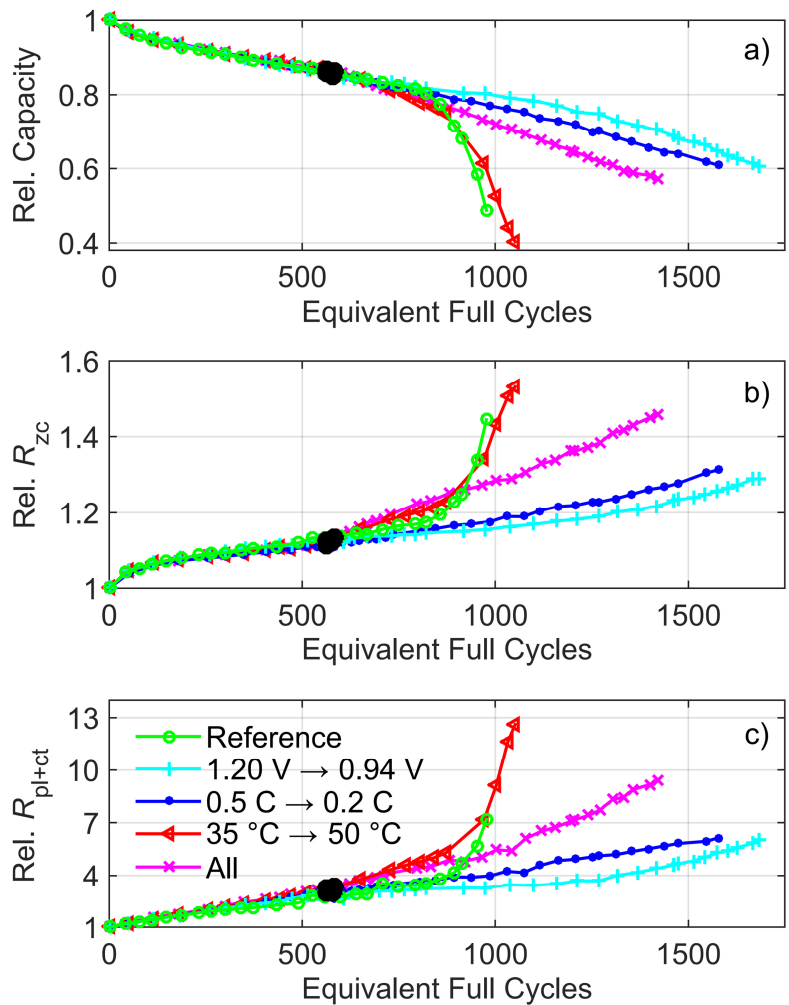


Figure 33: a) Development of the relative capacity versus equivalent full cycles upon prolonged cycling for the reference base case and the conducted load adaption test cases (marked by black circles); b) and c) show the corresponding development of R_{zc} and R_{pl+ct} versus EFC, respectively. ID (legend top down) = 3, 13, 15, 19, 20.

6.2.1.2 Continuous Charging Rate Adaption

The investigation of the effect of a continuous charging rate adaption has been conducted within an aging quick test experiment. At the start of it, with regard to the maximally allowed charging rate of 1.0 C for all adaption test cases, relevant reference is the test case with constant 1.0 C CCCV charging (ID 8). As the rates of the adaption test cases are decreased in accordance with Equation (13) (see Subchapter 5.2) up to a charging rate of approx. 0.1 C (for $\delta = 2$ and 4), an additional mild reference is given with constant 0.2 C CCCV charging (ID 6). The references correspond with the respective curves of the charging rate experiment which was shown in Figure 24. As the operation with a charging rate of 1.0 C led almost instantaneously to the effect of nonlinear aging, and adapted test cases are cycled for one week (until to the next checkup) with this maximally allowed rate, cell prejudice must be accepted within the scope of the aging quick test experiment. The term *close-to-the-edge charging* expresses the aim of charging with the aging dependent maximal rate which just does not trigger nonlinear aging. With regard to the capacity fade rate, the gain factor δ controls the extent of current reduction; in accordance with Equation (13), for a capacity loss of 5%, exemplarily, a gain factor $\delta = 1$ or 4, leads to a corresponding reduction of the charging rate of 5% or 20%, respectively. As a consequence, a higher gain factor guarantees a more safe operation with a decelerated aging behavior which is, however, paid by the price of a slower charging process.

Figure 34 a) shows the relative discharge capacity development versus EFC for the references and the adaption test cases of the experiment regarding the effect of a continuous charging rate adaption (with every checkup). Figure 34 b) shows the development of corresponding charging rates. It is observable for the adaption test case with a $\delta = 1$, that the effect of nonlinear aging is only slightly debilitated compared with the challenging reference with a constant rate of 1.0 C. Thus, as already assumed from the constant charging rate experiment, to keep the idea of the close-to-the-edge charging process, the maximal charging rate of 1.0 C (which is given by the manufacturer), is actually too high for the investigated type of LIC. Thus, as the *capacity-related charging rate stays constant without a gain* (i.e., $\delta = 1$), the adapted rate permanently exceeds the charging current capability of the cell at the same extent than when charging with 1.0 C in the new state.

In contrast to it, with an increase of the gain factor, the respective charging rates obviously fall below the critical threshold value with the progress of aging, as for both test cases (with a $\delta = 2$ and 4), nonlinear aging can be avoided within the timeframe of the experiment. Regarding the shape of the curve with a $\delta = 2$, nonlinear aging has apparently already started to onset, but could barely be suppressed by the continuous reduction of the charging rate. As the start of nonlinear aging was denoted before as a *point of no return*, due to the adverse circle of cyclable lithium and graphite active material loss which is inflicted by lithium plating, the term might only be adequate in the case of an operation with a constant load (like the charging rate). Regarding

an operation which considers cell aging, *the so called adverse circle is obviously possible to escape from*. Though, in any case, as the capacity fade rate of the test case with a $\delta = 2$ clearly outclasses the one of the reference with constant 0.2 C charging, the yielded quicker charging (up to approx. 350 EFC) is in no relation with the severely reduced service life.

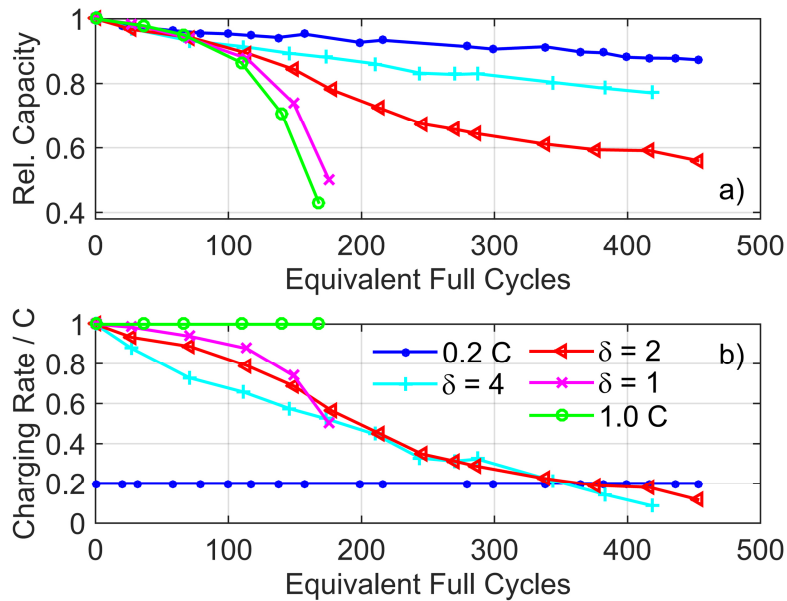


Figure 34: a) Development of the relative capacity versus equivalent full cycles for the test cases of the continuous charging rate adaption experiment; b) shows the development of corresponding charging rates; the gain factor δ controls the extent of current reduction. Constant parameters: $\Delta V = 1.2 \text{ V}$, $I_{\text{Dis}} = 1.0 \text{ C}$, $T = 35 \text{ }^\circ\text{C}$; ID of references (left right) = 6, 8. **Based on [181], extended data set.**

For the test case with a $\delta = 4$, the aging behavior stays completely linear within the timeframe of the experiment. However, the gradient in the linear area of aging is slightly more negative compared with the reference of constant charging with 0.2 C. At a number of approx. 350 EFC, as for the adaption test case with a $\delta = 2$, the charging rate is reduced to 0.2 C, which corresponds to the rate of the mild reference. However, in contrast to the smaller gain, the capacity fade rate is only slightly higher compared with the reference, but up to 350 EFC, the average charging rate is threefold as high. Thus, it depends on the individual application and the users' specific needs if the adapted test case would be preferred before the mild reference. The experiment of continuous charging rate adaption ended, as, for the test case with the maximal gain $\delta = 4$, the current had to be reduced below the value of the termination condition in the CCCV charging process (which was 0.1 C).

The presented close-to-the-edge charging process is beneficial for the maximal gain $\delta = 4$, if a high charging rate is preferred before a long service life (e.g. conceivable in the consumer electronics domain). However, the suggested charging process might be more useful for a

decreased charging rate in the beginning of operation, as cell prejudice would be reduced as a consequence. Alternatively, further functional interrelations of adapting the charging rate (referred to the capacity fade) should be tested, as it seems that the applied approach (according to Equation (13)) causes a charging rate adaption, which is too mild in the beginning of operation but progressively too low in the end. A multi-step charging rate adaption approach, in which aforementioned gain factors at high SoH are proportionately higher than at low SoH, is promising to solve this issue.

Moreover, as the presented experiment considered only the charging rate as control element parameter, a superior close-to-the-edge charging process should be designed based on the optimization of a variety of parameters (like voltage swing, charging rate, temperature, operational prehistory, etc.). In the following, the effects of different long-term storage conditions before the first time operation of a LIC are analyzed and assessed.

6.2.2 Storage Conditions before Cycling

As described in the beginning of Chapter 3, most models of LIC with layered transition metal cathodes (like NMC) suffer from calendric aging, which is generally increased at enhanced SoC and temperatures. The main aging mechanism under storage is the growth of passive layers [68, 69]. As a result of it, the capacity fades due to the loss of cyclable lithium; however, even more prevailing is the associated increase of impedance. Regarding the test cases with mild compared to challenging load profiles (for which time dependent aging mechanisms are assumed to dominate), the increase of impedance is higher at the same residual capacity, as is known from Figure 26 and Figure 30. The phenomenon, which is possibly related to the multilayered structure of the passive layers, is comprehensively analyzed in Chapter 8 (in addition, see Subchapter 3.2).

Figure 35 shows the relative discharge capacity development versus storage time in weeks for cells which have been stored at a SoC = 0%, 10%, 50%, 90% or 100% and a temperature of either 35 °C (ID 21-25) or 50 °C (ID 26-30). For both temperatures, the aging rate is increased with an increase of the SoC. Regarding the effect of the temperature, by comparing the residual capacity values of cells with a SoC = 100% at the end of the experiment (week 84), it can be estimated that an increase of 15 K leads to a doubled rate of calendric aging. As aforementioned, for LIC models with graphite anode and NMC cathode, calendric aging which is increased with increasing SoC and temperature is reported in the literature as well [65].

However, there is a currently inexplicable phenomenon as the capacities of cells with a SoC = 0% and 100% (and SoC = 10% at 35 °C) slightly rise from the new state to the next measuring point, even if respective cells have been preloaded with four cycles to avoid ongoing formation processes. For the cells stored at a SoC = 100%, only due to the more negative gradient of the capacity fade after this increase, the expected aging rate rank order ($0\% < 10\% < 50\% < 90\% <$

100%) is consecutively reached again. As a hypothesis, a long storage time at extreme SoC maybe provokes charge equalization processes in far-flung anode active material like in overlapping electrode areas or outermost layers (due to potential gradients). To test this hypothesis, calendric aging experiments with fully charged and discharged LIC models in different mechanical designs but with identical active materials should be conducted.

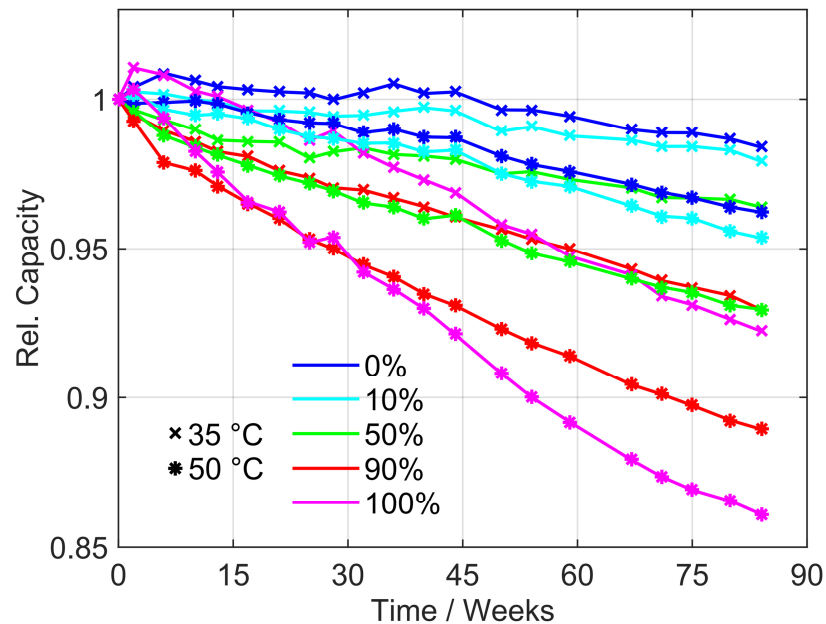


Figure 35: Development of the relative capacity versus storage time (in weeks) in dependency on the state of charge and temperature. ID (legend top down) = 21-30.

Regarding the effect of different long-term storage conditions before the first time operation of a LIC, an excessive impedance increase could quickly provoke lithium plating and thus, in turn, the breakdown of cell capacity. After the calendric aging experiment had been finished (week 84), the long-term stored cells were started to be operated with the reference base case (ID 3) of the two-step parameter adaption experiment ($\Delta V = 1.2 \text{ V}$, 0.5 C charging (CC), 1.0 C discharging (CC), $35 \text{ }^\circ\text{C}$). Figure 36 a) and b) present the relative discharge capacity development versus EFC of the mentioned reference test case and of the cells which have been stored in advance for 84 weeks at $35 \text{ }^\circ\text{C}$ and $50 \text{ }^\circ\text{C}$, respectively. To enable a better comparison with the reference, based on their initial residual capacity value, the curves of pre-stored cells were shifted to the corresponding residual capacity value of the reference. By that, the effect of pre-storing cells at different storage conditions can easily be assessed.

Regarding the test cases at $35 \text{ }^\circ\text{C}$ in Figure 36 a), those cells which have been stored in advance at a SoC = 100% and 90% immediately show a breakdown of cell capacity. In contrast, cells which have been stored in advance at a SoC = 0%, 10% or 50% basically behave like the

reference test case within the timeframe of the experiment. In Figure 36 b), it is observable that even capacities of cells which have been stored at 50 °C and low SoC break in after only a comparably low number of EFC. At high SoC and high temperatures, the growth of the SEI is accelerated, which leads to increased overpotentials at the anode. As a consequence, the anode potential is more prone to drop below the critical value of 0 V vs. Li/Li⁺ at the end of a charging process. Plated lithium then leads to an adverse circle which expresses itself as nonlinear aging [140, 144].

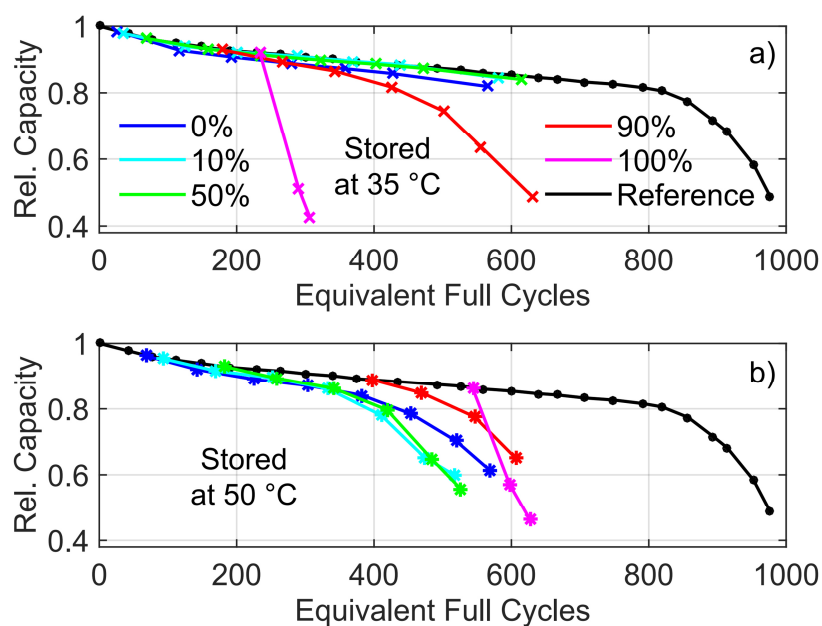


Figure 36: Development of the relative capacity versus equivalent full cycles of pre-stored cells and of the reference test case; based on their initial residual capacity value, curves of pre-stored cells were shifted to the corresponding value of the reference. Constant parameters: $\Delta V = 1.2$ V, $I_{Ch} = 0.5$ C, $I_{Dis} = 1.0$ C, $T = 35$ °C; reference ID = 3.

The presented results underline the importance of the storage SoC, especially in terms of the observed breakdown of cell capacity. With regard to cells, which have been in the shelf for a long time, usually storage SoC and temperature are adequately low. With regard to the aging behavior of the investigated type of cell, this is clearly recommended as test cases at 35 °C and low SoC (see Figure 36 a) *basically still behave like new cells* after a storage time of 84 weeks.

For that reason, the motivation for a current project of the Deutsche ACCUotive and the municipal utilities of Hannover, in which a storage with a capacity of 15 MWh (consisting of 3000 ALIB for E-Smarts) is used for PCRR to avoid long storage periods, is questionable; the pre-use of ALIB in the parts warehouse (before operation in the BEV) as a storage for PCRR is proposed to avoid the crucial effects of calendric aging, whereas simultaneously, economic profits can

even be generated [184]. This is regarded as interesting from the economic point of view, but as is observable from the presented pre-storage experiments, the effects of calendric aging on the performance of LIC can likewise be minimized by just choosing suited storage conditions.

In general, for applications with long inactive periods (such as BEV), optimized operational strategies should always aim at decreasing the storage SoC if possible (besides from temperature conditioning) [43]. With regard to the pre-aged state of SLB, due to the increased risk of nonlinear aging, related concern is even enhanced. In the following subchapter, the main results and statements of Chapter 6 are repetitively summarized.

6.3 Conclusion

In this chapter, the results of a large LIC aging experiment were presented; in the first phase of it, the parameters voltage swing, current rate and temperature were varied to detect their respective effect towards nonlinear aging (which is generally observed at residual capacities of approx. 80%). For the second phase, yielded results of the first one were used to define appropriate values of control element parameters. These in turn were used within further experiments which aimed at analyzing and assessing the controllability of nonlinear aging by either a two-step parameter (voltage swing, charging rate, temperature) or a continuous charging rate adaption. Furthermore, the effects of different long-term storage conditions before a first operation were investigated by combining calendric and cyclic aging experiments.

Lithium plating, which results in an adverse circle of cyclable lithium and graphite active material loss, is regarded as the cause of nonlinear aging. In accordance with the stress factors of lithium plating, i.e., high charging rates and end voltages at low temperatures, the onset of nonlinear aging could be offset within the first phase of aging experiments: while the maximally allowed charging rate of 1.0 C almost immediately triggered nonlinear aging, no increase of the aging rate was observed for the minimum charging rate of 0.2 C; a reduction of the voltage swing ΔV from 1.2 V to 0.94 V extended the area of linear aging around 42%. Regarding the temperature, an increase from 25 °C to 35 °C resulted in an extension of almost 40% before reaching the turning point, but cycling at 50 °C compared with 35 °C shortened the length of the linear area about 34%. To sum up, the onset of nonlinear aging could be delayed or even prevented by:

- a reduced voltage swing (decreased charging and/or increased discharging end voltage)
- a reduced charging rate
- operation at the cell specific temperature optimum

Between the development of considered impedance parts and corresponding capacity values, a linear negative correlation was clearly observable for almost all test cases, even after the onset of nonlinear aging; i.e., the impedance parts correspondingly exhibited an intense increase, simultaneously with the breakdown of capacity. The correlation between capacity fade and

impedance increase of LIC represents the base of a later presented (correlation based) aging quick test. Regarding its realization, an observed phenomenon could be critical: for test cases with a mild compared with a challenging load profile, impedance parts were observed to be higher at corresponding values of the residual capacity. The causes of the effect might be related to the multilayered structure of the passive layers (see Subchapter 3.2 and Chapter 8).

Regarding the results of the two-step parameter load adaption experiments in the second phase, for both, the voltage swing and the charging rate, a reduction led to a clear prolongation of the reachable service life, as nonlinear aging could be completely prevented. Due to the similar aging behavior of reference and adaption test cases, the effect of the operational prehistory appeared as only marginal. Furthermore, a causative relationship could be derived from the temperature experiments, as switching away from the optimum immediately triggered nonlinear aging in both the temperature increasing and decreasing experiment. In the reverse, considering the case of temperature adaption towards the optimum, a delay or prevention of nonlinear aging is assumed as the most likely result, as a consequence.

The close-to-the-edge charging process, which was derived from the continuous charging rate adaption experiment, was only useful for a gained adaption, as e.g. for a linear adaption of the current rate without a gain (referred to the capacity fade), capacity breakdown quickly occurred nevertheless. This was especially due to the acceleration of the aging experiment by starting with the maximally allowed charging rate of 1.0 C. However, for a reduced value of the charging rate in the beginning, the charging process, which considers the progress of aging, is regarded as promising and capable of enabling fast charging without a reduced service life.

The experiment, which addressed the effects of different long-term storage conditions before the first cell operation, underlined the detrimental effects of high storage temperatures and SoC. Only those cells which had been stored for 84 weeks at the lower temperature of 35 °C and lower SoC (0%, 10%, and 50%) could be operated afterwards in a satisfactory manner. The rest exhibited a quick breakdown of cell capacity from the beginning of operation.

With regard to the implementation of SLC, the findings on the effect of nonlinear aging are promising, as the adaption experiments clearly showed the possibility of extending the service life by load reduction. However, a major issue is to reliably predict the onset of nonlinear aging, which must not be missed under any circumstances. Thus, it is relevant to find the ideal hand-over time, i.e., when the respective ALIB is removed from the car, refurbished, and finally reused in a SLA as stationary energy storage (not compulsory). There, energy density is of minor importance and thus, the respective storage can simply be oversized to reach the required mild load profile (i.e., a reduced voltage swing and charging rate), with regard to the pre-aged state of the battery. Furthermore, regarding the effect of the temperature, especially low values are regarded as critical during operation (as the occurrence of lithium plating is promoted). Temperature conditioning should always ensure operation at the cell specific and aging

dependent temperature optimum (which is around room temperature). However, cooling or heating is in any case accompanied by a reduction of the battery system's efficiency. Contrary to active application periods, optimized operational strategies should always aim at decreasing the storage SoC and temperature, if possible, to avoid a strong rise of impedance. Due to the increased risk of nonlinear aging as a consequence of their pre-aged state, the related concern is especially enhanced for SLB. Finally, if the special characteristics of SLB are gratifyingly considered with regard to an adequate load and temperature, due to the resulting extension of the service life, SLC might be economically realizable (from the perspective of the aging behavior of a single LIC).

7 Lithium-Ion Cell-to-Cell Variation

Aside from the effect of nonlinear aging, the increasing cell-to-cell parameter variation is regarded as the second core issue towards the implementation of SLC. The value of the variation in the new state, which is a consequence of deviations in the production process, is inevitably increased with the progress of aging, even if the charge equalization and the temperature conditioning system work sufficiently effective. Regarding the implementation of SLC, cell-to-cell variation is crucial as only a fraction of the units of a BEV battery pack might be worthy to refurbish from an economic point of view. This is why the battery units must be measured to select only those, which are suitable for reuse. However, especially the measuring of capacity is time-consuming and thus, costly.

In complete, 484 new and 954 aged cells out of two identical BEV each (i.e., 1908 BEV cells in total) were characterized to yield a broad set of data for the distribution fit analysis, which is presented in Subchapter 7.1. Therein, the results are presented only from a pure mathematical perspective. However, afterwards in Subchapter 7.2, they are compared with the operational histories of the respective BEV (see Subchapter 5.3). Finally, as single cell outliers are capable of remarkably influencing whole cell compounds (in dependency on the respective cell interconnection configuration), they are characterized in Subchapter 7.3. Figure 37 clarifies the progress of work which is reached in Chapter 7.

With regard to the implementation of SLC, cell outliers are rather critical if the desired level of battery units, at which they are planned to be reinstalled in SLB, is the single cell; exemplarily, considering reuse constellations of large cells with bolted connections, the effect of cell-to-cell variation would be tremendous. However, reuse at the cell level is regarded as unlikely from the economic point of view, as, e.g., either the breakup of single cells' soldered joints or just the opening of bolts might be too costly even for large cells.

Regarding reuse constellations at the module level, cell outliers play only a minor role, if the BEV battery units consist of a large number of cells in parallel which is often the case. As a consequence, the effect of a single cell outlier is compensated. However, e.g. temperature gradients might result in whole areas of inferior and superior modules (in which all cells each are particularly bad or good) in a battery pack. Thus, as BEV modules are generally connected in series, the performance of the whole pack is limited to the worst; the sufficiently accurate online detection of wrongdoing modules, though, is currently not yet state-of-the-art, which is why modules must be costly measured to select those suitable for reuse. That is, cell-to-cell variation is rather relevant regarding the implementation of SLC, if not only single cell outliers are present, but cell-to-cell variation is scaled up to the next level due to affected whole areas of cell compounds (basically resulting in *module-to-module variation*). Regarding large-scale energy

storage projects with SLB, capacity measurement can probably be even skipped, as a scale-up effect of cell-to-cell or module-to-module variation is compensated by the high number of cells or modules, respectively; thus, it might be adequate, as a consequence, to select similar ones only based on comparing the mileage and the mean logged temperature values.

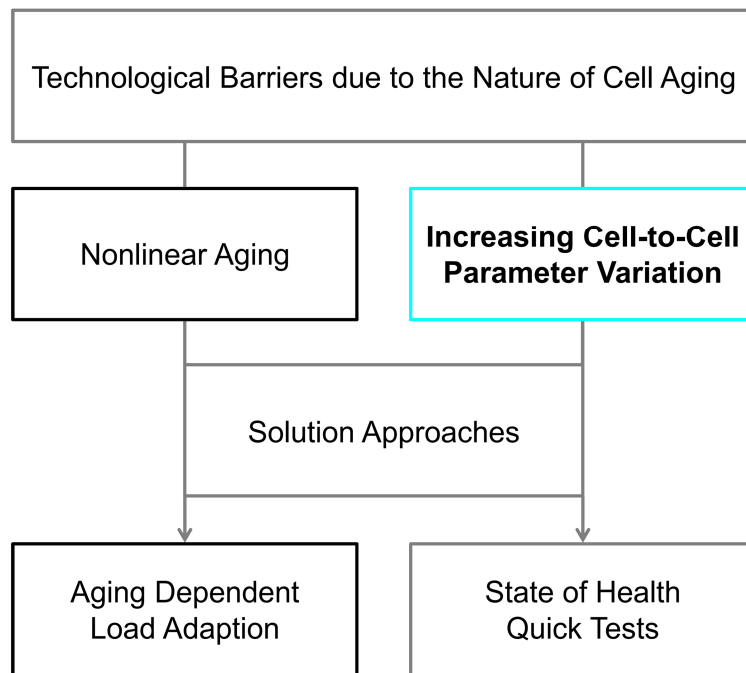


Figure 37: Progress of work in Chapter 7: the box of the presented core issue (increasing cell-to-cell variation) is colored in cyan.

7.1 Distribution Fit Analysis

This subchapter deals with the distribution of capacity, R_{zc} and R_{pl+ct} with consideration of all cells in the new and the aged state (out of BEV1 and BEV2). At first, no distinction is made regarding the position of cells in a module or of modules in the battery pack; likewise the influence of interconnections, the direction of the cooling air flow etc. is not considered. Focus is on the pure statistical analysis of the overall amount of investigated cells. All statistical calculations were thereby performed by use of the MATLAB Statistics Toolbox. Figure 38 shows nine histograms of the relative frequency of capacity, R_{zc} and R_{pl+ct} (row 1 - 3) for the batches of new cells, BEV1 and BEV2 (column a) - c)). Histograms are fitted to normal distribution according to Equation (4), represented by solid lines. Additionally, two-parameter Weibull distribution fits, marked by dotted lines, are calculated according to Equation (6). The two- instead of three-parameter Weibull distribution is chosen because no minimum life parameter γ

can be given as e.g. the capacity could drop to zero for a cell which has been cycled long enough. In addition, vertical dashed lines mark the mean values of each histogram.

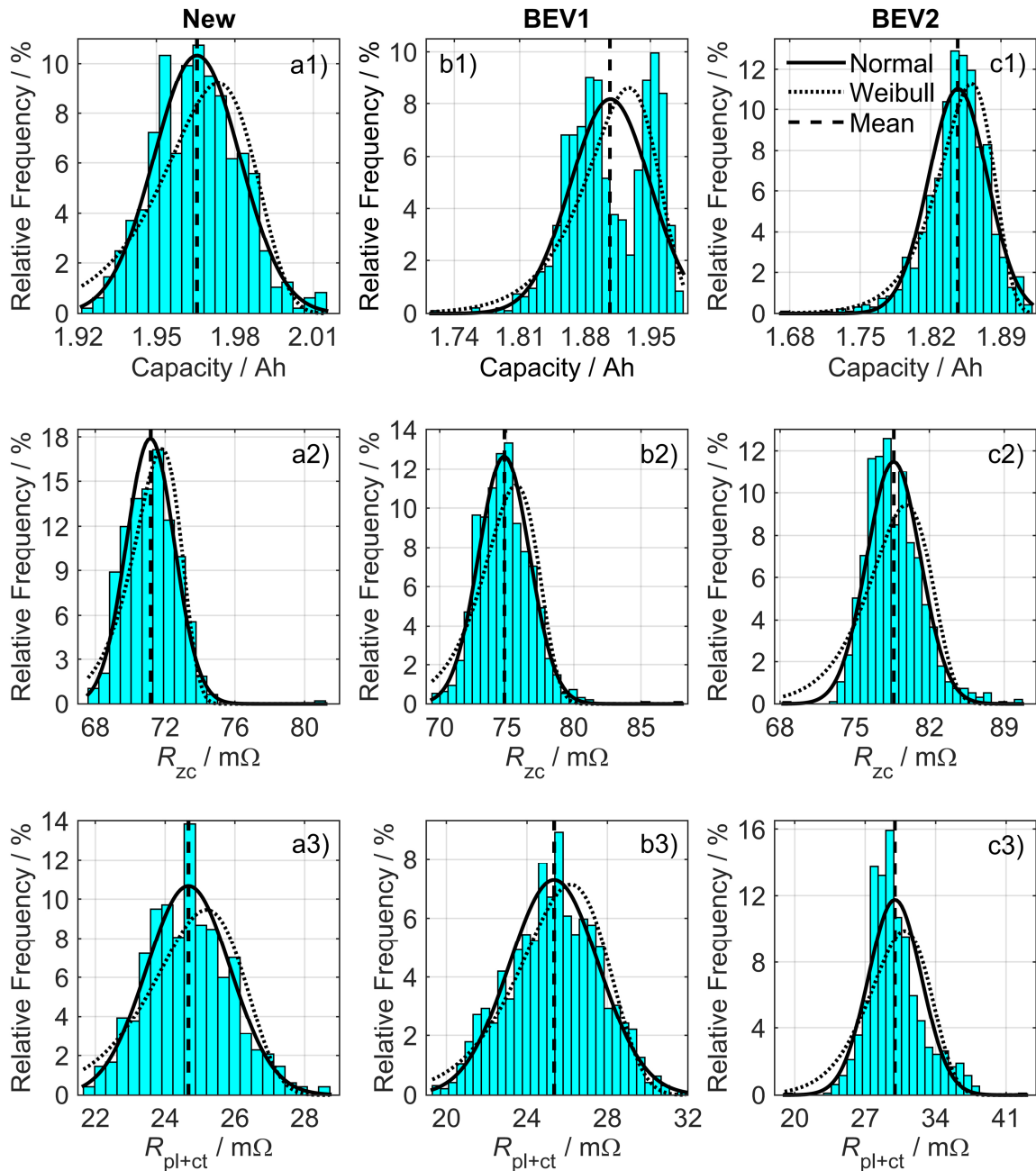


Figure 38: Overview of histograms with corresponding normal and Weibull distribution fits and mean values. [127]

It has to be mentioned that all data values are considered and plotted in the respective frequency class, but strong outliers are not regarded for distribution fit analysis. Strong outliers are defined here as bins more far away from the mean value before or after the first appearance of histogram classes equal to zero. This is useful because the distribution shape is strongly influenced by strong outliers and therefore quality of the fit decreases. In terms of supporting clarity, the total value range including outliers can be identified by the range of the distribution plots even for classes with bins which are invisible due to the small relative frequency value.

As already mentioned in Subchapter 5.3, the mean capacity value of the batch of new cells $\mu_{New,C} = 1.97$ Ah dropped to $\mu_{BEV1,C} = 1.91$ Ah and $\mu_{BEV2,C} = 1.85$ Ah, respectively. Besides of the capacity fade due to the progress of aging, also the parameter variation is reported to alter as a result of it [142, 160-162]. This is reflected by $\kappa_{New,C} = 0.8\%$, $\kappa_{BEV1,C} = 2.25\%$ and $\kappa_{BEV2,C} = 1.57\%$ with regard to the normal distribution fit. As BEV2 exhibits the lowest mean capacity value but BEV1 the highest coefficient of variation κ , the assumed relationship of increasing dispersion with the progress of aging can only partially, i.e., referred to the new state, be proven. However, this ambiguous tendency could originate from distinct reasons like local weak spots in the battery pack of BEV1 as the histogram itself appears to be bimodal. Regarding the development of R_{zc} , the mean value of the new state with $\mu_{New,zc} = 71.15$ m Ω is increased to $\mu_{BEV1,zc} = 74.08$ m Ω or $\mu_{BEV2,zc} = 78.64$ m Ω , respectively. Assumption of increased parameter variation with the progress of aging is unambiguous with regard to R_{zc} , as $\kappa_{New,zc} = 1.94\%$, $\kappa_{BEV1,zc} = 2.56\%$ and $\kappa_{BEV2,zc} = 3.19\%$. Considering R_{pl+ct} , the average value of the batch of new cells is increased from $\mu_{New,pl+ct} = 24.67$ m Ω to $\mu_{BEV1,pl+ct} = 25.35$ m Ω or $\mu_{BEV2,pl+ct} = 29.95$ m Ω , respectively. Same as for R_{zc} , there is a clear correlation for the progress of aging and the coefficients of variation with $\kappa_{New,pl+ct} = 4.86\%$, $\kappa_{BEV1,pl+ct} = 8.76\%$ and $\kappa_{BEV2,pl+ct} = 8.78\%$. As a conclusion from the normal distribution fit analysis, the assumption of an increased parameter spread with the progress of aging, i.e., new < BEV1 < BEV2, is justified for the three investigated parameters. However, regarding capacity values, tendency is ambiguous due to the bimodal shape of the histogram of BEV1 which leads to a disproportionately high coefficient of variation κ .

After normal distribution fit analysis, same is performed for the two-parameter Weibull distribution. In contrast to arithmetic mean values μ and coefficients of variation κ , when dealing with normal distribution, the scale and shape parameter η and β are used to parameterize the Weibull distribution fit. Thereby, all Weibull fits are calculated by the maximum likelihood estimation method. Regarding capacities, results with the same tendency as for normal distribution fit analysis are obtained for the Weibull approach, with scale parameters of $\eta_{New,C} = 1.97$ Ah, $\eta_{BEV2,C} = 1.93$ Ah and $\eta_{BEV1,C} = 1.86$ Ah. Comparing the scale parameters η to the corresponding mean values μ of BEV1 and BEV2, deviation is small with approx. 1.05% and 0.54%, respectively. However, parameters must be interpreted differently as the scale parameter η in classical reliability analysis reflects the value of the data set for which 63.2% of devices will have failed. Calculated values for the corresponding shape parameters $\beta_{New,C} = 116.06$, $\beta_{BEV1,C} =$

51.68 and $\beta_{\text{BEV2,C}} = 70.69$ exhibit an untypical magnitude with usually $\beta < 10$ in classical life time data analysis [177]. Mathematical explanation for this abnormality is the untypical small spread of data values for this kind of *before end of life distribution analysis*. To give an example, the capacity spread for the new batch of cells $\Delta C_{\text{New}} = C_{\text{New,max}} - C_{\text{New,min}} = 0.09$ Ah referred to the corresponding scale parameter $\eta_{\text{New,C}} = 1.97$ Ah, i.e., $\Delta C / \eta_{\text{New,C}} = 4.57\%$, is very small compared with a typical spread of failure times of classical reliability or *life cycle distribution analysis*. In [185] for example, a spread of $\Delta \text{cycles} = 1373$ cycles – 886 cycles = 487 cycles referred to the corresponding scale parameter $\eta_{[185]} = 1138$ cycles, yields a relative value $\Delta \text{cycles} / \eta_{[185]} = 42.79\%$.

Concerning the impedance part parameters which were calculated by Weibull distribution fit analysis, same tendency (new < BEV1 < BEV2) as for normal distribution analysis is observed with: $\eta_{\text{New,zc}} = 71.83$ m Ω , $\eta_{\text{BEV1,zc}} = 75.75$ m Ω and $\eta_{\text{BEV2,zc}} = 79.92$ m Ω , as well as $\eta_{\text{New,pl+ct}} = 25.25$ m Ω , $\eta_{\text{BEV1,pl+ct}} = 26.36$ m Ω and $\eta_{\text{BEV2,pl+ct}} = 31.21$ m Ω . Corresponding shape parameters $\beta_{\text{New,zc}} = 54.25$, $\beta_{\text{BEV1,zc}} = 38.19$ and $\beta_{\text{BEV2,zc}} = 28.31$, as well as $\beta_{\text{New,pl+ct}} = 20.20$, $\beta_{\text{BEV1,pl+ct}} = 12.54$ and $\beta_{\text{BEV2,pl+ct}} = 10.78$ monotonously decrease with the progress of aging. As already mentioned before, this is linked to the increased parameter spread which is inflicted by the aging progress.

The distribution of capacities seems to turn from normal to Weibull distribution with the progress of aging. Regarding Figure 38 a1), b1) and c1), alteration to left-skewness is observable which is expressed by $s_{\text{New,C}} = 0.18$, $s_{\text{BEV1,C}} = -0.17$ and $s_{\text{BEV2,C}} = -0.58$. For the distribution of impedance parts, there is obviously a pronounced weak quality of the Weibull fits for LIC in the aged state. Especially the histograms of R_{zc} which are shown in Figure 38 b2) and c2) appear more like a *reverse Weibull distribution* due to an obvious right-skewness, also shown by calculation of $s_{\text{New,zc}} = 0.04$, $s_{\text{BEV1,zc}} = 0.24$ and $s_{\text{BEV2,zc}} = 0.64$.

For a clearer illustration and analysis of central tendency, skewness and outliers, box-plots should be preferred over histograms. Therefore, box-plots of all histograms of Figure 38 are resumed in Figure 39. The medians of data sets are marked by a cyan cross each, while the bold black line marks the interquartile range. Hence, the left end of the box marks the first quartile q_1 , i.e., the 25th percentiles, and the right end the third quartile q_3 , i.e., the 75th percentiles. Thus, the interquartile range q is defined by the difference $q_3 - q_1$. The position of the median inside the box represents the skewness of the investigated data set. For example in Figure 39 b) for the data set of R_{zc} of BEV2, the median is more on the left side of the box which represents right-skewness as compared to Figure 38 c2). The thin whisker lines generally exhibit a maximum length of $1.5 q$ and are plotted to the adjacent value, which is the most extreme data value not being an outlier. In the box-plot of Figure 39, outliers are marked as small crosses and are defined as values larger than $q_3 + 1.5 q$ or smaller than $q_1 - 1.5 q$. Thus, the definition of an outlier differs from the one which was used for the calculations exhibited in Figure 38. The one-

dimensionality of box-plots allows easy and straight-forward optical comparison of the data sets of the new state and those of BEV1 and BEV2.

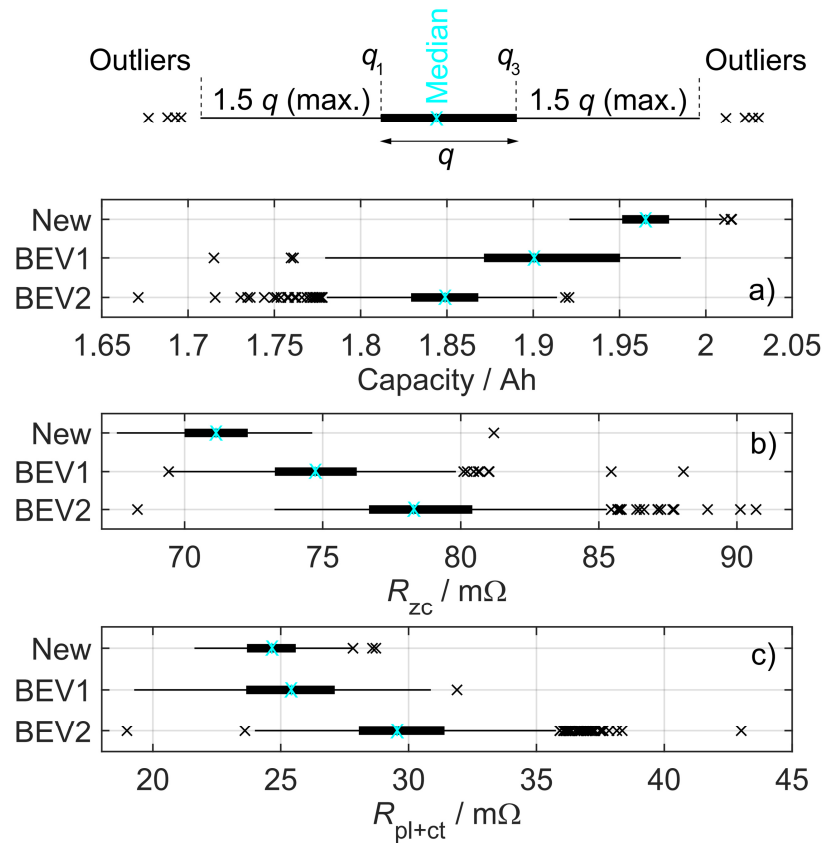


Figure 39: Box-plots of investigated data sets to elucidate skewness, medians, interquartile ranges, outliers, etc. [127]

Thereby, two main aspects can clearly be seen in Figure 39 when comparing the data set of the new state with the one of BEV2. First: the number of outliers is strongly increased with the progress of aging for all three parameters. To give an example, the highest amount of outliers is visible for the parameters of BEV2, but none or only a few are observable in the new state of cells. Second: with only a few exceptions, all outliers can be found on the side of higher degradation, i.e., left of the median for capacities but right of it for impedance parts. This observance is called *unidirectional diversification* henceforth. Generally, such a behavior of the majority of outliers being worse as the distribution mode is very common for wear-out of electronic components and usually described in terms of Weibull distributions.

In the following, only BEV2 (and not BEV1) is considered for further investigation because of the higher amount of outliers and progress of aging, and the more regular distribution in contrast to the bimodal shape which is visible in Figure 38 b1). For Weibull distributions with a $\beta > 3.6$, the

majority of outliers are situated left from the median due to the resulting left-skewness. As already mentioned earlier, this is invalid for the description of impedance parts in the aged state of cells, as an obvious right-skewness of respective distributions is observable. Calculation of the reciprocal values of investigated impedance parts, i.e., raising the conductances $G_{zc} = 1 / R_{zc}$ and $G_{pl+ct} = 1 / R_{pl+ct}$, can solve that issue. Exemplarily, the yielded data sets of BEV2 are plotted as histograms in Figure 40 and analyzed again by the normal and the Weibull distribution fitting approach. In case of the normal distribution fit, calculated values of the skewness are $s_{BEV2,zc,cond} = -0.45$ and $s_{BEV2,pl+ct,cond} = -0.17$, which represents left-skewness. For the Weibull fit, parameters obtained are $\eta_{BEV2,zc,cond} = 12.91$ S, $\eta_{BEV2,pl+ct,cond} = 34.92$ S, $\beta_{BEV2,zc,cond} = 36.54$ and $\beta_{BEV2,pl+ct,cond} = 12.64$. Especially for $G_{BEV2,zc}$, whose histogram is depicted in Figure 40 a), the resulting shape fits much better to a Weibull distribution as compared with the data set of $R_{BEV2,zc}$ which is illustrated in Figure 38 c2). Again as already explained for the histograms which are depicted in Figure 38, outliers appear as invisible due to the low height of histogram bins but the lines of distribution fit analyses mark the total value range.

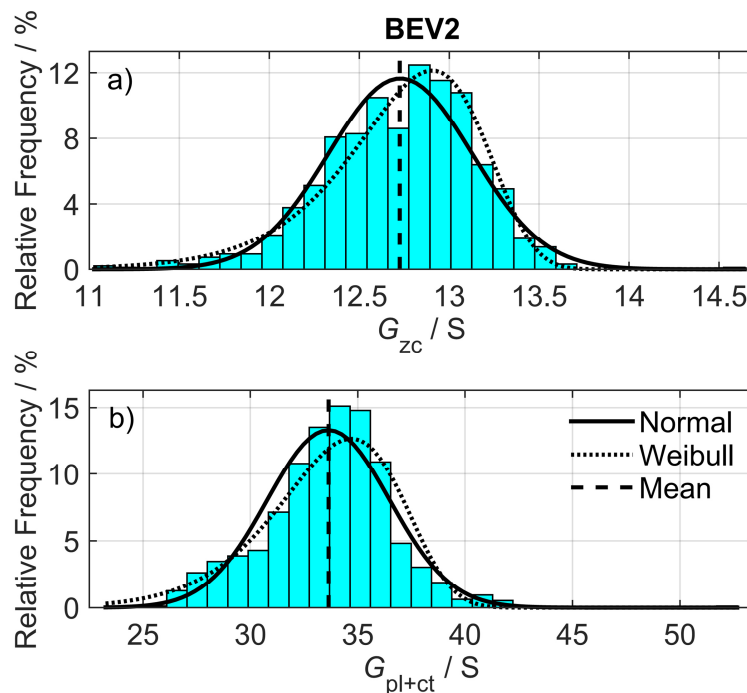


Figure 40: Histograms of a) $G_{BEV2,zc}$ and b) $G_{BEV2,pl+ct}$ with corresponding normal and Weibull distributions and mean values. [127]

For $G_{BEV2,pl+ct}$, the quality of the normal and Weibull fit is difficult to assess due to ambiguous results. For the capacity distributions which are shown in Figure 38 a1) and c1), and $R_{BEV2,zc}$ resp. $G_{BEV2,zc}$ distributions which are shown in Figure 38 a2) and Figure 40 a), the new hypothesis is constructed that described *histograms turn from a normal to a Weibull distribution*

with the progress of aging. This hypothesis is further tested and validated by the inspection of normal and Weibull probability nets which are presented in Figure 41 and Figure 42. Therein, the complete data sets including all outliers are considered. In Figure 41, the data sets of the three investigated parameters (a), b), c)) of LIC in the new state and out of BEV2, marked by crosses and plus signs, vs. the corresponding ideal normal distributions, marked by dotted and dashed lines, are illustrated. Especially when regarding capacities and the values of G_{zc} (a), b)), it is clearly visible that the quality of normal fits turns from a good one in the new state of cells to a worse one in the aged state. To further corroborate the claimed hypothesis of alteration from normal to Weibull distribution with the progress of aging, same data sets are presented in Weibull instead of normal probability nets in Figure 42.

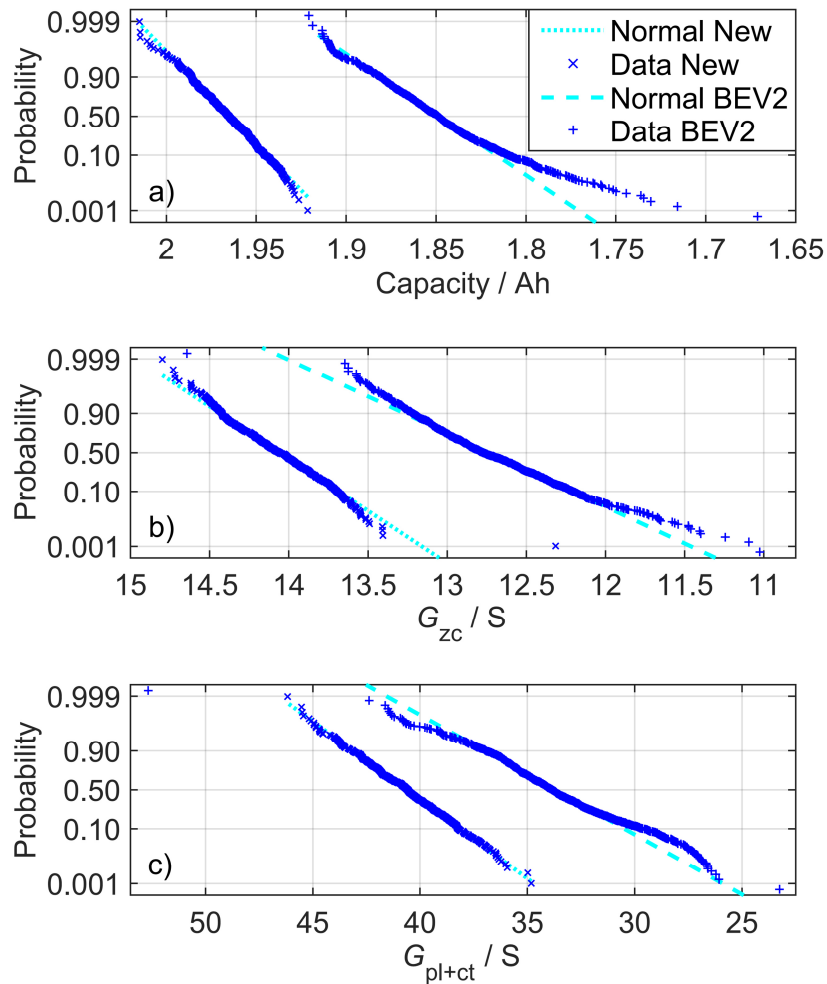


Figure 41: Normal probability nets of investigated parameters showing the development from the new to the aged state of lithium-ion cells; ordinate scaling is chosen so that the ideal normal distribution appears as linear in the respective normal probability net. [127]

When comparing the development of investigated parameters (a), b), c)) in the Weibull probability nets in Figure 42, the tendency is just contrary to the findings depicted in Figure 41: the quality of Weibull fits turns from a bad one in the new state to a better one in the aged state. Although claimed hypothesis cannot be sustained by the development of $G_{\text{pl+ct}}$, capacity values and those of G_{zc} definitely corroborate it by the parameter developments depicted in Figure 41 and Figure 42.

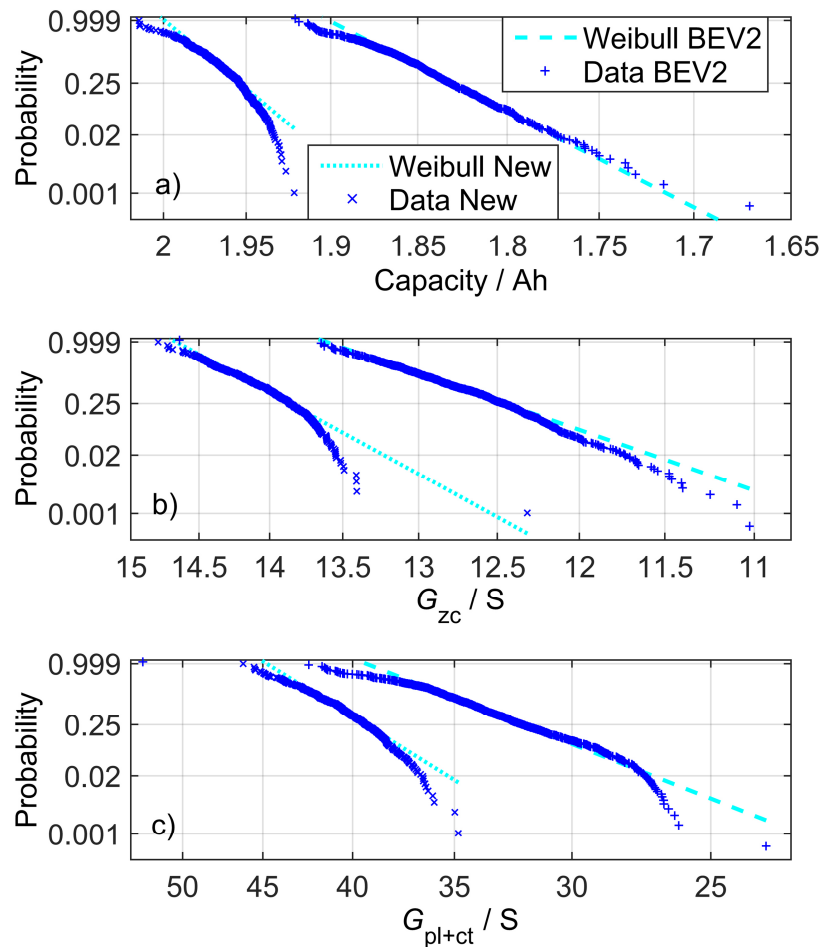


Figure 42: Weibull probability nets of investigated parameters showing the development from the new to the aged state of lithium-ion cells; ordinate scaling is chosen so that the ideal Weibull distribution appears as linear in the respective Weibull probability net. [127]

To summarize yielded observations, it can be said that the data sets of capacity, G_{zc} and $G_{\text{pl+ct}}$ for new cells can optimally be described by normal distributions. Additionally, due to the symmetric shape in the new state, it does not matter if impedance (R_{zc} , $R_{\text{pl+ct}}$) or admittance parts (G_{zc} , $G_{\text{pl+ct}}$) are raised. During the progress of aging, alteration from normal to Weibull distribution is shown for capacities and, albeit a bit less precise, for G_{zc} . However, no clear

statement can be made for G_{pl+ct} in the aged state regarding the available data. Probably, longer operation time and thus pronounced aging could deliver clearer results.

In the following, the reasons of the parameters (capacity, G_{zc}) to turn from normal to Weibull distribution with the progress of aging are discussed more specifically. Thereby, extrinsic reasons like temperature gradients in a battery pack are excluded, but considered in the upcoming subchapter. Focus here is the interaction between deviations in the production process and aging mechanisms at the cell level. Possibly linked with the production process, even for pre-selected cells cycled with the same load profile under controlled atmosphere in the laboratory, the aging behavior is reported to vary [160]. In the production process, cells are manufactured with the aim to yield the respective nominal capacity as accurately as possible. Therefore, e.g. the active materials or electrodes are controlled to stay within predefined mixing or thickness tolerances, respectively, in order to obtain the desired characteristics of the fabricated cell model [50, 163, 164]. Result of such a manufacturing and screening process is that the normal distribution is optimally suited to describe the parameter variation of LIC in the new state.

However, a minimum deviation e.g. in the thickness of electrodes is only scarcely avoidable, as an additional reduction of tolerances would result in excessively increased manufacturing costs at a comparably low improvement of performance [163]. Although when satisfying the required tolerances, e.g. deviations in the mixture of the electrolyte might influence the evolution of passive layers; or deviations in the thickness of electrodes might lead to differently pronounced aging effects caused by the electrodes' volumetric changes. For the latter, thicker electrodes result in higher capacities in the new state which is paid by the price of pronounced cyclic aging; or in the reverse, thinner electrodes lead to lower capacities but also to a deceleration of cyclic aging [50, 163, 164].

The reason for alteration from normal to Weibull distribution with the progress of aging might be explainable by such an interrelationship between deviations in the production process and a variety of aging mechanisms of LIC. As the majority of new cells exhibits parameters in the near of the normal distribution mode (average), aging behavior can also be assumed to proceed ordinarily. It is mainly provoked by unavoidable mechanisms like passive layer growth, irreversible structural changes of the cathode or aforementioned volumetric changes which especially lead to anode active material loss [67, 68]. However, there are also cells which have just barely complied with required tolerances. As already mentioned before, thinner electrodes might result in reduced cyclic aging due to lower volumetric changes, reduced overpotentials and heat generation. However, zero aging behavior can never be reached with common LIC technologies as there are unavoidable aging mechanisms like passive layer growth [67]. According to this, thicker electrodes might provoke accelerated cyclic aging behavior. If it is assumed, that cells which bear characteristics at the upper and lower bound of tolerances (like

electrode thickness) are uniformly distributed, it is still questionable why there are more cells in the aged state at the higher side of degradation.

This *unidirectional diversification*, which is typical for Weibull distribution, might be explained by additional aging or *failure* mechanisms, like e.g. detachment of active materials from the current collectors, pronounced aging which results from local lithium plating, or faulty triggering of internal safety devices [48, 140]. Due to such mechanisms, cells may exhibit strong dispersion as degradation itself is strong compared with conventional, unavoidable aging mechanisms which were described before. As a conclusion, there is an interrelationship between deviations in the production process and a variety of aging mechanisms, which might be the reason that the aging rate of LIC (and so the parameter variation in the aged state) can be described by Weibull distribution.

7.2 Influence of Operational Histories of Examined Vehicles

In the distribution fit analysis, no distinction is made regarding the position of modules, SoC drifts or temperature gradients along the cooling air flow in the battery pack, but treats every LIC in the same manner. These influences which could e.g. lead to local weak spots in the battery pack are combined henceforth in the umbrella term *extrinsic influences*. So, this subchapter aims at explaining abnormalities of cell parameters (capacity, R_{zc} resp. G_{zc} , R_{pl+ct} resp. G_{pl+ct}) which were observed in the distribution fit analysis by comparison with the data of operational histories of examined BEV. In the literature, it is mentioned that although if intrinsic cell-to-cell variation (caused by the production process) is minimized by pre-selection of most similar cells, the LIC of a multi-cell battery system will inevitably spread due to extrinsic influences like described above [142, 160-162].

However, the calculation of the mean values of the module temperatures at begin and end of each drive showed a maximum deviation of approx. 2 K between the coolest and hottest module without a clear linkage to the module position in the battery pack or the rank order with regard to the cooling air flow (see Figure 19). If the limited sensor accuracy of ± 1 K is considered, no hot spots in the battery pack or insufficiently cooled modules can clearly be stated. Additionally, also the mean voltage (or SoC) dispersion of battery units versus all drives shows to be smaller than the sensor measurement accuracy of ± 10 mV. As a conclusion, it can be stated that both the charge equalization and the temperature conditioning system work sufficiently effective and thus, without creating locally situated weak spots in the battery packs of the investigated cars.

For the most part, the investigation of the aged modules of BEV1 reveals equally distributed outliers regarding the values of cell capacity within the analyzed modules. The bimodal or two-peak distribution, which is depicted in Figure 38 b1), is observable again at the module level as four modules exhibit a mean capacity of approx. 1.95 Ah, whereas the residual five modules have only one of approx. 1.87 Ah. However, no clear linkage to the position of these two groups

of modules with distinct performance values is observable. Also when regarding the values of R_{zc} of these modules, outliers mostly concentrate on definite modules but again no clear linkage to the position of modules within the pack can be made. In addition, also for BEV2, no influence of the position of modules on the investigated parameters and their dispersion is observable. Besides, the assumption of a missing correlation between the module position and the performance of cells within the progress of aging is corroborated by comparing the six completely identically located modules of BEV1 and BEV2 (see Figure 19). Also for these 12 modules in total, no clear tendency can be observed as e.g. weak modules from a concrete position in the battery pack of BEV1 face good modules in the corresponding position of BEV2. Though, for a definite statement, all 48 modules of both cars instead of only nine should be investigated; resulting measurement effort would be enormous, however, whereas it can be assumed that the same results would be obtained.

Because of the measured homogenous temperature and voltage distribution and due to the non-existing dependency on the position of battery units within the pack, prevalence of cell outliers is assumed to be of cell-intrinsic nature provoked by tolerances during the production process, distinct thermal loads of cells in the soldering process and the aforementioned interrelationship of these deviations with a variety of aging mechanisms.

7.3 Characterization of Cell Outliers

As aforementioned, a negative correlation between capacity fade and impedance increase has been observed for a variety of loads, even after the onset of nonlinear aging (see Subchapter 6.1). Generally, most people would expect a negative correlation also for outlier cells, meaning a cell with a remarkably high or low capacity coming along with low or high impedance, respectively. This appears especially logical in the discharge direction (no CV phase), as the discharge end voltage is reached earlier for cells with an increased impedance due to enhanced overpotentials; as a consequence, the available discharge capacity is limited. In the following, different types of cell outliers within two exemplary battery modules are tried to be characterized, also with regard to the cooling air flow of the temperature conditioning system (see Figure 19).

Figure 43 shows the value pairs of capacity and R_{zc} of the 106 cells of the two exemplary battery modules, arranged in accordance with the cooling air flow of the temperature conditioning system. That is, cells are numbered consecutively along their rank regarding the cooling air flow through the module, i.e., cell number one is the first at the cooling air entrance, while cell number 106 being the last at the side of deflection. Both capacity and R_{zc} for BEV1 and BEV2, which are represented by dotted and solid lines, respectively, do not exhibit dependency from the cell positioning, because the parameters appear randomly distributed around a relatively constant mean value. Thus, no hot spots are detectable within the two exemplary battery modules.

With regard to the correlation between capacity and R_{zc} of outlier cells, results are ambiguous. Based on the exemplary battery module of BEV1, which is shown in Figure 43 a), the assumption of negative correlation must be rejected, as cell number 4 and 20 exhibit high values of R_{zc} but simultaneously regular ones of capacity. A possible cause of the phenomenon could be the aforementioned faulty triggering of cell integrated safety devices, like e.g. the pore closing mechanism of shutdown separators. However, regarding the cell outliers in the exemplary battery module of BEV2 in Figure 43 b), negative correlation is observable as cell number 6 exhibits a high value of capacity, but a low one of R_{zc} ; and, in the reverse, cell number 20 has a low capacity but a high R_{zc} . Here, the constellation of the first could e.g. result from a lost cell contact (thus, the charge throughput is just smaller), whereas the latter might have an intrinsic origin (i.e., a certain fault in the production process has been present). As these ambiguous observations might be critical towards an aging quick test (which is based on the correlation between capacity and impedance), more focus is put on it in Chapter 8.

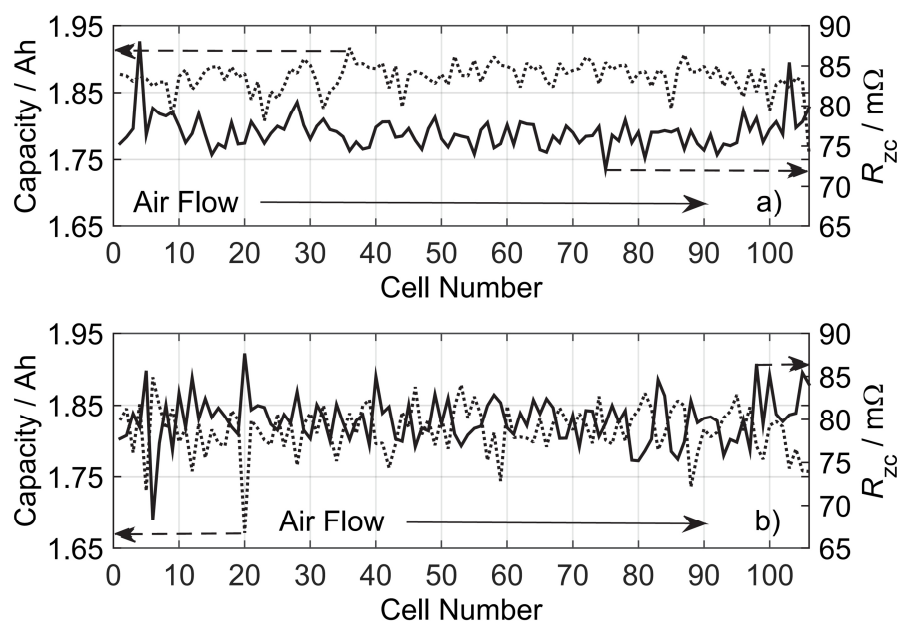


Figure 43: Cells arranged regarding the cooling air flow within one module with an example out of BEV1 for a) “not correlating outliers” and out of BEV2 for an example of b) “correlating outliers”. [127]

7.4 Conclusion

Within the scope of this chapter, 484 new cells and 1908 cells out of two identical BEV (i.e., 954 cells each), were characterized by capacity and impedance measurements to yield a broad set of data for statistical distribution fit analysis. With it, distributions of characteristic parameters of LIC (capacity, R_{zc} , R_{pl+ct}) in the new state were compared with those after approx. 3 years of

BEV customer operation. Obtained results indicated alteration from normal to left-skewed Weibull distribution especially for the values of capacities and conductances G_{zc} with the progress of aging. As a majority of the values of R_{zc} in the aged state of LIC was observed to be higher than compared with the mode of distribution, this suggested right-skewness which was the reason to raise the reciprocal value, i.e., the conductance G_{zc} . In general, with only a few exceptions, all the cell outliers were found on the side of higher degradation, i.e., left of the median for capacities (and admittance parts) but right of it for impedance parts. This unidirectional diversification is very common for wear-out of electronic components which in turn is usually described by Weibull distributions. An interrelationship between deviations in the LIC production process and a variety of aging mechanisms is assumed to be responsible for the alteration from normal to Weibull distribution. Furthermore, the total amount of cell outliers and the lithium-ion cell-to-cell parameter spread were generally observed to increase with the progress of aging.

Besides of the pure statistical analysis of data sets of new and aged LIC, obtained results were additionally compared with the operational history of examined BEV by raising logged data of operation of approx. 3 years of customer usage. Thereby, it was especially aimed at linking suspicious values of parameters to weak spots of the battery pack, which e.g. could had been caused by an insufficiently working charge equalization or temperature conditioning system. However, because of the measured homogenous temperature and voltage distribution and due to the non-existing dependency on the position of battery units (modules, cells) within the battery pack, prevalence of cell outliers was assumed to be of cell-intrinsic nature provoked by tolerances during the production process or distinct thermal loads of cells in the soldering process. These deviations might then have been again in interrelationship with a variety of aging mechanisms of LIC. By inspection of different sorts of outlier cells, there were those to list which exhibited a negative correlation between capacity and impedance, but this was not always the case. Furthermore, for one of the two investigated vehicles, examined modules could be split in two groups with respect to their performance (see bimodal variation in BEV1); however, as aforementioned, the relevant causes for this module-to-module variation stayed inexplicable, especially as general local weak spots in the battery pack could be excluded by car-to-car comparison.

Finally, as cell outliers appear unavoidably even in the presence of sufficiently effective charge equalization and temperature conditioning systems, it is of major importance that the BMS reliably detects LIC with suspicious parameters and effectively balances resulting SoC drifts to guarantee a safe way of operation of the installed battery storage. Regarding the thereby resulting decrease of efficiency, though, nothing else remains than to replace defect battery units, i.e., to remanufacture the BEV battery pack. Furthermore, if battery unit parameters are not monitored by the BMS at the cell level, consideration of cell parameter variation by

implementation of respective distributions is not useful, as a systematic deviation would be created; deviations are minimized by referring to the mean parameter values instead.

From the perspective of SLC implementation, observed appearance of cell outliers is considered to be uncritical, as the effect of only a few cell outliers in modules is usually compensated (depending on the cell interconnection configuration). However, as e.g. temperature gradients in a battery pack can lead to local areas of inferior and superior modules (in which all cells are either remarkably bad or good, respectively), cell-to-cell variation is basically scaled up to the module level. Regarding reuse constellations at the module level, this is critical as the effect basically underlines the need of costly capacity measuring to select only those which are capable for reuse. A less expensive approach of detecting the status of aging is presented in the following. Regarding large-scale energy storage projects with SLB, capacity measurement can probably be skipped in general, as a scale-up effect of cell-to-cell or module-to-module variation is compensated by the high number of cells or modules, respectively; thus, it might be adequate, as a consequence, to select similar ones only based on comparing the mileage and the mean logged temperature value.

8 Correlation between Capacity Fade and Impedance Increase of Lithium-Ion Cells

As aforementioned, e.g. temperature gradients might lead to local whole areas of inferior and superior modules (in which all cells each are particularly bad or good) in BEV battery packs. That is, parameter variation which starts at the cell level is basically scaled up to the module level. Besides of the severe impact on the performance of the respective automotive battery, regarding reuse constellations at the module level, this is critical as consequently capacity measuring is required to select only those modules which are still suited. Unfortunately, capacity measuring is time-consuming and thus, costly (see Subchapter 2.2).

In this chapter, a SoH quick test approach is presented, which is based on the correlation between capacity fade and impedance increase. Regarding the aging behavior of nearly all conducted test cases, which were presented in Chapter 6, a (negative) linear correlation behavior was observed even after the onset of nonlinear aging. Thus, *nonlinear aging would not affect the functionality of the SoH quick test*. Though, possibly critical for SoH quick test implementation, it was also observed, that for challenging compared with mild load profiles at high temperatures, the latter led to higher values of impedance parts at corresponding residual capacities (i.e., for an assumed linear relationship, the respective gradients differed). As was described in Subchapter 3.2, this phenomenon is possibly linked to the multilayered structure of passive layers, as calendric aging might only provoke a growth of the respective outer layers, whereas cyclic aging could make complete reconstruction necessary. The observed phenomenon is discussed again in this chapter specifically with regard to its meaning for the suggested SoH quick test.

Thereby, as the name of the chapter already suggests, the correlation behavior during the progress of aging is comprehensively analyzed and assessed (not only focused on the realization of the SoH quick test). Based on the fundamental investigation of the correlation behavior, with regard to the quick test approach, though, the most suitable impedance part is selected and its reachable scope of precision is presented. Therefore, for reuse constellations at the module level, either module aging data sets must be available (which is unlikely in terms of the enormous effort), or the *scalability of respective cell aging data must be assumed* as a consequence. In the case of this work, presented in Subchapter 8.1, single aging state correlation analysis is conducted based on the data sets of the 484 new and 1908 aged BEV cells. The regression functions of the SoH quick test, presented in Subchapter 8.2, are basically parameterized by the complete laboratory data sets of the first phase of aging experiments, accompanied by data from supplementary cell measurements (see Subchapter 5.2). The validation of the suggested quick test approach, which is given in Subchapter 8.3, is based

again on the data sets of both examined BEV. Finally, the previous single aging state analysis is extended in Subchapter 8.4, with a special focus on the effect of cell outliers. Figure 44 clarifies the progress of work which is reached in Chapter 8, implicating the end of the main part of this work.

In the following, to provide an unambiguous and most manageable nomenclature for the used PPMCC $r_{X,Y}$ (see Subchapter 4.2), X is not used for capacity, but for the raised data set (New, BEV1, BEV2, etc.), whereas Y describes the analyzed part of impedance. This is useful, as always the correlation between capacity, but either R_{zc} or R_{p+ct} , is considered. So, for example, $r_{BEV1,zc}$ is the PPMCC between capacity and R_{zc} for the data set of BEV1.

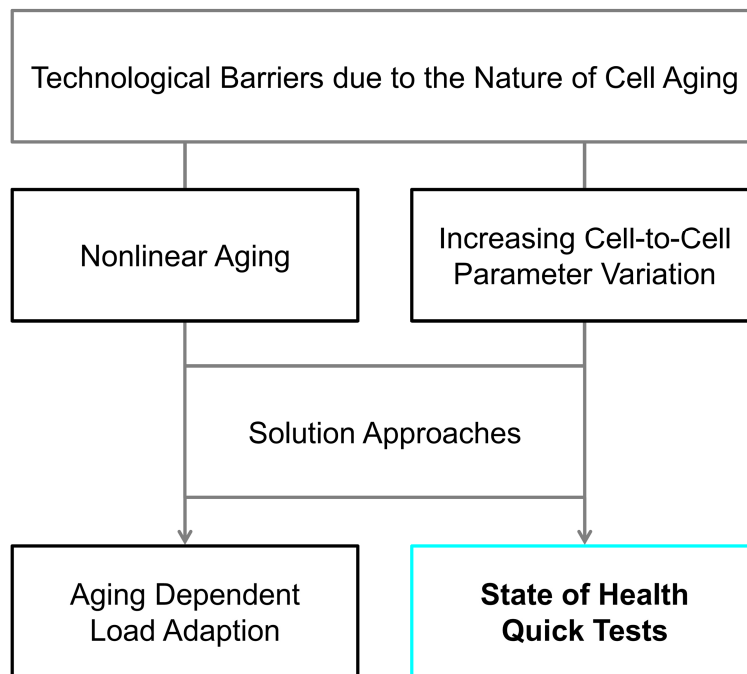


Figure 44: Progress of work in Chapter 8: the box of the presented solution approach (state of health quick test) is colored in cyan.

8.1 Single Aging State Analysis

The scatter plot in Figure 45 illustrates the pairs of capacities and a) R_{zc} or b) R_{p+ct} for the batches of the 484 new cells and the 954 aged cells each out of BEV1 and BEV2. Comparing the point clouds of the new cells and those of both cars, it is obvious that the mean values of capacity have been decreasing and the mean impedance values rising during BEV operation due to the progress of aging. With respect to the more demanding operational history of BEV2, as was summarized in Table 4, the aging progress of its cells appears to be slightly advanced.

Regarding the gradation values of the PPMCC which were presented in Subchapter 4.2, with $r_{\text{New,zc}} = 0.13$, no correlation exists between capacity and R_{zc} in the *new state* which could be a result from tolerances (e.g., mixing or electrode thickness) in the cell production process. Additionally, $r_{\text{New,zc}}$ is positive against expectations which is also explainable by the production process as e.g. thicker electrode layers lead to higher cell capacities but also to increased impedance values [50, 163, 164]. However, no further clarification should be given here as there is no correlation anyway.

In contrast to that, with $r_{\text{BEV1,zc}} = -0.52$ and $r_{\text{BEV2,zc}} = -0.55$, a moderate correlation is calculated for the cells out of both BEV, representing the *aged state*. This increased correlation could be interpreted as a result of electrolyte decomposition which in turn leads to passive layer growth (as was described in Subchapter 3.1). However, as the number of cell outliers appears to be clearly increased in the aged state, this could affect the PPMCC values as well. For this reason, the effect of cell outliers on the strength of correlation is further investigated in Subchapter 8.4. For the correlation between capacity and $R_{\text{pl+ct}}$, the trend is just contrary, as at least a weak correlation with $r_{\text{New,pl+ct}} = -0.32$ exists in the new state, but it fades with $r_{\text{BEV1,pl+ct}} = -0.08$ and $r_{\text{BEV2,pl+ct}} = -0.28$ for the point clouds of BEV1 and BEV2, respectively.

As a conclusion, only the (absolute) correlation between capacity and R_{zc} in contrast to $R_{\text{pl+ct}}$ is increased in the aged compared with the new state. However, between both impedance parts and capacity, a linear functional dependency is imaginable, which is represented by the *shifted point clouds towards lower capacities and higher impedance parts* with the *progress of aging* (here new \rightarrow BEV1 \rightarrow BEV2). This aging induced shift of point clouds is mathematically represented by strong and moderate PPMCC values for the entirety of the three cell batches (new, BEV1 and BEV2) with $r_{\text{Total,zc}} = -0.80$ and $r_{\text{Total,pl+ct}} = -0.60$, respectively.

For the shift of point clouds on the assumed functional line in Figure 45 a), $\text{cov}_{\text{New,zc}} = 3.1 \mu\Omega \cdot \text{Ah}$ is increased (absolute) about fourteen fold to $\text{cov}_{\text{BEV1,zc}} = -44.60 \mu\Omega \cdot \text{Ah}$ and $\text{cov}_{\text{BEV2,zc}} = -43.30 \mu\Omega \cdot \text{Ah}$. In contrast to that, the product of $\sigma_{\text{New,zc}} \cdot \sigma_{\text{New,C}} = 1.45 \text{ m}\Omega \cdot 16.40 \text{ mAh} = 23.78 \mu\Omega \cdot \text{Ah}$ is only increased approx. fourfold to $\sigma_{\text{BEV1,zc}} \cdot \sigma_{\text{BEV1,C}} = 1.97 \text{ m}\Omega \cdot 43.40 \text{ mAh} = 85.50 \mu\Omega \cdot \text{Ah}$ and $\sigma_{\text{BEV2,zc}} \cdot \sigma_{\text{BEV2,C}} = 2.60 \text{ m}\Omega \cdot 30.00 \text{ mAh} = 78.00 \mu\Omega \cdot \text{Ah}$. This disproportionately higher increase of the covariance compared with the product of standard deviations leads to the increased correlation between capacity and R_{zc} in the aged state. This issue can be imagined as a shift of point clouds on the functional line while the diameters of these clouds both are approx. equally increased (due to higher standard deviations). Simultaneously, proportionately more data points are situated close to the assumed functional line (due to the disproportionately higher increase of the covariance).

In contrast to that, for the point clouds in Figure 45 b), $\text{cov}_{\text{New,pl+ct}} = -6.30 \mu\Omega \cdot \text{Ah}$ is only slightly increased (absolute) to $\text{cov}_{\text{BEV1,pl+ct}} = -8.20 \mu\Omega \cdot \text{Ah}$ or approx. quadrupled to $\text{cov}_{\text{BEV2,pl+ct}} = -22.60 \mu\Omega \cdot \text{Ah}$. The product of $\sigma_{\text{New,pl+ct}} \cdot \sigma_{\text{New,C}} = 1.20 \text{ m}\Omega \cdot 16.40 \text{ mAh} = 19.68 \mu\Omega \cdot \text{Ah}$ is also

increased approx. fourfold to $\sigma_{\text{BEV1,pl+ct}} \cdot \sigma_{\text{BEV1,C}} = 2.23 \text{ m}\Omega \cdot 43.40 \text{ mAh} = 96.78 \text{ }\mu\Omega\cdot\text{Ah}$ and $\sigma_{\text{BEV2,pl+ct}} \cdot \sigma_{\text{BEV2,C}} = 2.69 \text{ m}\Omega \cdot 30.00 \text{ mAh} = 80.70 \text{ }\mu\Omega\cdot\text{Ah}$. This is why the correlation between $R_{\text{pl+ct}}$ and capacity in the aged state fades for BEV1 and is slightly decreased for BEV2. Again, it can be imagined as a shifted point cloud whose diameters approx. equally increase, but in contrast to the above mentioned example, proportionately, no more data points are concentrated in the near of the assumed functional line.

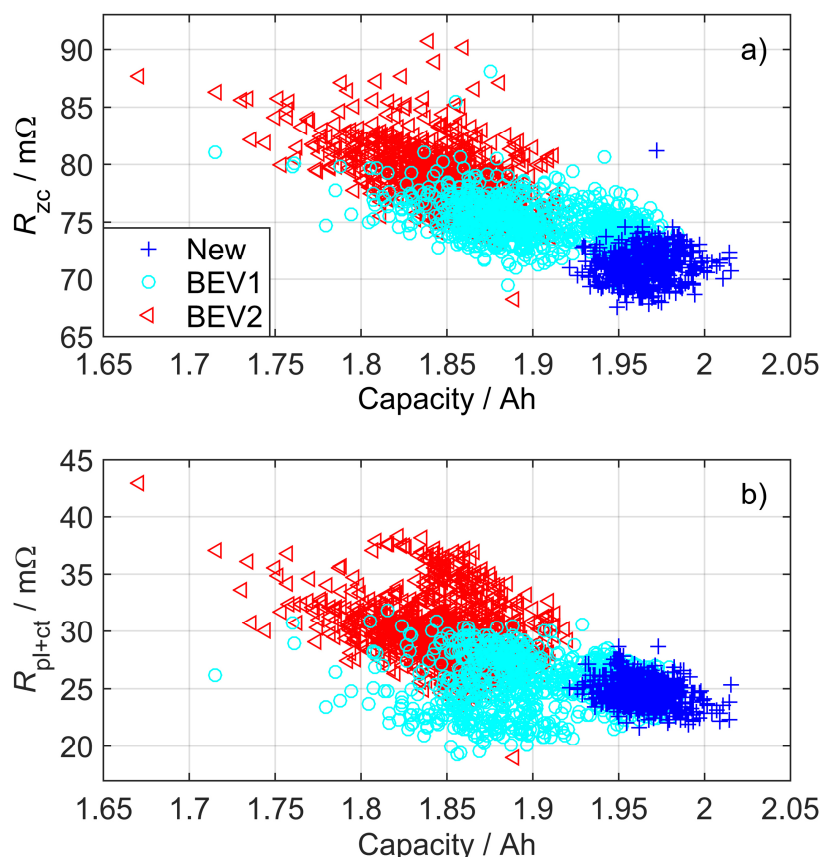


Figure 45: Scatter plot of capacity and a) R_{zc} or b) $R_{\text{pl+ct}}$ of 484 new cells and 954 aged cells each out of BEV1 and BEV2. [186]

The functional dependency (shifted point clouds) of both investigated impedance parts from the capacity during the progress of aging enables the proposed correlation based SoH quick test in theory, while the increased PPMCC value regarding capacity and R_{zc} in the aged state even implies a continuous reduction of the thereby resulting error (on average). So, besides of the dependency from the SoC of $R_{\text{pl+ct}}$, in contrast to R_{zc} [54, 58, 59], a further disadvantage of this impedance part is the increasing error with the progress of aging.

For a quick classification of cells in the new state, with disregard of the SoC dependency, raising the correlation between $R_{\text{pl+ct}}$ and capacity would be the better choice (for the investigated type of cell), as its PPMCC is initially higher. However, correlation based quick classification of cells in the new state is critical nevertheless as no or only a weak correlation exists between capacity and R_{zc} or $R_{\text{pl+ct}}$, respectively. As aforementioned, this is assumed to be linked with tolerances in the production process. The slightly increased absolute PPMCC values between capacity and $R_{\text{pl+ct}}$ compared with R_{zc} in the new state could be a result from the SEI formation process in which the passive layer is firstly created under the consumption of active lithium.

In the next subchapter, data sets of both calendric and cyclic aging experiments are investigated by linear regression analysis and PPMCC value calculation. By the first, a functional interrelation between capacity and respective impedance parts is yielded, which is required for the SoH quick test. By the latter, its reachable precision can be estimated. As aforementioned, $R_{\text{pl+ct}}$ cannot be used for the SoH quick test because of its SoC dependency; nevertheless, same investigations than for R_{zc} are presented in the following, which aim at a fundamental understanding of the correlation behavior between capacity and different impedance parts.

8.2 Aging Progress Regression Analysis

In this subchapter, regression curves are calculated for capacity and corresponding impedance parts *during the progress* of aging. Thereby, it is important to distinguish from the inspection of point clouds of single *aging states* (as shown in Figure 45), compared with a data set describing the *progress of aging* as presented in Figure 46. In the first, each measuring point represents a single cell, in contrast to the latter, in which a variety of points belongs to the same cell, basically quantifying the number of checkups during the aging experiment.

The scatter plot in Figure 46 illustrates the pairs of capacities and a) R_{zc} or b) $R_{\text{pl+ct}}$ for 83 cells during the progress of aging in the laboratory under a variety of storage and operational conditions (as presented in Subchapter 5.2; first phase of experiments). Thereby, it is apparent in Figure 46 a) that cells from calendric (ID 21-30 + cells from supplementary measurements, see Table 2) and cyclic (ID 1-11 + cells from supplementary measurements, see Table 1) aging experiments, represented by plus-signs and triangles, form two different branches. For the same value of capacity, the value of R_{zc} is higher for cells which have been stored only. A special case, henceforth named as “Mild Cyclic” (represented by circles, ID 12, see Table 1), exhibits the same behavior as observed for the cells of the calendric aging experiment. Cells of this test case have been cycled with a rather mild load profile, i.e., current rates of 0.5 C / 1.0 C for charging / discharging (both CC) within a small voltage swing $\Delta V = 0.94$ V at a high temperature of 50 °C. Such an observance of prevailing time-controlled aging mechanisms for cells cycled with an unchallenging load profile at high temperatures has e.g. been reported in [141].

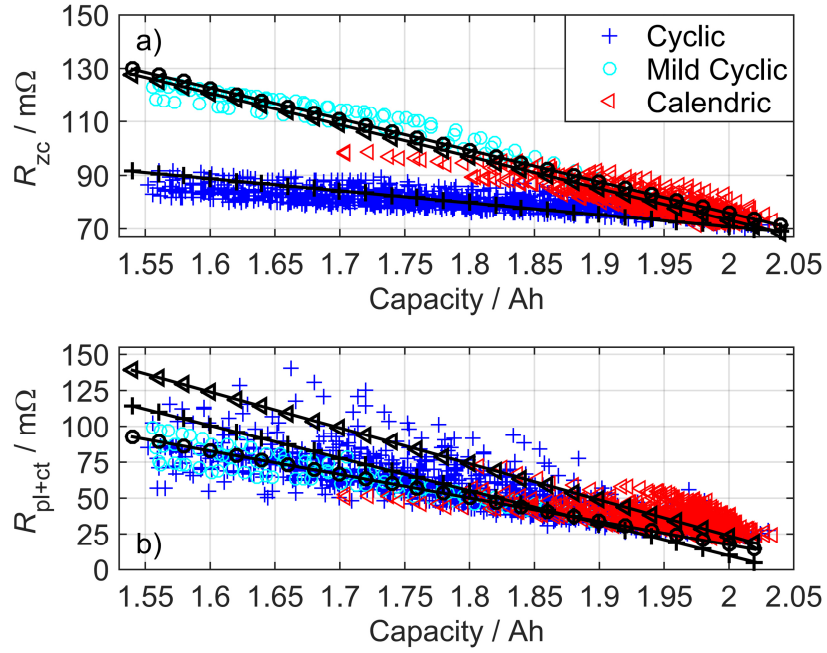


Figure 46: Scatter plot of capacity and a) R_{zc} or b) R_{pl+ct} of 83 cells aged in the laboratory under different operational conditions in conjunction with corresponding regression curves. [186]

Regarding the PPMCC values of the data sets in Figure 46 a), a moderate correlation with a $r_{Cyclic,zc} = -0.76$ is calculated for the batch of cycled cells, and both a strong one with $r_{Mild,zc} = -0.97$ and $r_{Calendric,zc} = -0.88$ is determined for mildly cycled and stored cells, respectively. However, when comparing these values to those of the point clouds in Figure 45, no wrong interpretation should be done as a comparison of data sets describing either single aging states or the progress of aging is not useful.

By linear regression analysis, based on the least squares method, the required regression curves were calculated for capacity C and R_{zc} for the three different data sets:

$$C_{Cyclic} = 3.57 \text{ Ah} - 2.22 \cdot 10^{-2} \text{ A}^2\text{hV}^{-1} \cdot R_{Cyclic,zc} \quad (14)$$

$$C_{Mild} = 2.65 \text{ Ah} - 8.54 \cdot 10^{-3} \text{ A}^2\text{hV}^{-1} \cdot R_{Mild,zc} \quad (15)$$

$$C_{Calendric} = 2.62 \text{ Ah} - 8.43 \cdot 10^{-3} \text{ A}^2\text{hV}^{-1} \cdot R_{Calendric,zc} \quad (16)$$

Regarding the point clouds of different operational conditions in the scatter plot of Figure 46 b), no different branches appear for capacity and R_{pl+ct} . For the cells of the cyclic aging experiment, represented by plus-signs, measured data seems to spread more as compared with corresponding values depicted in Figure 46 a). A moderate correlation with $r_{Calendric,pl+ct} = -0.64$ is calculated for the data set of stored cells. For the sets of cycled and mildly cycled cells, a strong correlation is calculated with $r_{Cyclic,pl+ct} = -0.81$ and $r_{Mild,pl+ct} = -0.95$, respectively. The regression curves for capacity C and R_{pl+ct} were calculated as follows:

$$C_{\text{Cyclic}} = 2.04 \text{ Ah} - 4.40 \cdot 10^{-3} \text{ A}^2\text{hV}^{-1} \cdot R_{\text{Cyclic,pl+ct}} \quad (17)$$

$$C_{\text{Mild}} = 2.11 \text{ Ah} - 6.12 \cdot 10^{-3} \text{ A}^2\text{hV}^{-1} \cdot R_{\text{Mild,pl+ct}} \quad (18)$$

$$C_{\text{Calendric}} = 2.10 \text{ Ah} - 3.99 \cdot 10^{-3} \text{ A}^2\text{hV}^{-1} \cdot R_{\text{Calendric,pl+ct}} \quad (19)$$

In the following subchapter, the correlation based SoH quick test is validated by usage of the BEV data sets.

8.3 Validation of the State of Health Quick Test Approach

By inserting the measured impedance values of the BEV data sets in the detected equations (which describe the functional interrelation between capacity and impedance values), *SoH quick test capacity* is given as a result. To illustrate the approach of validation, BEV point clouds are shown in the scatter plots of Figure 47 a) and b) in combination with the detected regression curves. Thereby, it is obvious from Figure 47 a), that only a SoH quick test, which is based on the regression curve of the data set of regularly cycled cells, can deliver good results. For the entirety of operated cells, only cells of the “Mild Cyclic” batch which were operated with a mild load profile at 50 °C formed an additional branch, as aforementioned. As the average module temperature of both BEV was even lower than 30 °C, though, it was expectable that the BEV data sets would rather behave like the one of the “Cyclic” batch.

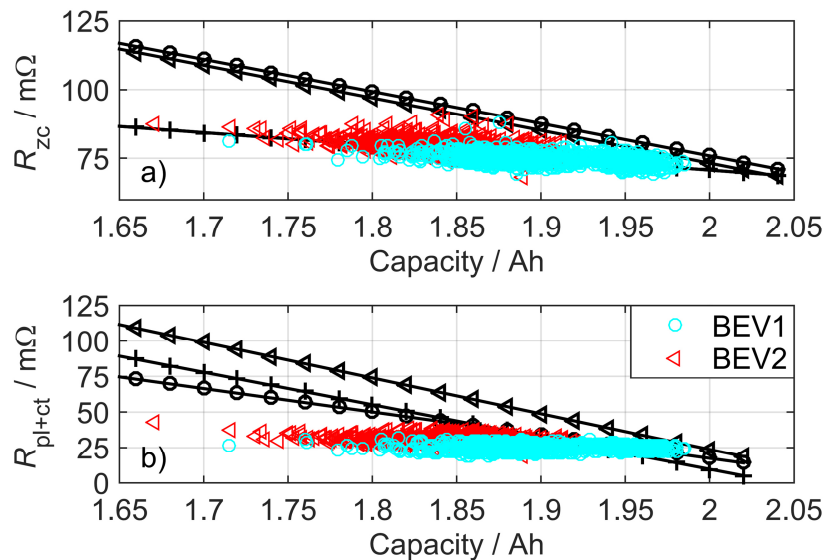


Figure 47: Comparison of the value pairs of BEV1 and BEV2 with the linear regression functions. [186]

Because of that obviousness, only the regression curve of the “Cyclic” aging data set is raised for further validation. By inserting the impedance values of BEV cells in the corresponding regression functions, SoH quick test capacities are yielded as a result; then, these are each

compared with the corresponding measured capacity values. The relative deviation of measured and calculated capacity is given by $\delta = (C_{\text{calc}} - C_{\text{meas}}) / C_{\text{meas}}$ and plotted in relative frequency histograms (with a number of bins equal to the square root of the number of measured points of the BEV data sets). The histograms of BEV1 for the deviation of capacities, yielded by inserting R_{zc} in Equation (14) or $R_{\text{pl+ct}}$ in Equation (17), are shown in Figure 48 a1) and a2), respectively. Corresponding histograms of BEV2 are given in Figure 48 b1) and b2). Additionally, in all graphs the arithmetic mean values of relative deviation are marked by a dashed vertical line. For BEV1, except from a few outlier cells, most of the values of δ_{zc} range from -5% to 5% with a mean of 0.2%. Regarding BEV2, most of the values of δ_{zc} are within a range of -9% and 5% with a mean of -1.2%. For $\delta_{\text{pl+ct}}$, most of the values of BEV1 range from -3% to 9% with a mean of 1.4%. For BEV2, except from a few outlier cells, values range from -1% to 9% with a mean of 3.5%. If the respective value pairs of data sets, which were used for the parameterization of detected equations, would be used in the same way for validation, the presented mean values of deviation would be equal to zero.

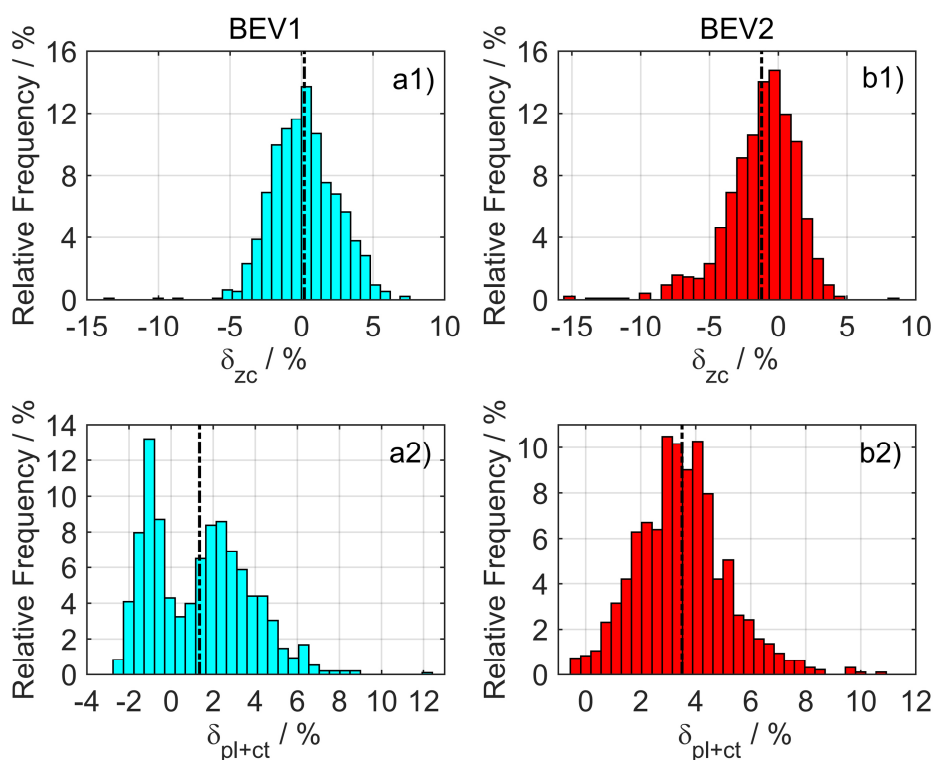


Figure 48: Relative frequency versus deviation of calculated capacities of a) BEV1 and b) BEV2; mean deviations are represented by dashed vertical lines. [186]

If a deviation of approx. 10% (absolute deviation maximum, if obvious outlier cells are excluded) can be accepted for the intended field of application, the proposed SoH quick test is a viable

approach. However, as especially the requirement of suitable aging data is critical, further approaches should be investigated. In addition, the ranges of deviation were seriously increased, if the respective regression curves of the calendric aging experiment would have been used, for example. Thus, the choice of a suitable load profile to create the required aging data set, which is used for *parameterization*, is *crucial but absolutely essential*.

8.4 Extended Single Aging State Analysis

In this subchapter, the single aging state analysis from Subchapter 8.1 is extended with a special focus on the effect of cell outliers. As described in Subchapter 3.2, aging mechanisms which lead both to capacity fade and impedance increase, could theoretically lead to a continuous rise of correlation values. This was observed for the correlation between capacity and R_{zc} but rebutted for R_{pl+ct} of the shifted point clouds in Figure 45. However, results and interpretations might have been distorted due to an increased amount of cell outliers in the aged state. So, investigation of the correlation of single aging states (during the progress of aging) is repeated by a stepwise PPMCC value calculation for the “Cyclic” data set (plus-signs in Figure 46). As only this data set is further investigated, the term “Cyclic” is omitted in the indexes of following parameters.

Therefore, all capacity values were normalized related to the corresponding values in the new state, and then, grouped in intervals within a range of 100% and 80%. For each interval, the strength of correlation between relative capacity and R_{zc} or R_{pl+ct} was calculated. Regarding the size of investigated intervals, a trade-off between a too low one, which would produce unstable results, and a too big one not being assumable as a single aging state, had to be found. Approx. 100 data points each were finally grouped in 5% intervals.

The strength of correlation between capacity and R_{zc} or R_{pl+ct} for each interval is shown in Figure 49. Principally, same tendency (increase of R_{zc} , decrease of R_{pl+ct}) as for the point clouds in Figure 45 is observable again: from the first interval with $r_{zc} = -0.17$ and $r_{pl+ct} = -0.47$, PPMCC values turn to $r_{zc} = -0.39$ and $r_{pl+ct} = -0.35$ in the fourth interval. However, it is noticeable that PPMCC values in the fourth interval both represent only a weak correlation with similar values. Results were clearer for the point clouds of BEV1 and BEV2 in Figure 45, as there was a moderate correlation between capacity and R_{zc} , but no one for R_{pl+ct} in the aged state. As aforementioned, the increased amount of cell outliers in the aged ALIB might have influenced the PPMCC calculation and biased results.

So, as the results of the single aging state analysis from Subchapter 8.1 (new and BEV cells) and the extended one in this subchapter (“Cyclic” aging data set) partially collide, it is investigated whether results get clearer when considering only the capacity interquartile range of BEV cells. By excluding cells from the highest and lowest quarter of capacities, the correlation between capacity and R_{zc} indeed fades for both cars with $r_{BEV1,zc} = -0.52$ turning to $r_{BEV1,zc,interquart}$

= -0.18 and $r_{\text{BEV2,zc}} = -0.55$ to $r_{\text{BEV2,zc,interquart}} = -0.16$. For $R_{\text{pl+ct}}$, PPMCC values turn from $r_{\text{BEV1,pl+ct}} = -0.08$ to $r_{\text{BEV1,pl+ct,interquart}} = -0.06$ and $r_{\text{BEV2,pl+ct}} = -0.28$ to $r_{\text{BEV2,pl+ct,interquart}} = -0.09$. Thus, outlier cells seem to have a strong effect when calculating PPMCC values, which is why precaution must be exercised when interpreting results.

By eliminating outlier cells (like only regarding the interquartile range), no or only a weak correlation exists between both investigated impedance parts and capacity in the new as well as in the aged state. For the proposed SoH quick test, this means that there is no systematic deviation in dependency from the actual SoH (in the absence of outliers), as there is no clear tendency for the correlation itself during the progress of aging. Most important, however, the SoC dependency of $R_{\text{pl+ct}}$ is a disqualifier for SoH quick tests as a prior SoC adjustment would result in a loss of any temporal advantage. So, only the correlation between capacity and R_{zc} seems to be useful for the proposed SoH quick test – regardless of the correlation between investigated impedance parts and capacity in any specific state of aging.

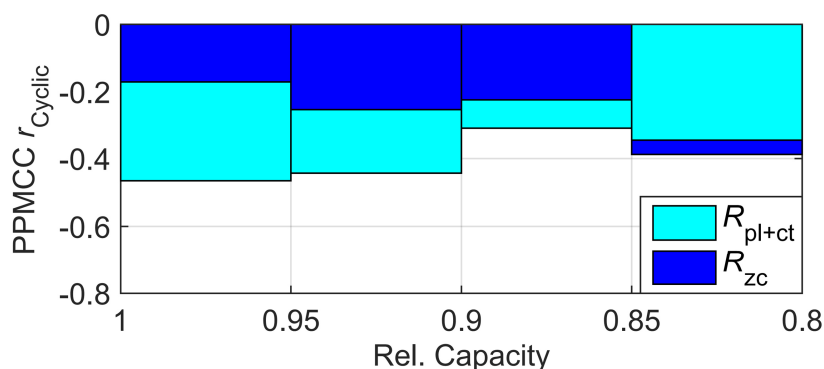


Figure 49: Stepwise calculation of single aging state PPMCC values for the batch of “Cyclic” cells. [186]

8.5 Conclusion

In this chapter, the correlation between capacity and impedance parts of LIC during calendar and cycle life was investigated. Therefore, again the characterization data sets of the 484 new cells and 954 aged cells, out of two BEV each, were used. In addition, the aging data of 83 cells from the first phase of the laboratory aging experiments was considered, which in turn consisted of a variety of storage and operational conditions.

By analyzing yielded data sets of single aging states with PPMCC calculation, results let assume an increase of correlation between R_{zc} and capacity, but a decrease between capacity and $R_{\text{pl+ct}}$. However, these tendencies seemed to depend strongly on the amount of cell outliers and thus, should not be used for interpretation with regard to any specific aging mechanisms.

Regression curves for impedance parts and corresponding capacity values were calculated by linear regression analysis. By inserting values of respective impedance parts in these equations, SoH quick test capacity for a LIC (of the same type) in any specific state of aging was quickly given as a result. Thereby, the main reason to use the impedance part R_{zc} in contrast to R_{pl+ct} for the SoH quick test was its SoC independency and occurrence at high frequencies in the impedance spectrum. However, a major issue was the observance of different “branches” in the scatter plots; the values of R_{zc} of stored compared with cycled cells were higher at corresponding residual capacities. The branch of cells cycled with an unchallenging load profile at high temperatures was congruent with the one of stored cells.

The appearance of different branches for cycled and stored cells might origin from the multilayered structure of passive layers with mainly inorganic or organic salts close to the electrode or electrolyte, respectively; therefore, the effects on capacity and impedance could vary for calendric and cyclic aging as the first may only lead to a thickening of the layer close to the electrolyte but the second provoke complete reconstruction. As a result, capacity and impedance development could correlate nevertheless for each single case, but impedance increase for the same capacity fade would differ. Thus, the choice of a suited load profile to create the required aging data set, which is used for *parameterization*, is *crucial but absolutely essential*.

With regard to the refurbishing process of SLB, optical failure inspection, serial number based aging detection and analysis of logged BEV data is usually conducted before the costly capacity measuring process. As a consequence, battery units which are apparently not suited for reuse are sorted out in advance to minimize refurbishing costs. Generally, if a deviation of approx. 10% can be accepted for the intended field of application, the proposed SoH quick test is regarded as a viable approach. Though, with regard to the limited precision, it is recommended to use the suggested approach in the refurbishing process only to additionally reduce the amount of battery units in advance to the capacity measuring process. To omit it completely, the precision of SoH quick test must be generally increased on the one hand, whereas on the other, legal certainty should be created, as there are currently no related standards.

9 Final Conclusion

To finally conclude the thesis “Reuse of Automotive Lithium-Ion Batteries: An Assessment from the Cell Aging Perspective”, at first, the main findings are summarized in the following subchapter. Additionally, a short outlook is given, pointing out still present SLC research fields. Afterwards, in Subchapter 9.2, for a most successful realization of battery reuse scenarios, the top three priority recommendations for action are presented. These special tasks were worked out, and after all decided by vote, by the authors of [14] in cooperation with a study related advisory board. Those recommended actions are discussed and assessed within the scope of this work.

9.1 Summary

In Chapter 1, former battery reuse studies were concisely summed up, and the topic was put into an actual broader context, which is basically, the energy revolution and the launch of BEV. Latest studies consistently state, on the one hand, that the potential of SLC to reduce the acquisition costs of BEV must be regarded as rather low, but, on the other hand, there are positive effects, which especially arise from the availability of cheap SLB for stationary energy storage. Moreover, reuse concepts of aged ALIB can be imagined as a temporal bridge from uneconomic to economic times of recycling (whereas the latter are expected to be reached in the near future).

The different battery life cycle stages within a SLC were presented in Chapter 2. Aside from an adequate operation of SLB, which especially considers their pre-aged state, the refurbishing process, i.e., all necessary steps from automotive battery removal to the development of “new” SLB, has been identified to play an essential role in reaching profitability of SLC. As a part of the refurbishing process, SoH detection of respective battery units is regarded as the crucial point. Thereby, either SoH quick tests, or ideally, algorithm implementation which enables online logging of relevant state variables in BEV with sufficient precision, could lead to clearly reduced costs of the refurbishing process and thus, to an increase of the residual value of aged ALIB.

The different aging mechanisms, which are known to occur in LIC, were described in Chapter 3. Thereby, focus was laid particularly on those mechanisms, which lead to the so called effect of nonlinear aging. This aging phenomenon is critical regarding the implementation of SLC, as the desired second service life would be severely limited by its occurrence (which is usually observed at residual capacities of approx. 80%). At the turning point, i.e., the start of nonlinear aging, lithium plating is assumed to occur as a result of the increased overpotentials and reduced capacity of the graphite anode. Because of the self-reinforcing nature of lithium plating,

which is accompanied by an increased distortion of the electrode balancing, an adverse circle of lithium and graphite active material loss is finally assumed to provoke the effect of nonlinear aging. With regard to the stress factors, which promote the occurrence of lithium plating, i.e., high charging rates and end voltages at low temperatures, SLC specific operational strategies can be derived (which especially aim at extending the second service life of SLB by suppressing nonlinear aging). Furthermore, at the end of Chapter 3, causes were described, which lead to a continuous increase of the cell-to-cell variation in multi-cell battery applications (such as BEV); thereby, an intrinsic cell-to-cell variation, which results from deviations in the production process, is basically increased with the progress of aging due to external influences like SoC drifts of cells or temperature gradients in a battery pack.

The required statistical fundamentals (univariate and bivariate analysis, link to the battery cell and module interconnection configuration) were presented in Chapter 4. Afterwards, in Chapter 5, the experimental setup was described. Moreover, background information on the examined BEV was provided. The main part of the work *“Reuse of Automotive Lithium-Ion Batteries: An Assessment from the Cell Aging Perspective”* (Chapter 6, 7 and 8) was structured in two technological core issues, which directly originate from the nature of LIC aging, and two corresponding solution approaches. As the respective chapters in the main part of the work already end in each case with a conclusion, to avoid unnecessary repetition, the results were additionally reduced to the essential, and presented here in headword style.

Core Issue: Nonlinear Aging → Solution Approach: Aging Dependent Load Adaption

- nonlinear aging can be delayed or even avoided by a reduction of the charging rate; by a reduction of the voltage swing (reduced charging end voltage, increased discharging end voltage); by operation at the cell specific temperature optimum
- two-step parameter (voltage swing, charging rate, temperature) load adaption, shortly before the onset of nonlinear aging, is effective towards its suppression
- the influence of the operational prehistory is marginal for cells (of the investigated model) which mainly suffered from cyclic aging
- the influence of the operational prehistory is significant for cells (of the investigated model) which severely suffered from calendric aging (i.e., those stored at high SoC and temperature) as they quickly exhibit capacity breakdown after the start of cycling
- continuous charging rate adaption (close-to-the-edge charging) principally enables fast charging without a reduction of the reachable service life

Finally, nonlinear aging is considered to be controllable by aging dependent load adaption; though, as its onset must not be missed under any circumstances, reliable and precise online SoH detection of battery modules is the key to success. In general, a well-coordinated operational strategy appears to be capable of reducing the risk of nonlinear aging up to the minimum.

Core Issue: Increasing Cell-to-Cell Variation → Solution Approach: SoH Quick Tests

- strength of variation and amount of outlier cells is increased with the progress of aging
- outlier cells are mostly found on the side of higher degradation (lower capacity, higher impedance; “unidirectional diversification”)
- alteration from symmetric normal to skewed Weibull distribution
- appearance of outlier cells seems to be random and inevitable
- cell-to-cell variation, which is transferred to the module level, is more critical than cell outliers with regard to the implementation of SLC
- correlation (between capacity and impedance) based SoH quick tests must be parameterized with aging data which is similar to the practical use
- SoH quick tests (with limited precision) are capable of sorting out battery units in advance to the costly capacity measuring process

After all, to support the profitability of SLC, reversible and easily detachable cell and module interconnection techniques should be favored, as reduced refurbishing costs clearly increase the residual value of aged ALIB. With regard to the limited precision of SoH quick tests, currently only a supporting role in the pre-selection process of battery units is recommended. Following the flow charts of the main and the refurbishing process of SLC (shown in Figure 3 and Figure 4), an adapted battery unit characterization and selection process is presented in Figure 50, in which the SoH quick test is upstream to the capacity (and impedance) measurement. Main aim is to sort out battery units, which are not reusable, in advance to the costly capacity measuring process. Ideally, no further battery unit classification based on costly measurements would be needed at all after retrieval of aging dependent BMS state variables. Therefore, it is necessary to develop highly-precise SoH quick tests, which are runnable on the BMS of an ALIB.

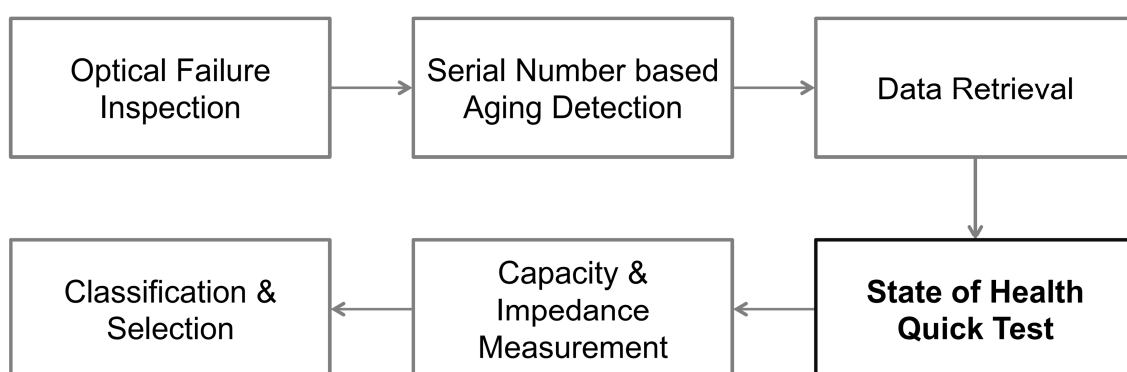


Figure 50: Adapted battery unit characterization and selection process with the state of health quick test only to support the steps of pre-selection.

Finally, with regard to the technological barriers which emerge directly from the nature of LIC aging, battery SLC are regarded as well implementable (especially if online SoH detection is refined); in contrast, legal and logistic issues (which are especially present due to the high number of involved actors) are considered to be the more challenging part of economic SLC realization. Here, the key is to revise present standards and norms, specifically with regard to battery reuse concepts and thus, creating legal certainty for an utterly new market.

9.2 Recommendations for Action

The top three priority recommended actions to promote the implementation of battery reuse scenarios (determined by vote by the authors of [14] and a study related advisory board) are:

- interface standardization to enable simple insight in the battery operational history
- definition of safety specific norms and standards for pre-aged batteries
- comprehensive analysis of the SLB market

The interface standardization is needed for straightforward data acquisition. In the ideal case, as aforementioned, aging dependent BMS state variables already enable to separate reusable battery units from those which are not. The costly capacity measurement process would then be obsolete. Thus, the refinement of online SoH detection methodologies is of great importance regarding the implementation of SLC, and the operation of LIB in general.

In the literature, there are contradicting statements regarding the issue if the safety of LIB is influenced by the progress of aging. Exemplarily, it is stated in [81, 187] that aging leads to reduced safety but just the opposite is mentioned in [188]. With regard to the implementation of SLC, results of commonly prescribed safety tests, performed with new batteries and aged ones with residual capacities smaller than 80%, should be compared to answer this serious question. By that, insurance companies could be encouraged to offer coverage to SLB storage operators. Furthermore, as strong capacity fade (like residual capacities smaller than 80%) can be an indicator e.g. for small internal short-circuits, quickly classifying a battery as “safe” is actually just possible if the battery operational prehistory is available. If the respective data set does not disclose any signs of nonlinear aging, the battery can principally be regarded as safe even if the battery aging progress is heavily advanced (but still in the area of linear aging).

The market acceptance towards used batteries is generally a considerable uncertainty. The target groups of the, at present, imaginary SLB market and simultaneously their willingness to pay must therefore be analyzed in more detail. Additionally, the availability of aged automotive batteries must be compared with storage capacities of applications which are suitable for SLB, via supply and demand analysis. Finally, the market acceptance towards used batteries is also influenced by a variety of technological aspects, like the aforementioned safety level or the ecological impact of batteries. Thus, upcoming battery research and development is decisive for

SLC implementation, but could also counteract its profitability as a SLB has always to compete with a technologically superior, new battery model.

List of References

- [1] B.G. Pollet, I. Staffell, J.L. Shang, Current status of hybrid, battery and fuel cell electric vehicles: From electrochemistry to market prospects, *Electrochim. Acta* 84 (2012) 235-249.
- [2] O. van Vliet, A.S. Brouwer, T. Kuramochi, M. van den Broek, A. Faaij, Energy use, cost and CO₂ emissions of electric cars, *J. Power Sources* 196 (2011) 2298-2310.
- [3] R. McCarthy, C. Yang, Determining marginal electricity for near-term plug-in and fuel cell vehicle demands in California: Impacts on vehicle greenhouse gas emissions, *J. Power Sources* 195 (2010) 2099-2109.
- [4] S. Dunn, Hydrogen futures: toward a sustainable energy system, *Int. J. Hydrogen Energ.* 27 (2002) 235-264.
- [5] Kraftfahrtbundesamt (29. October 2015):
http://www.kba.de/DE/Statistik/Fahrzeuge/Bestand/Umwelt/2014_b_umwelt_duсл_absolut.html
- [6] Prognos AG, Energiewirtschaftliches Institut an der Universität Köln, Gesellschaft für wirtschaftliche Strukturforchung, Entwicklung der Energiemärkte – Energiereferenzprognose, Project Nr. 57/12, Basel, Cologne, Osnabrück, 2015.
- [7] K. Kairies, D. Haberschusz, D. Magnor, M. Leuthold, J. Badeda, D.U. Sauer, Wissenschaftliches Mess- und Evaluierungsprogramm Solarstromspeicher, Institut für Stromrichtertechnik und Elektrische Antriebe (iSEA), Annual Report, Aachen, 2015.
- [8] B. Battke, T.S. Schmidt, D. Grosspietsch, V.H. Hoffmann, A review and probabilistic model of lifecycle costs of stationary batteries in multiple applications, *Renew. Sustainable Energy Rev.* 25 (2013) 240-250.
- [9] H. Vikström, S. Davidsson, M. Höök, Lithium availability and future production outlooks, *Appl. Energy* 110 (2013) 252-266.
- [10] E. Rahimzei, K. Sann, M. Vogel, Kompendium: Li-Ionen-Batterien - Grundlagen, Bewertungskriterien, Gesetze und Normen, VDE Verband der Elektrotechnik, Frankfurt am Main, 2015.
- [11] D.C.R. Espinosa, A.M. Bernardes, J.A.S. Tenório, An overview on the current processes for the recycling of batteries, *J. Power Sources* 135 (2004) 311-319.
- [12] L. Gaines, R. Cuenca, Costs of Lithium-Ion Batteries for Vehicles, Argonne National Laboratory, Technical Report ANL/ESD-42, Chicago, 2000.

- [13] M. Gellner, L. Wuschke, H. Jäckel, U.A. Peuker, Akkus mechanisch aufbereiten, RECYCLING Magazin 16 (2015) 26-29.
- [14] S. Fischhaber, A. Regett, S.F. Schuster, H. Hesse, Second-Life-Konzepte für Lithium-Ionen-Batterien aus Elektrofahrzeugen, Ergebnisrapport Nr. 18 (Begleit- und Wirkungsforschung), Frankfurt am Main, 2016.
- [15] B. Nykvist, M. Nilsson, Rapidly falling costs of battery packs for electric vehicles, Nat. Clim. Chang. 5 (2015) 329-332.
- [16] EFS, DNV GL, What's driving tomorrow's electricity grid, Position Paper, Høvik, Wien, 2015.
- [17] B.D. Williams, T.E. Lipman, Strategies for transportation electric fuel implementation in California: Overcoming battery first-cost hurdles, California Energy Commission, PIER Transportation Program, Final Report CEC-500-2009-091, Berkeley, 2010.
- [18] California Environmental Protection Agency: Air Resources Board (6. September 2015): <http://www.arb.ca.gov/msprog/zevprog/zevprog.htm>
- [19] N. Pinsky, Electric Vehicle Battery 2nd Use Study, Argonne National Laboratory, Lemont, 1998.
- [20] E. Cready, J. Lippert, J. Pihl, I. Weinstock, P. Symons, R.G. Jungst, Technical and Economic Feasibility of Applying Used EV Batteries in Stationary Applications: A Study for the DOE Energy Storage Systems Program, U.S. Department of Energy, Sandia National Laboratories, Final Report SAND2002-4084, Albuquerque, Livermore, 2003.
- [21] A. Burke, Performance, Charging, and Second-use Considerations for Lithium Batteries for Plug-in Electric Vehicles, Institute of Transportation Studies, Research Report UCD-ITS-RR-09-17, Davis, 2009.
- [22] B. Williams, T. Lipman, Analysis of the combined vehicle- and post-vehicle-use value of lithium-ion plug-in-vehicle propulsion batteries. Task 3, Second life applications and value of "traction" lithium batteries, Transportation of Sustainability Research Center, Final Report 500-02-004, Berkeley, 2011.
- [23] C.K. Narula, R. Martinez, O. Onar, M.R. Starke, G. Andrews, Economic analyses of deploying used batteries in power systems, U.S. Department of Energy, Oak Ridge National Laboratory, Final Report ORNL/TM-2011/151, Oak Ridge, 2011.
- [24] J. Neubauer, K. Smith, E. Wood, A. Pesaran, Identifying and Overcoming Critical Barriers to Widespread Second Use of PEV Batteries, National Renewable Energy Laboratory, Technical Report NREL/TP-5400-63332, Golden, 2015.

- [25] M. Bowler, J. Weber, D. Bodde, J. Taiber, T. Kurfess, Battery second use: Sustainable life cycle design through the extension of tools used in the vehicle development process, 5th International Conference on Sustainable Automotive Technologies (ICSAT), Ingolstadt, September 2013.
- [26] E.N. Elkind, S. Hecht, C. Horowitz, S. Weissman, REUSE AND REPOWER - How to Save Money and Clean the Grid with Second-Life Electric Vehicle Batteries, CLEE, Emmett Institute, Final Report, California, 2014.
- [27] D. Beverungen, C. Fabry, W. Ganz, M. Matzner, G. Satzger, Dienstleistungsinnovationen für Elektromobilität, DELFIN, Final Report, Aachen, Karlsruhe, Münster, Stuttgart, 2015.
- [28] J. Warner, The Handbook of Lithium-Ion Battery Pack Design, 1st ed., Elsevier Science, 2015.
- [29] R. Sathre, C.D. Scown, O. Kavadia, T.P. Hendrickson, Energy and climate effects of second-life use of electric vehicle batteries in California through 2050, J. Power Sources 288 (2015) 82-91.
- [30] D. Hustadt, Vattenfall Company Blog (21. August 2015):
<http://blog.vattenfall.de/das-zweite-leben-der-e-mobility-batterien/>
- [31] Heise Autos, Heise online (26. October 2015):
<http://www.heise.de/autos/artikel/Joint-Venture-baut-Speicher-aus-gebrauchten-E-Auto-Akkus-2854938.html>
- [32] S.J. Tong, A. Same, M.A. Kootstra, J.W. Park, Off-grid photovoltaic vehicle charge using second life lithium batteries: An experimental and numerical investigation, Appl. Energy 104 (2013) 740-750.
- [33] Forsee Power - Designing Tomorrow (10. July 2015):
http://www.forseepower.fr/wp-content/uploads/2015/07/10072015_2nd-Life-Project_DE.pdf
- [34] Battery University Website (3. November 2015):
http://batteryuniversity.com/learn/article/battery_statistics
- [35] J. Neubauer, A. Pesaran, The ability of battery second use strategies to impact plug-in electric vehicle prices and serve utility energy storage applications, J. Power Sources 196 (2011) 10351-10358.
- [36] J.S. Neubauer, A. Pesaran, B. Williams, M. Ferry, J. Eyer, A Techno-Economic Analysis of PEV Battery Second Use Repurposed-Battery Selling Price and Commercial and Industrial End-User Value, SAE International 2012-01-0349 (2012).
- [37] H. Ambrose, D. Gershenson, A. Gershenson, D. Kammen, Driving rural energy access: a second-life application for electric-vehicle batteries, Environ. Res. Lett. 9 (2014) 094004.

- [38] K.N. Genikomsakis, C.S. Ioakimidis, A. Murillo, A. Trifonova, D. Simic, A Life Cycle Assessment of a Li-ion urban electric vehicle battery, 27th International Electric Vehicle Symposium and Exhibition (EVS), Barcelona, November 2013.
- [39] D. Kim, A. Geissler, C. Menn, D. Hengevoss, Quantifizierung des Umweltnutzens von gebrauchten Batterien aus Elektrofahrzeugen als gebäudeintegrierte 2nd-Life-Stromspeichersysteme, *Bauphysik* 37 (2015) 213-222.
- [40] R. Faria, P. Marques, R. Garcia, P. Moura, F. Freire, J. Delgado, A.T. de Almeida, Primary and secondary use of electric mobility batteries from a life cycle perspective, *J. Power Sources* 262 (2014) 169-177.
- [41] L. Ahmadi, A. Yip, M. Fowler, S.B. Young, R.A. Fraser, Environmental feasibility of re-use of electric vehicle batteries, *Sust. Energy Tech. Assess.* 6 (2014) 64-74.
- [42] E. Wood, M. Alexander, T.H. Bradley, Investigation of battery end-of-life conditions for plug-in hybrid vehicles, *J. Power Sources* 11 (2011) 5147-5154.
- [43] B. Lutz, Z. Yan, J.B. Gerschler, D.U. Sauer, Influence of plug-in hybrid electric vehicle charging strategies on charging and battery degradation costs, *Energy Policy* 46 (2012) 511-519.
- [44] J. Neubauer, A. Brooker, E. Wood, Sensitivity of plug-in hybrid electric vehicle economics to drive patterns, electric range, energy management, and charge strategies, *J. Power Sources* 236 (2013) 357-364.
- [45] C. Heymans, S.B. Walker, S.B. Young, M. Fowler, Economic analysis of second use electric vehicle batteries for residential energy storage and load-levelling, *Energy Policy* 71 (2014) 22-30.
- [46] M. Naumann, R.C. Karl, C.N. Truong, H. Hesse, A. Jossen, Lithium-ion battery cost analysis in PV-household application, 9th International Renewable Energy Storage Conference (IRES), Düsseldorf, March 2015.
- [47] C. Guenther, M. Taumann, J. Li, M.A. Danzer, Calculation of the Residual Value of Used Electric Vehicle Batteries for Stationary Second Life Applications, European Advanced Automotive & Stationary Battery Conference (AABC), Mainz, January 2015.
- [48] M.J. Brand, S.F. Schuster, T. Bach, E. Fleder, M. Stelz, S. Gläser, J. Müller, G. Sextl, A. Jossen, Effects of vibrations and shocks on lithium-ion cells, *J. Power Sources* 288 (2015) 62-69.
- [49] S.M. Rezvanizani, Z. Liu, Y. Chen, J. Lee, Review and recent advances in battery health monitoring and prognostics technologies for electric vehicle (EV) safety and mobility, *J. Power Sources* 256 (2014) 110-124.

- [50] Y. Zheng, L. Lu, X. Han, J. Li, M. Ouyang, LiFePO₄ battery pack capacity estimation for electric vehicles based on charging cell voltage curve transformation, *J. Power Sources* 226 (2013) 33-41.
- [51] K. Ridder, J. Holzhäuser, ADR 2015, 30st ed., ecomed - Storck GmbH, Heidelberg, Munich, Landsberg, Frechen, Hamburg, 2014.
- [52] S. Grolleau, A. Delaille, H. Gualous, P. Gyan, R. Revel, J. Bernard, E. Redondo-Iglesias, J. Peter, Calendar aging of commercial graphite/LiFePO₄ cell - Predicting capacity fade under time dependent storage conditions, *J. Power Sources* 255 (2014) 450-458.
- [53] A. Barré, B. Deguilhem, S. Grolleau, M. Gérard, F. Suard, D. Riu, A review on lithium-ion battery ageing mechanisms and estimations for automotive applications, *J. Power Sources* 241 (2013) 680-689.
- [54] K. Takeno, M. Ichimura, K. Takano, J. Yamaki, S. Okada, Quick testing of batteries in lithium-ion battery packs with impedance-measuring technology, *J. Power Sources* 128 (2004) 67-75.
- [55] G. Hunt, Electric Vehicle Battery Test Procedures Manual. U.S. Adv. Battery Consort., LLC, 1996.
- [56] R.B. Wright, J.P. Christophersen, C.G. Motloch, J.R. Belt, C.D. Ho, V.S. Battaglia, J.A. Duong, R.A. Sutula, Power fade and capacity fade from cycle-life testing of Advanced Technology Development Program lithium-ion batteries, *J. Power Sources* 119-121 (2003) 865-869.
- [57] W. Waag, S. Käbitz, D.U. Sauer, Experimental investigation of the lithium-ion battery impedance characteristic at various conditions and aging states and its influence on the application, *Appl. Energy* 102 (2013) 885-897.
- [58] C.T. Love, M.B.V. Virji, R.E. Rocheleau, K.E. Swider-Lyons, State-of-health monitoring of 18650 4S packs with a single-point impedance diagnostic, *J. Power Sources* 266 (2014) 512-519.
- [59] D. Andre, M. Meiler, K. Steiner, Ch. Wimmer, T. Soczka-Guth, D.U. Sauer, Characterization of high-power lithium-ion batteries by electrochemical impedance spectroscopy. I. Experimental investigation, *J. Power Sources* 196 (2011) 5334-5341.
- [60] F.M. Kindermann, A. Noel, S.V. Erhard, A. Jossen, Long-term equalization effects in Li-ion batteries due to local state of charge inhomogeneities and their impact on impedance measurements, *Electrochim. Acta* 185 (2015) 107-116.
- [61] H. Dong, X. Liu, Y. Lou, C. Wang, Lithium-ion battery state of health monitoring and remaining useful life prediction based on support vector regression-particle filter, *J. Power Sources* 271 (2014) 114-123.

- [62] P. Keil, S.F. Schuster, C. von Lüders, H. Hesse, R. Arunachala, A. Jossen, Lifetime Analyses of Lithium-Ion EV Batteries, Electromobility Challenging Issues Conference (ECI), Singapore, December, 2015.
- [63] J. Schmalstieg, S. Käbitz, M. Ecker, D.U. Sauer, A holistic aging model for Li(NiMnCo)O₂ based 18650 lithium-ion batteries, *J. Power Sources* 257 (2014) 325-334.
- [64] J. Wang, P. Liu, J. Hicks-Garner, E. Sherman, S. Soukiazian, M. Verbrugge, H. Tataria, J. Musser, P. Finamore, Cycle-life model for graphite-LiFePO₄ cells, *J. Power Sources* 196 (2011) 3942-3948.
- [65] M. Ecker, N. Nieto, S. Käbitz, J. Schmalstieg, H. Blanke, A. Warnecke, D.U. Sauer, Calendar and cycle life study of Li(NiMnCo)O₂-based 18650 lithium-ion batteries, *J. Power Sources* 248 (2014) 839-851.
- [66] D.A. Stevens, R.Y. Ying, R. Fathi, J.N. Reimers, J.E. Harlow, J.R. Dahn, Using High Precision Coulometry Measurements to Compare the Degradation Mechanisms of NMC/LMO and NMC-Only Automotive Scale Pouch Cells, *J. Electrochem. Soc.* 161 (2014) A1364-A1370.
- [67] M. Wohlfahrt-Mehrens, C. Vogler, J. Garche, Aging mechanisms of lithium cathode materials, *J. Power Sources* 127 (2004) 58-64.
- [68] J. Vetter, P. Novák, M.R. Wagner, C. Veit, K.-C. Möller, J.O. Besenhard, M. Winter, M. Wohlfahrt-Mehrens, C. Vogler, A. Hammouche, Ageing mechanisms in lithium-ion batteries, *J. Power Sources* 147 (2005) 269-281.
- [69] P. Keil, S.F. Schuster, J. Wilhelm, J. Travi, A. Hauser, R.C. Karl, A. Jossen, Calendar Aging of Lithium-Ion Batteries. Part I: Impact of the Graphite Anode on Capacity Fade, *J. Electrochem. Soc.* 163 (2016) A1872-A1880.
- [70] T. Waldmann, M. Wilka, M. Kasper, M. Fleischhammer, M. Wohlfahrt-Mehrens, Temperature dependent ageing mechanisms in Lithium-ion batteries - A Post-Mortem study, *J. Power Sources* 262 (2014) 129-135.
- [71] M. Kassem, J. Bernard, R. Revel, S. Pélissier, F. Duclaud, C. Delacourt, Calendar aging of a graphite/LiFePO₄ cell, *J. Power Sources* 208 (2012) 296-305.
- [72] P. Balbuena, Y. Wang, *Lithium-Ion Batteries - Solid-Electrolyte Interphase*, first ed., World Scientific Pub Co, London, 2004.
- [73] M. Shikano, H. Kobayashi, S. Koike, H. Sakaebe, Y. Saito, H. Hori, H. Kageyama, K. Tatsumi, X-ray absorption near-edge structure study on positive electrodes of degraded lithium-ion battery, *J. Power Sources* 196 (2011) 6881-6883.

- [74] M.K. Rahman, Y. Saito, Investigation of positive electrodes after cycle testing of high-power Li-ion battery cells III: An approach to the power fade mechanism using FT-IR-ATR, *J. Power Sources* 174 (2007) 889-894.
- [75] N. Dupré, J. Martin, J. Oliveri, P. Soudan, A. Yamada, R. Kanno, D. Guyomard, Relationship between surface chemistry and electrochemical behavior of $\text{LiNi}_{1/2}\text{Mn}_{1/2}\text{O}_2$ positive electrode in a lithium-ion battery, *J. Power Sources* 196 (2011) 4791-4800.
- [76] V. Agubra, J. Fergus, Lithium Ion Battery Anode Aging Mechanisms, *Mater.* 6 (2013) 1310-1325.
- [77] S. Kim, A.C.T. van Duin, V.B. Shenoy, Effect of electrolytes on the structure and evolution of the solid electrolyte interphase (SEI) in Li-ion batteries: A molecular dynamics study, *J. Power Sources* 196 (2011) 8590-8597.
- [78] B. Rieger, S. Schlueter, S.V. Erhard, J. Schmalz, G. Reinhart, A. Jossen, Multi-scale investigation of thickness changes in a commercial pouch type lithium-ion battery, *J. Energy Storage* 6 (2016) 213-221.
- [79] M. Broussely, P. Biensan, F. Bonhomme, P. Blanchard, S. Herreyre, K. Nechev, R.J. Staniewicz, Main aging mechanisms in Li ion batteries, *J. Power Sources* 146 (2005) 90-96.
- [80] H.J. Ploehn, P. Ramadass, R.E. White, Solvent Diffusion Model for Aging of Lithium-Ion Battery Cells, *J. Electrochem. Soc.* 151 (2004) A456-A462.
- [81] P. Röder, B. Stiaszny, J. Ziegler, N. Baba, P. Lagaly, H. Wiemhöfer, The impact of calendar aging on the thermal stability of a $\text{LiMn}_2\text{O}_4\text{-Li}(\text{Ni}_{1/3}\text{Mn}_{1/3}\text{Co}_{1/3})\text{O}_2$ /graphite lithium-ion cell, *J. Power Sources* 268 (2014) 315-325.
- [82] E. Sarasketa-Zabala, I. Gandiaga, L.M. Rodriguez-Martinez, I. Villarreal, Calendar ageing analysis of a LiFePO_4 /graphite cell with dynamic model validations: Towards realistic lifetime predictions, *J. Power Sources* 272 (2014) 45-47.
- [83] J. Choi, A. Manthiram, Role of Chemical and Structural Stabilities on the Electrochemical Properties of Layered $\text{LiNi}_{1/3}\text{Mn}_{1/3}\text{Co}_{1/3}\text{O}_2$ Cathodes, *J. Electrochem. Soc.* 152 (2005) A1714-A1718.
- [84] D. Mohanty, H. Gabrisch, Microstructural investigation of $\text{Li}_x\text{Ni}_{1/3}\text{Mn}_{1/3}\text{Co}_{1/3}\text{O}_2$ ($x \leq 1$) and its aged products via magnetic and diffraction study, *J. Power Sources* 220 (2012) 405-412.
- [85] R. Chen, F. Liu, Y. Chen, Y. Ye, Y. Huang, F. Wu, L. Li, An investigation of functionalized electrolyte using succinonitrile additive for high voltage lithium-ion batteries, *J. Power Sources* 306 (2016) 70-77.

- [86] J. Zhou, P.H.L. Notten, Studies on the degradation of Li-ion batteries by the use of microreference electrodes, *J. Power Sources* 177 (2008) 553-560.
- [87] J. Xia, M. Nie, L. Ma, J.R. Dahn, Variation of coulombic efficiency versus upper cutoff potential of Li-ion cells tested with aggressive protocols, *J. Power Sources* 306 (2016) 233-240.
- [88] I. Buchberger, S. Seidlmayer, A. Pokharel, M. Piana, J. Hattendorff, P. Kudejova, R. Gilles, H.A. Gasteiger, Aging Analysis of Graphite/LiNi_{1/3}Mn_{1/3}Co_{1/3}O₂ Cells Using XRD, PGAA, and AC Impedance, *J. Electrochem. Soc.* 162 (2015) A2737-A2746.
- [89] F. Lin, I.M. Markus, D. Nordlund, T. Weng, M.D. Asta, H.L. Xin, M.M. Doeff, Surface reconstruction and chemical evolution of stoichiometric layered cathode materials for lithium-ion batteries, *Nat. Commun.* 5 (2014) Art. 3529.
- [90] B. Stiaszny, J.C. Ziegler, E.E. Krauß, M. Zhang, J.P. Schmidt, E. Ivers-Tiffée, Electrochemical characterization and post-mortem analysis of aged LiMn₂O₄-NMC/graphite lithium ion batteries part II: Calendar aging, *J. Power Sources* 258 (2014) 61-75.
- [91] J. Wang, Y. Tang, J. Yang, R. Li, G. Liang, X. Sun, Nature of LiFePO₄ aging process: Roles of impurity phases, *J. Power Sources* 238 (2013) 454-463.
- [92] L. Bodenes, R. Naturel, H. Martinez, R. Dedryvère, M. Menetrier, L. Croguennec, J. Pérès, C. Tessier, F. Fischer, Lithium secondary batteries working at very high temperature: Capacity fade and understanding of aging mechanisms, *J. Power Sources* 236 (2013) 265-275.
- [93] J.C. Burns, A. Kassam, N.N. Sinha, L.E. Downie, L. Solnickova, B.M. Way, J.R. Dahn, Predicting and Extending the Lifetime of Li-ion Batteries, *J. Electrochem. Soc.* 160 (2013) A1451-A1456.
- [94] J. Wang, J. Purewal, P. Liu, J. Hicks-Garner, S. Soukazian, E. Sherman, A. Sorenson, L. Vu, H. Tataria, M.W. Verbrugge, Degradation of lithium ion batteries employing graphite negatives and nickel-cobalt-manganese oxide + spinel manganese oxide positives: Part 1, aging mechanisms and life estimation, *J. Power Sources* 269 (2014) 937-948.
- [95] T. Ohzuku, Y. Iwakoshi, K. Sawai, Formation of Lithium-Graphite Intercalation Compounds in Nonaqueous Electrolytes and Their Application as a Negative Electrode for a Lithium Ion (Shuttlecock) Cell, *J. Electrochem. Soc.* 140 (1993) 2490-2498.
- [96] W.H. Woodford, W.C. Carter, Y. Chiang, Design criteria for electrochemical shock resistant battery electrodes, *Energy Environ. Sci.* 5 (2012) 8014-8024.

- [97] W. Yoon, K.Y. Chung, J. McBreen, X. Yang, A comparative study on structural changes of $\text{LiCo}_{1/3}\text{Ni}_{1/3}\text{Mn}_{1/3}\text{O}_2$ and $\text{LiNi}_{0.8}\text{Co}_{0.15}\text{Al}_{0.05}\text{O}_2$ during first charge using in situ XRD, *Electrochem. Commun.* 8 (2006) 1257-1262.
- [98] M. Klett, R. Eriksson, J. Groot, P. Svens, K.C. Höglström, R.W. Lindström, H. Berg, T. Gustafson, G. Lindbergh, K. Edström, Non-uniform aging of cycled commercial LiFePO_4 /graphite cylindrical cells revealed by post-mortem analysis, *J. Power Sources* 257 (2014) 126-137.
- [99] J. Groot, State-of-Health Estimation of Li-ion Batteries: Cycle Life Test Methods, Chalmers University of Electronics, Licentiate Thesis, Gothenburg, 2012.
- [100] K. Xu, "Charge-Transfer" Process at Graphite/Electrolyte Interface and the Solvation Sheath Structure of Li^+ in Nonaqueous Electrolytes, *J. Electrochem Soc.* 154 (2007) A162-A167.
- [101] M.D. Levi, E. Markevich, D. Aurbach, The Effect of Slow Interfacial Kinetics on the Chronoamperometric Response of Composite Lithiated Graphite Electrodes and on the Calculation of the Chemical Diffusion Coefficient of Li Ions in Graphite, *J. Phys. Chem. B* 109 (2005) 7420-7427.
- [102] C. Uhlmann, J. Illig, M. Ender, R. Schuster, E. Ivers-Tiffée, In situ detection of lithium metal plating on graphite in experimental cells, *J. Power Sources* 279 (2015) 428-438.
- [103] M. Petzl, M. Kasper, M. Danzer, Lithium plating in a commercial lithium-ion battery - A low-temperature aging study, *J. Power Sources* 275 (2015) 799-807.
- [104] B. Bitzer, A. Gruhle, A new method for detecting lithium plating by measuring the cell thickness, *J. Power Sources* 262 (2014) 297-302.
- [105] M. Fleischhammer, T. Waldmann, G. Bisle, B. Hogg, M. Wohlfahrt-Mehrens, Interaction of cyclic ageing at high-rate and low temperatures and safety in lithium-ion batteries, *J. Power Sources* 274 (2015) 432-439.
- [106] W. Lu, C.M. López, N. Liu, J.T. Vaughey, A. Jansen, D.W. Dennis, Overcharge Effect on Morphology and Structure of Carbon Electrodes for Lithium-Ion Batteries, *J. Electrochem. Soc.* 159 (2012) A566-A570.
- [107] A.N. Jansen, D.W. Dees, D.P. Abraham, K. Amine, G.L. Henriksen, Low-temperature study of lithium-ion cells using Li_3Sn micro-reference electrode, *J. Power Sources* 174 (2007) 373-379.
- [108] S.S. Zhang, K. Xu, T.R. Jow, Study of the charging process of a LiCoO_2 -based Li-ion battery, *J. Power Sources* 160 (2006) 1349-1354.

- [109] R.V. Bugga, M.C. Smart, Lithium plating behavior in lithium-ion cells, *ECS Transactions* 25 (2010) 241-252.
- [110] R. Mukherjee, A.V. Thomas, D. Datta, E. Singh, J. Li, O. Eksik, V.B. Shenoy, N. Koratkar, Defect-induced plating of lithium metal within porous graphene networks, *Nat. Commun.* 5 (2014) Art. 3710.
- [111] N. Legrand, B. Knosp, P. Desprez, F. Lopicque, S. Rael, Physical characterization of the charging process of a Li-ion battery and prediction of Li plating by electrochemical modelling, *J. Power Sources* 245 (2014) 208-216.
- [112] V. Zinth, C. von Lüders, M. Hofmann, J. Hattendorff, I. Buchberger, S. Erhard, J. Rebelo-Kornmeier, A. Jossen, R. Gilles, Lithium plating in lithium-ion batteries at sub-ambient temperatures investigated by in situ neutron diffraction, *J. Power Sources* 271 (2014) 152-159.
- [113] S. Schindler, M. Bauer, M. Petzl, M.A. Danzer, Voltage relaxation and impedance spectroscopy as in-operando methods for the detection of lithium plating on graphitic anodes in commercial lithium-ion cells, *J. Power Sources* 304 (2016) 170-180.
- [114] J. Wandt, C. Marino, H.A. Gasteiger, P. Jakes, R. Eichel, J. Granwehr, Operando electron paramagnetic resonance spectroscopy - formation of mossy lithium on lithium anodes during charge-discharge cycling, *Energy Environ. Sci.* 8 (2015) 1358-1367.
- [115] F. Sagane, R. Shimokawa, H. Sano, H. Sakaebe, Y. Iriyama, In-situ scanning electron microscopy observations of Li plating and stripping reactions at the lithium phosphorus oxynitride glass electrolyte/Cu interface, *J. Power Sources* 225 (2013) 245-250.
- [116] M. Petzl, M.A. Danzer, Nondestructive detection, characterization, and quantification of lithium plating in commercial lithium-ion batteries, *J. Power Sources* 254 (2014) 80-87.
- [117] S.S. Zhang, The effect of the charging protocol on the cycle life of a Li-ion battery, *J. Power Sources* 161 (2006) 1385-1391.
- [118] P.H.L. Notten, J.H.G. Op het Veld, J.R.G. van Beek, Boostcharging Li-ion batteries: A challenging new charging concept, *J. Power Sources* 145 (2005) 89-94.
- [119] M.C. Smart, R.V. Bugga, Effects of Electrolyte Composition on Lithium Plating in Lithium-Ion Cells, *J. Electrochem. Soc.* 158 (2011) A379-A389.
- [120] C. Peabody, C.B. Arnold, The role of mechanically induced separator creep in lithium-ion battery capacity fade, *J. Power Sources* 196 (2011) 8147-8153.
- [121] J. Cannarella, C.B. Arnold, Stress evolution and capacity fade in constrained lithium-ion pouch cells, *J. Power Sources* 245 (2014) 745-751.

- [122] J. Cannarella, C.B. Arnold, The Effects of Defects on Localized Plating in Lithium-Ion Batteries, *J. Electrochem. Soc.* 162 (2015) A1365-A1373.
- [123] K. Jalkanen, J. Karppinen, L. Skogström, T. Laurila, M. Nisula, K. Vuorilehto, Cycle aging of commercial NMC/graphite pouch cells at different temperatures, *Appl. Energy* 154 (2015) 160-172.
- [124] L. Terborg, S. Weber, F. Blaske, S. Passerini, M. Winter, U. Karst, S. Nowak, Investigation of thermal aging and hydrolysis mechanisms in commercial lithium ion battery electrolyte, *J. Power Sources* 242 (2013) 832-837.
- [125] J. Li, E. Murphy, J. Winnick, P.A. Kohl, The effects of pulse charging on cycling characteristics of commercial lithium-ion batteries, *J. Power Sources* 102 (2001) 302-309.
- [126] Z. Ma, J. Jiang, W. Shi, W. Zhang, C.C. Mi, Investigation of path dependence in commercial lithium-ion cells for pure electric bus applications: Aging mechanism identification, *J. Power Sources* 274 (2015) 29-40.
- [127] S.F. Schuster, M.J. Brand, P. Berg, M. Gleissenberger, A. Jossen, Lithium-ion cell-to-cell variation during battery electric vehicle operation, *J. Power Sources* 297 (2015) 242-251.
- [128] D.J. Moosbauer, Elektrochemische Charakterisierung von Elektrolyten und Elektroden für Lithium-Ionen-Batterien, University Regensburg, Doctoral Thesis, Regensburg, 2010.
- [129] S. Bourlot, P. Blanchard, S. Robert, Investigation of aging mechanisms of high power Li-ion cells used for hybrid electric vehicles, *J. Power Sources* 196 (2011) 6841-6846.
- [130] S.S. Zhang, Electrochemical study of the formation of a solid electrolyte interphase on graphite in a $\text{LiBC}_2\text{O}_4\text{F}_2$ -based electrolyte, *J. Power Sources* 163 (2007) 713-718.
- [131] H. Jannesari, M.D. Emami, C. Ziegler, Effect of electrolyte transport properties and variations in the morphological parameters on the variation of side reaction rate across the anode electrode and the aging of lithium ion batteries, *J. Power Sources* 196 (2011) 9654-9664.
- [132] M.B. Pinson, M.Z. Bazant, Theory of SEI Formation in Rechargeable Batteries: Capacity Fade, Accelerated Aging and Lifetime Prediction, *J. Electrochem. Soc.* 160 (2013) A243-A250.
- [133] S.K. Martha, H. Sclar, Z.S. Framowitz, D. Kovacheva, N. Saliyski, Y. Gofer, P. Sharon, E. Golik, B. Markovsky, D. Aurbach, A comparative study of electrodes comprising nanometric and submicron particles of $\text{LiNi}_{0.50}\text{Mn}_{0.50}\text{O}_2$, $\text{LiNi}_{0.33}\text{Mn}_{0.33}\text{Co}_{0.33}\text{O}_2$ and $\text{LiNi}_{0.40}\text{Mn}_{0.40}\text{Co}_{0.20}\text{O}_2$ layered compounds, *J. Power Sources* 189 (2009) 248-255.

- [134] X. Xiong, Z. Wang, P. Yue, H. Guo, F. Wu, J. Wang, X. Li, Washing effects on electrochemical performance and storage characteristics of $\text{LiNi}_{0.8}\text{Co}_{0.1}\text{Mn}_{0.1}\text{O}_2$ as cathode material for lithium-ion batteries, *J. Power Sources* 222 (2013) 318-325.
- [135] B.Y. Liaw, E.P. Roth, R.G. Jungst, G. Nagasubramanian, H.L. Case, D.H. Doughty, Correlation of Arrhenius behaviors in power and capacity fades with cell impedance and heat generation in cylindrical lithium-ion cells, *J. Power Sources* 119-121 (2003) 874-886.
- [136] A. Barré, F. Suard, M. Gerard, M. Montaru, D. Riu, Statistical Method Tools to Analyze Ageing Effects on Li-Ion Battery Performances, SAE International (2013) 2013-01-1429.
- [137] K. Smith, J. Neubauer, E. Wood, M. Jun, A. Pesaran, Models for Battery Reliability and Lifetime - Applications in Design and Health Management, Battery Congress, Ann Arbor, April 2013, National Renewable Laboratory Website (25. December 2015): <http://www.nrel.gov/docs/fy13osti/58550.pdf>
- [138] E. Sarasketa-Zabala, F. Aguesse, I. Villarreal, L.M. Rodriguez-Martinez, C.M. López, P. Kubiak, Understanding Lithium Inventory Loss and Sudden Performance Fade in Cylindrical Cells during Cycling with Deep-Discharge Steps, *J. Phys. Chem. C*, 119 (2015) 896-906.
- [139] M. Ouyang, Z. Chu, L. Lu, J. Li, X. Han, X. Feng, G. Liu, Low temperature aging mechanism identification and lithium deposition in a large format lithium iron phosphate battery for different charge profiles, *J. Power Sources* 286 (2015) 309-320.
- [140] S.F. Schuster, T. Bach, E. Fleder, J. Müller, M. Brand, G. Sextl, A. Jossen, Nonlinear aging characteristics of lithium-ion cells under different operational conditions, *J. Energy Storage* 1 (2015) 44-53.
- [141] A.J. Smith, H.M. Dahn, J.C. Burns, J.R. Dahn, Long-Term Low-Rate Cycling of LiCoO_2 /Graphite Li-Ion Cells at 55 °C, *J. Electrochem. Soc.* 159 (2012) A705-A710.
- [142] T. Baumhöfer, M. Brühl, S. Rothgang, D.U. Sauer, Production caused variation in capacity aging trend and correlation to initial cell performance, *J. Power Sources* 247 (2014) 332-338.
- [143] M. Dubarry, C. Truchot, M. Cugnet, B.Y. Liaw, K. Gering, S. Sazhin, D. Jamison, C. Michelbacher, Evaluation of commercial lithium-ion cells based on composite positive electrode for plug-in hybrid electric vehicle applications. Part I: Initial characterization, *J. Power Sources* 196 (2011) 10328-10335.
- [144] T.C. Bach, S.F. Schuster, E. Fleder, J. Müller, M.J. Brand, H. Lormann, A. Jossen, G. Sextl, Nonlinear aging of cylindrical lithium-ion cells linked to heterogeneous compression, *J. Energy Storage* 5 (2016) 212-223.

- [145] Y. Wu, *Lithium-Ion Batteries: Fundamentals and Applications*, 1st ed., CRC Press, Tokyo, 2015.
- [146] P.J. Osswald, S.V. Erhard, J. Wilhelm, H.E. Hoster, A. Jossen, Simulation and Measurement of Local Potentials of Modified Commercial Cylindrical Cells I: Cell Preparation and Measurements, *J. Electrochem. Soc.* 162 (2015) A2099-A2105.
- [147] S.V. Erhard, P.J. Osswald, J. Wilhelm, A. Rheinfeld, S. Kosch, A. Jossen, Simulation and Measurement of Local Potentials of Modified Commercial Cells II: Multi-Dimensional Modeling and Validation, *J. Electrochem. Soc.* 162 (2015) A2707-A2719.
- [148] D.P. Finegan, M. Scheel, J.B. Robinson, B. Tjaden, I. Hunt, T.J. Mason, J. Millichamp, M. Di Michiel, G.J. Offer, G. Hinds, D.J.L. Brett, P.R. Shearing, In-operando high-speed tomography of lithium-ion batteries during thermal runaway, *Nat. Commun.* 6 (2015) Art. 7924.
- [149] M. Wang, H. Li, Spatiotemporal modeling of internal states distribution for lithium-ion battery, *J. Power Sources* 301 (2016) 261-270.
- [150] R. Gonzalez-Arrabal, M. Panizo-Laiz, K. Fujita, K. Mima, A. Yamazaki, T. Kamiya, Y. Oriksa, Y. Uchimoto, H. Sawada, C. Okuda, Y. Kato, J.M. Perlado, Meso-scale characterization of lithium distribution in lithium-ion batteries using ion beam analysis techniques, *J. Power Sources* 299 (2015) 587-595.
- [151] D.S. Eastwood, V. Yufit, J. Gelb, A. Gu, R.S. Bradley, S.J. Harris, D.J.L. Brett, N.P. Brandon, P.D. Lee, P.J. Withers, P.R. Shearing, Lithiation-Induced Dilation Mapping in a Lithium-Ion Battery Electrode by 3D X-Ray Microscopy and Digital Volume Correlation, *Adv. Energy Mat.* 4 (2014) Art. 130050.
- [152] K.B. Oldham, Edge effects in semiinfinite diffusion, *J. Electroanal. Chem. Interfacial Electrochem.* 122 (1981) 1-17.
- [153] M. Dollé, L. Sannier, B. Beaudoin, M. Trentin, J. Tarascon, Live Scanning Electron Microscope Observations of Dendritic Growth in Lithium/Polymer Cells, *Electrochem. Solid-State Lett.* 5 (2002) A286-A289.
- [154] J. Cannarella, C.B. Arnold, Ion transport restriction in mechanically strained separator membranes, *J. Power Sources* 226 (2013) 149-155.
- [155] L. Cai, K. An, Z. Feng, C. Liang, S.J. Harris, In-situ observation of inhomogeneous degradation in large format Li-ion cells by neutron diffraction, *J. Power Sources* 236 (2013) 163-168.
- [156] M. Tang, P. Albertus, J. Newman, Two-Dimensional Modeling of Lithium Deposition during Cell Charging, *J. Electrochem. Soc.* 156 (2009) A390-A399.

- [157] S. Saxena, C. Le Floch, J. MacDonald, S. Moura, Quantifying EV battery end-of-life through analysis of travel needs with vehicle powertrain models, *J. Power Sources* 282 (2015) 265-276.
- [158] E. Musk, Tesla Motors Website (31. January 2016):
<https://www.teslamotors.com/blog/infinite-mile-warranty>
- [159] S. Viehmann, Focus Online (31. January 2016):
http://www.focus.de/auto/fahrberichte/tid-34017/fahrbericht-bmw-i3-nie-wieder-tanken-trotzdem-vollgas-rollendes-iphone-fuer-reiche-der-bmw-i3-im-ersten-test-das-muessen-sie-sonst-noch-zum-i3-wissen_aid_1124731.html
- [160] S. Paul, C. Diegelmann, H. Kabza, W. Tillmetz, Analysis of ageing inhomogeneities in lithium-ion battery systems, *J. Power Sources* 239 (2013) 642-650.
- [161] Y. Zheng, M. Ouyang, L. Lu, J. Li, Understanding aging mechanisms in lithium-ion battery packs: From cell capacity loss to pack capacity evolution, *J. Power Sources* 278 (2015) 287-295.
- [162] M. Dubarry, C. Truchot, A. Devie, B.Y. Liaw, State-of-Charge Determination in Lithium-Ion Battery Packs Based on Two-Point Measurements in Life, *J. Electrochem. Soc.* 162 (2015) A877-A884.
- [163] S. Santhanagopalan, R.E. White, Quantifying Cell-to-Cell Variations in Lithium Ion Batteries, *Int. J. Electrochem.* (2012) Art. 395838.
- [164] B. Kenney, K. Darcovich, D.D. MacNeil, I.J. Davidson, Modelling the impact of variations in electrode manufacturing on lithium-ion battery modules, *J. Power Sources* 213 (2012) 391-401.
- [165] M. Dubarry, N. Vuillaume, B.Y. Liaw: Origins and accomodation of cell variations in Li-ion battery pack modeling, *Int. J. Energ. Res.* 34 (2010) 216-231.
- [166] R. Gogoana, M.B. Pinson, M.Z. Bazant, S.E. Sarma, Internal resistance matching for parallel-connected lithium-ion cells and impacts on battery pack cycle, *J. Power Sources* 252 (2014) 8-13.
- [167] R. Leonhart, *Lehrbuch Statistik: Einstieg und Vertiefung*, 3rd ed., Hans Huber, Bern, 2013.
- [168] J. Hartung, B. Elpelt, K. Klösener, *Statistik, Lehr- und Handbuch der angewandten Statistik*, 1st ed., Oldenbourg, Munich, 2005.
- [169] H. Degen, P. Lorscheid, *Statistik-Lehrbuch: Methoden der Statistik im wirtschaftswissenschaftlichen Bachelor-Studium*, 3rd ed., Oldenbourg, Munich, 2012.

- [170] J. Li, J.K. Barillas, C. Guenther, M.A. Danzer, Multicell state estimation using variation based sequential Monte Carlo filter for automotive battery packs, *J. Power Sources* 277 (2015) 95-103.
- [171] L. Papula, *Mathematik für Ingenieure und Naturwissenschaftler Band 3: Vektoranalysis, Wahrscheinlichkeitsrechnung, Mathematische Statistik, Fehler- und Ausgleichsrechnung*, 6th ed., Vieweg+Teubner, Wiesbaden, 2011.
- [172] C.M. Harmann, Accelerated life cycle testing and analysis for early failure prediction using two types of lead/acid batteries, *J. Power Sources* 37 (1992) 363-368.
- [173] W. Spindler, How handy is Weibull? or, the use of failure distributions in the planning and analysis of battery experiments, *Journal of Power Sources* 17 (1986) 269-278.
- [174] K. Aström, E. Fontell, S. Virtanen, Reliability analysis and initial requirements for FC systems and stacks, *J. Power Sources* 171 (2006) 46-54.
- [175] E.S. Kumar, B. Sarkar, Improvement of life time and reliability of battery, *Int. J. Engin. Sci. Adv. Tech.* 5 (2012) 1210-1217.
- [176] R. Li, J. Wu, H. Wang, J. Guo, G. Li, Reliability assessment and failure analysis of lithium iron phosphate batteries, *Inform. Sci.* 259 (2014) 359-368.
- [177] P. O'Connor, A. Kleyner, *Practical Reliability Engineering*, 5th ed., John Wiley & Sons, West Susses, 2012.
- [178] H. Zuse, *A framework of software measurement*, 1st ed., Walter de Gruyter, Berlin, 1998.
- [179] D.J. Sheshkin, *Handbook of parametric and nonparametric statistical procedures*, 5th ed., Taylor & Francis Ltd., Boca Raton, 2011.
- [180] A. Jossen, Fundamentals of battery dynamics, *J. Power Sources* 154 (2006) 530-538.
- [181] S. Schuster, P. Keil, C. von Lüders, H. Hesse, A. Jossen, New Charging Method to Avoid Nonlinear Aging of Lithium-Ion Batteries, Batteries Event, Nice, October 2015.
- [182] J. Gallardo-Lozano, E. Romero-Cadaval, M.I. Milanés-Montero, M.A. Guerrero-Martinez, Battery equalization active methods, *J. Power Sources* 246 (2014) 934-949.
- [183] M.S. Lepiorz, Betriebsbedingte Alterung von Lithium-Ionen-Batterien in stationären und mobilen Anwendungen, Technical University of Munich, Doctoral Thesis, Munich, 2015.
- [184] D. Stoller, *INGENIEUR.de* (2. February 2016):
<http://www.ingenieur.de/Themen/Energiespeicher/Wie-Daimler-Smart-Batterien-Verkauf-Geld-verdient>
- [185] S. Eom, M. Kim, I. Kim, S. Moon, Y. Sun, H. Kim, Life prediction and reliability assessment of lithium secondary batteries, *J. Power Sources* 174 (2007) 954-958.

- [186] S.F. Schuster, M.J. Brand, C. Campestri, M. Gleissenberger, A. Jossen, Correlation between capacity and impedance of lithium-ion cells during calendar and cycle life, *J. Power Sources* 305 (2016) 191-199.
- [187] M. Wu, P.J. Chiang, J. Lin, Y. Jan, Correlation between electrochemical characteristics and thermal stability of advanced lithium-ion batteries in abuse tests—short-circuit tests, *Electrochim. Acta* 49 (2004) 1803-1812.
- [188] E.P. Roth, D.H. Doughty, Thermal abuse performance of high-power 18650 Li-ion cells, *J. Power Sources* 128 (2004) 308-318.

List of Abbreviations

ALIB	automotive lithium-ion battery / batteries
BattG	German battery law (from German, “Batteriegesetz”, battery law)
BEV	battery electric vehicle / vehicles
BMS	battery management system / systems
CC	constant current
CCCV	constant current constant voltage
CO ₂ e	CO ₂ equivalent / equivalents
CV	constant voltage
DVA	differential voltage analysis
EFC	equivalent full cycles
EoL	end of life
Eo1L	end of first life
Eo2L	end of second life
GHG	greenhouse gas
HEV	hybrid electric vehicle / vehicles
ICA	incremental capacity analysis
ICP-OES	inductively coupled plasma optical emission spectroscopy
ID	identifier / identifiers
LCO	lithium-cobalt-oxide
LFP	lithium-iron-phosphate
LIB	lithium-ion battery / batteries
LIC	lithium-ion cell / cells
LMO	lithium-manganese-spinel
LTO	lithium-titanate-oxide
NCA	lithium-nickel-cobalt-aluminum-oxide
NiMH	nickel metal hydride

NMC	lithium-nickel-manganese-cobalt-oxide
PbB	lead-acid battery / batteries (from Latin, “plumbum”, lead)
PCRR	primary control reserve regulation
PPMCC	Pearson product-moment correlation coefficient / coefficients
PVDF	polyvinylidene difluoride
SEI	solid electrolyte interphase
SEM	scanning electron microscopy
SLA	second life application / applications
SLB	second life battery / batteries
SLC	second life concept / concepts
SoC	state / states of charge
SoH	state / states of health
SPI	solid permeable interphase
TCO	total cost / costs of ownership
USABC	United States Advanced Battery Consortium
XRD	X-ray diffraction